SAPIENZA UNIVERSITY OF ROME

DOCTORAL THESIS

Constraining Inflationary Models Using Cosmological Observables

Author:
Mehdi SHOKRI

Supervisor:
Alessandro MELCHIORRI

A thesis submitted in fulfillment of the requirements
for the degree of Doctor of Philosophy
in Physics of Sapienza University of Rome

January 8, 2020

Declaration of Authorship

I, Mehdi SHOKRI, declare that this thesis titled, "Constraining Inflationary Models Using Cosmological Observables" is the result of work undertaken between November 2016 and February 2020 under the supervision of Prof. Alessandro Melchiorri. I confirm that:

- This work was done wholly or mainly while in candidature for a research degree at this University.
- Where I have consulted the published work of others, this is always clearly attributed.
- Where I have quoted from the work of others, the source is always given. With the exception of such quotations, this thesis is entirely my own work.
- The author's research works carried out during Ph.D. period are listed as:

  [6] "*What is the amplitude of the Gravitational Waves background expected in the Starobinski model?*" with F. Renzi and A. Melchiorri, **Phys. Dark Univ. 27 (2020) 100450**, [arxiv: astro-ph/1909.08014].

  [5] "*Cosmic Microwave Background constraints on non-minimal couplings in inflationary models with power-law potentials*", with F. Renzi and A. Melchiorri, **Phys. Dark Univ. 24 (2019) 100297**, [arxiv: astro-ph/1905.00649].

  [4] "*The relation between non-commutative and Finsler geometry in Horava-Lifshitz black holes*" with Z. Nekouee and J. Sadeghi, [arxiv: hep-th/1711.10482].

  [3] "*The Lagrangian of charged test particle in Horava-Lifshitz black hole and deformed phase space*" with Z. Nekouee and J. Sadeghi [arxiv: hep-th/1711.02534].

  [2] "*A Revision to the Issue of Frames by Non-minimal Large Field Inflation*" as the single author, [arxiv: hep-th/1710.04990].

  [1] "*Deformation of the quintom cosmological model and its consequences*" with J. Sadeghi, B. Pourhassan and Z. Nekouee, **Int. Mod. Phys. D 27 (2018) 1850025**, [arxiv:hep-th/1708.04319].

- The chapters 5 and 6 of the present thesis are based on the publications 5 and 6, respectively.

Sapienza University of Rome — Mehdi SHOKRI

February 2020

"I am enough of an artist to draw freely upon my imagination. Imagination is more important than knowledge. Knowledge is limited. Imagination encircles the world."

Albert Einstein

SAPIENZA UNIVERSITY OF ROME

Abstract

Department of Physics

Doctor of Philosophy

Constraining Inflationary Models Using Cosmological Observables

by Mehdi SHOKRI

In the present thesis, we attempt to find the constraints imposed by recent observational data on two widely-used inflationary models, including non-minimal inflation and Starobinsky inflation. The first part of the manuscript is dedicated to introducing some theoretical and observational foundations of cosmology which are necessary for the research chapters and the second part is devoted to present the results obtained by my published papers.

In the first part, we start by introducing the principles of Einstein's gravity and the field equations as the foundation of the standard cosmology. Then, we study the dynamical universe for different single-component cases and also the present time. The thermal history of the universe is examined in detail based on the temperature and time of the universe in each stage. Then, we review the observational proofs and also shortcomings of the Hot Big Bang model. We introduce the idea of cosmic inflation and show how inflation can remove the mentioned defects of the Hot Big Bang model. In the following, we go dipper into cosmic inflation by presenting the standard inflationary formalism and some common inflationary models. Moreover, the reheating process and the primordial perturbations generated during the inflationary era are discussed in detail. The thesis is followed by dedicating a chapter to study the physics of cosmic microwave background radiation as the main source of inflationary observables. Particularly, we study the primary temperature and polarization anisotropies of cosmic background photons generated by inflationary perturbations in the early universe and also express how can we use the observables to constraint our inflationary models.

The second part of the thesis is devoted to the research works carried out during my Ph.D. course about finding the observational constraints on inflationary models. The main purpose of the first research work is finding the cosmic microwave background anisotropies constraints on parameters space of power-law inflationary potentials in the context of non-minimal coupling of gravity and inflaton. Also, we study the effects of the presence of the non-minimal coupling term on the predicted amount of gravitational waves in such models. We carry out the inflationary analysis for the power-law potentials with the non-minimal coupling term in the Einstein frame as the easier frame which is conformally connected to the Jordan frame as the non-minimal frame. We consider two main classes of large field potentials, e.g., $n = 4$ and $n \neq 4$ with integer and fractional values. The inflationary parameters in both cases are calculated up to the first order of the slow-roll parameters, where we are assure that the results of the two frames are the same. In order to use the observational data, we use a model-depended analysis method in which N and ξ as

the independent parameters driven by modified CosmoMC code can be randomly sampled in a given range and to calculate the inflationary parameters of the model. Finally, we provide the final results by the corresponded plots and tables.
Our second research work is dedicated to finding constraints on inflationary parameters using a set of recent cosmic microwave background data and under the assumption of the Starobinski model. Also, we consider a particular class of inflationary models that generalize Starobinsky inflation and the possibility of an extension to ΛCDM described by the A_{lens} parameter. We present the inflationary analysis for the generalized form of the Starobinsky model and use the conformal transformation to mapping to the Einstein frame as the conformal frame. Then, we follow the inflationary analysis in the presence of a new scalar field, which is called scaleron, created due to using the conformal transformation. We calculate the inflationary parameters up to the first order of the slow-roll parameters for two main classes, $p = 1$ or Starobinsky model and $p \neq 1$ for a generalized case. Similar to the previous model, we use a model-depended analysis method wherein N and p as the independent parameters driven by modified CosmoMC code, can be randomly sampled in a given range and to calculate the inflationary parameters of the model. Lastly, we examine the final results by the corresponded plots and tables.

Keywords: Non-minimal inflation, Starobinsky inflation, Jordan frame, Einstein frame, Power-law potential, Observational constraints.

Acknowledgements

First, I would like to dedicate my deepest thanks to **Alessandro Melchiorri** as my supervisor during the Ph.D. period. He introduced me to the excellence of theoretical and in particular observational aspects of inflationary cosmology. He taught me the trade of research with a lot of patience. I learnt a lot from his great intellectual honesty and his deep curiosity. He offered me a very pleasant environment for carrying out research activities.

I want to thank my external evaluators **Pierluigi Monaco** and **Lauro Moscardini** for their helpful comments on the present manuscript. I profoundly appreciate their time and effort and I am grateful for their scientific interest in my work.

I want to thank my collaborators, **Jafar Sadeghi**, **Fabrizio Renzi**, **Zohreh Nekouee** and **Behnam Pourhassan** and with whom I worked closely and from whom I learnt a lot.

I want to thank **Paolo Di Beranrdies** and **Silvia Masi** as the directors of the G31 lab at the physics department of Sapienza University Rome for the great hospitality during these three years.

Finally, I would like to dedicate my special thanks to my great family for their motivation and support during all the years of my education.

Contents

List of Figures

List of Tables

Dedicated to my family

Chapter 1

Introduction

Alan Guth first introduced the idea of *Cosmic Inflation* as the accelerating phase of the early universe to overcome the shortcomings of Hot Big Bang theory, including flatness, horizon and monopole problems. It provides a good mechanism to produce the primordial density perturbations as the seed of the structure formation of the universe and also the tensor perturbations as the main responsible to generate the primordial gravitational waves. The generated scalar and tensor perturbations due to the primordial quantum fluctuations can be entitled as the leading cause of derivation from the homogeneous and isotropic early universe and we are forced to combine particle physics and cosmology to explain the main features of cosmic inflation. Hence, the standard formalism of inflation has been established on the scalar fields proposed by particle physics. An acceptable inflationary model must supply the main properties of cosmic inflation, including having a graceful exit from the inflationary era to the radiation-dominated epoch, producing the inflationary perturbations pointed out in the above discussion, having the specific amount of number of e-folds to remove the defects of hot big bang model and proposing a reheating mechanism to reheat the universe when inflation ends. The simplest inflationary model is based on a single scalar field as the sole component of the universe during the inflationary era which decays to the other particles at the end of inflation through the reheating process. Also, hybrid models as a widely used form of multi-filed models have benn considered in many inflationary scenarios in which an assistant field aids to inflaton to stop inflation. Besides the standard inflationary models, people also concern to explain inflation in the context of modified theories of gravity such as $f(R)$, Braneworld and scalar-tensor gravity theories. Eternal inflation considers the little bubbles of space which could have randomly stopped inflating instead of ending inflation all at once. Therefore, we can find a wide range of inflationary models among the cosmological papers.
One of the most crucial parts of inflation is finding an efficient inflationary model covering all features of cosmic inflation between hordes of models. The inflationary observations based on the analysis of cosmic background radiation help us to clarify the puzzle. The relic big bang photons released from the last scattering surface plays a significant role in modern cosmology since they contain valuable information from all stages of the universe due to traveling from recombination time to present. In particular, we focus on the temperature and polarization anisotropies created through the inflationary perturbations in order to perform a better judgment between different inflationary models.
The present manuscript is based on the published papers carried out by me and my colleagues during a three years Ph.D. course at the physics department of Sapienza University of Rome under the supervision of Alessandro Melchiorri. We found the CMB observational constraints on two popular inflationary models, including non-minimal coupling and R^{2p} inflationary models which are discussed in chapters 5

and 6, respectively.
Let's review how is organized the present thesis. In chapter 2, we present some fundamental concepts of cosmology that would be useful in the next chapters. Hence, we start by talking about the main principles of Einstein's gravity and it follows by the observational probes of the theory. Then, we examine the Einstein field equations by using the action principle. For the sake of completeness, we list some essential solutions to Einstein's field equations, in particular, the Friedman Robertson Walker metric describing the homogeneous and isotropic universe. The chapter follows by analyzing the standard model of cosmology and the appropriated dynamical relations for different universes, including the single and compound universe. Then, we provide a detailed discussion about the thermal history of the universe based on cosmic time and temperature. The chapter ends with an explanation of the strengths and weaknesses of the hot big bang model. We dedicate the chapter 3 to introduce the inflation theory and the corresponded issues. We begin with solving the shortcoming of the big bang theory by inflation. Then, we present the standard inflationary analysis based on the single scalar field under the slow-roll approximation. Also, we study the reheating process occurred at the end of inflation due to decaying the scalar field. The chapter tracks by reviewing some usual inflationary models. In the final section of the chapter, we examine the perturbations produced during inflation by using the SVT decomposition in order to divide the perturbations into scalar, vector and tensor cases. The thesis follows with a brief and useful discussion about cosmic microwave background radiation in chapter 4. We start with the timeline of prediction, discovery, and interpretation of cosmic background photons. Then, we study the temperature anisotropies of cosmic background photons created by the primary and secondary effects. Finally, we briefly express about E-mode and B-mode polarization anisotropies of cosmic background photons. We devote chapter 5 to our first research work which is dedicated to finding the CMB anisotropies constraints on space parameters of power-law inflationary potentials, in particular, the coupling constant ξ when gravity non-minimally connects to inflaton. We start with a brief discussion about the idea of NMC and its corresponded expressions. Then, we describe the inflationary analysis in Jordan and Einstein frames defined due to using the conformal transformation, separately. Because of the physical equivalency of two frames, we continue the inflationary study in the Einstein frame as the easier frame, for the general form of power-law potentials $\lambda\varphi^n$ wherein n can accept the integer and fractional values. In order to find the observational constraints on the parameters space of the model, first, we give a short description of the used analysis method and then we discuss the final results through the corresponded plots and tables. In chapter 6, we turn to the description of the second research paper in which we evaluate the amount of gravitational waves predicted by the Starobinski model by considering the current uncertainties on n_s and the possibility of an extension to the ΛCDM model parameterized by A_{lens}. First, we begin by studying the R^{2p} model as a generalized form of the Starobinsky model and perform the inflationary calculations in the Einstein frame using the conformal transformation. In such the previous work, we present the analysis method used for our model and then, we discuss the result for Starobinsky and near Starobinsky cases based on the allowed values of p by the obtained plots and tables. Finally, in chapter 7, we conclude our findings and present some remarks and possible prospects for the present works. Also, in the appendix A, we talk about the conformal transformation as an essential mathematical tool used in many gravitational situations, especially at the classical level. First, we introduce the connecting relations of the geometrical quantities in

Jordan and Einstein frames which are linked to each other by the conformal transformation. Then, we apply the conformal transformation for three important classical theories of gravity, including $f(R)$ and scalar to tensor gravity as the modified theories of gravity and also the gravitational theories represented in the presence of non-minimal coupling term between gravitational and scalar field.

Chapter 2

Fundamental Cosmology

The human mind has involved various fundamental questions about the universe since many years ago. *Where do we come from?*, *What are we?*, *Where are we going?*. Cosmology deals with these basic puzzles since it studies the situation of the universe from the creation to the present time and even predicts the future based on the existing theories. Cosmology talks about very large scales of distance in the range of Parsec (intergalactic distances), time in the range of billion years (age of the universe) and mass in the range of 10^{30} kg (the mass of the sun). In contrast, cosmology has been entwined with small scales in the early universe where particle physics and cosmology meet each other. These scales which are known to the *Planck scales*, have established on the fundamental constants of physics, the light speed (c), the reduced Planck constant ($\hbar$) and the gravitational constant (G). In principle, cosmology attempts to describe the past, explain the present and predict the future of the universe via studying the cosmological phenomena in different scales. This goal can be fulfilled by comparing the theoretical ideas with cosmological observations. Consequently, using modern technologies to fabricate high precision observational tools, plays a great role in progressing cosmology. The present chapter dedicates to explaining the primary concepts of the standard cosmology which are further discussed in a wide range of cosmological textbooks [1, 2, 3, 4, 5, 6, 7, 8, 9, 10, 11].

2.1 The Principles of General Relativity

Although gravity is the weakest force among the fundamental forces of nature, it has the most contribution to structure formation of the universe. In classical physics, there are two different approaches to describe gravity. Newton's view based on direct gravitational interaction between objects and Einstein's view of gravity or General Relativity (GR) talking about the influence of the gravitational fields on surrounded spacetime. In other words, GR deals with the spacetimes which have been curved because of gravitational fields. The mentioned pictures present a different concept of gravity. However, due to the *correspondence principle*, GR approaches to the Newtonian view in the limit of weak spatial curvature. Let's review the main principles of GR as one of the greatest achievements of the human mind [12].

2.1.1 Mach's Principle

To explain Mach's principle [13], we start with defining the inertial force acting opposite in direction to an accelerating or rotating force in a non-inertial frame. This means that the inertial forces are detectable in non-inertial frameworks. Imagine a non-inertial frame moving with a uniform acceleration a relative to an inertial frame S (see Figure 2.1) as

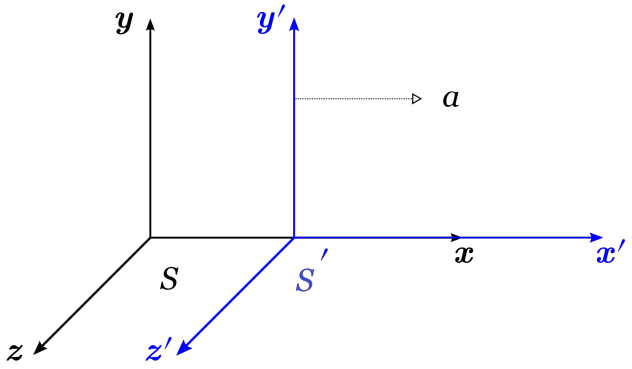

FIGURE 2.1: Two frameworks S and $\acute{S}$ are shown as inertial and non-inertial systems, respectively. The non-inertial system $\acute{S}$ is moving with a uniform acceleration a relative to the inertial frame S along x axis.

$$x \to \acute{x} + s, \tag{2.1}$$

where x and $\acute{x}$ are positions in the inertial and non-internal systems, respectively. Also, s denotes the displacement in the non-inertial system. By setting Newton's second law for a particle with a mass of m under the effect of the force F, we have

$$F - ma = m\ddot{x}. \tag{2.2}$$

By taking a look at the above expression, one can find that the inertial force reduces the effects of the non-inertial force. Newton attempted to show the result by a Bucket of water in a rotating system relative to the absolute space where remains steady independent from any matter and interactions (for a detailed discussion of Newton's original argument, see [14]). Based on the experiment, suppose that a bucket filled with water is suspended from a fixed point by a rope. The rope twists and then the bucket releases. The result can be expressed in four different situations:

- **First Phase**. The bucket begins to rotate because of the twisted rope. But, the water in the bucket does not turn with and remains steady. (see the picture (b) of Figure 2.2).
- **Second Phase**. The frictional force between the bucket and water produces a centrifugal force. Eventually, the water starts to rotate and the surface becomes concave. (see the picture (c) of Figure 2.2).
- **Third Phase**. The bucket will hold gradually, but the water is rotating yet with a concave surface. (see the picture (d) of Figure 2.2).
- **Forth Phase**. Water will stop with a flat surface.

Newton explained that the curvature of the surface belongs to the centrifugal effects of rotating water relative to the absolute space not the bucket rotation since the surface of the water is flat when the bucket is rotating in the first phase and it is curved when the bucket is in the rest in the third phase. In other words, he believed that the inertial forces are detectable in a non-inertial system relative to the absolute space and they are independent of other surrounded matters.
In contrast, the Mach approach says the motion is meaningful when the role of other

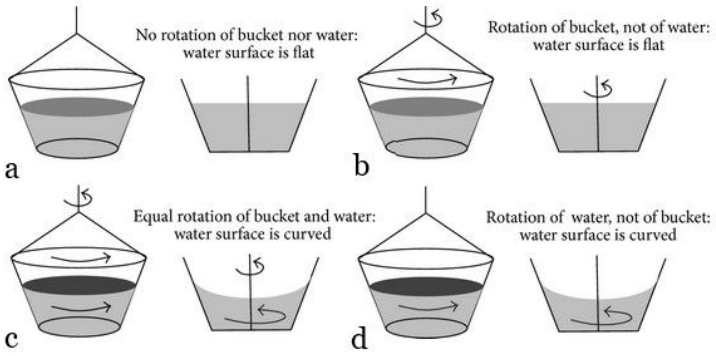

FIGURE 2.2: The result of the Newton bucket experiment can be divided into four parts. After twisting the rope and releasing the bucket, first the bucket begins to rotate, but the water is in rest and the water surface is flat. Second, by frictional effects between bucket and water, the centrifugal force is produced and then water starts to rotate with a concave surface. Third, The bucket will stop, but the water is turning with a curved surface yet. Forth, the water will stop and there is a flat surface for water.

matters is taken into account since without any matter there is nothing to which the motion can be refereed. Moreover, the inertial forces are produced due to the interactions of matters with each other and it means that the inertial forces can be counted in a non-inertial frame relative to other matters. For the bucket experiment, Mach believes that the curvature of the water surface is through the motion of water relative to other matters, not relative to absolute space.
In conclusion, we can summarize Mach's principles into three laws [15]:

- *The motion of a physical system is related to the other matter, not absolute space.*
- *The inertial forces are detectable in the non-inertial frames relative to the other matters, not absolute space.*
- *It is not acceptable to talk about motion and geometry in an empty space. If there is no matter there is no geometry. It means that space is relative, not absolute.*

In the next sections, we will see the footprint of Mach's principle in the Einstein field equations.

2.1.2 Equivalence Principle

In the Newtonian gravity, space is Euclidian and independent from matter. It means that the shortest distance between two points is a straight line. In such a case, gravity between two gravitational masses m_g and M_g acts as

$$F = -G\frac{M_g m_g}{r^2}, \tag{2.3}$$

where r and G are the distance between two masses and the universal gravitational constant, respectively. Also, the negative sign implies that gravity is an attractive force. On the other hands, regarding the second law of motion, we can attribute an inertial mass m_i to every object which acquires the acceleration a by a specific force F as

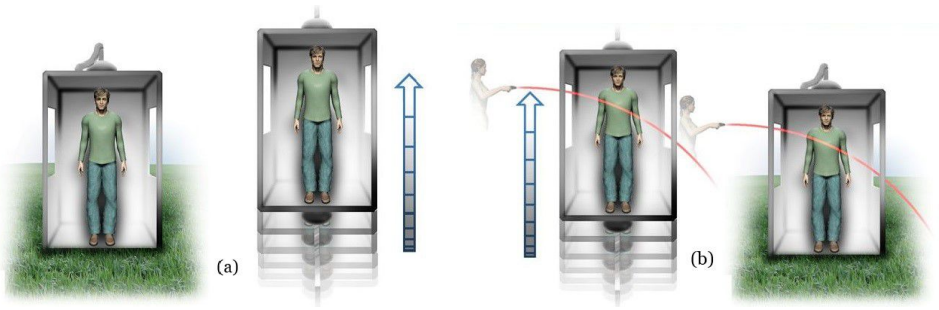

FIGURE 2.3: Picture (a) shows the strong equivalence principle between two physical systems in which the left elevator is settled on the earth with gravitational acceleration 9.8 ms^{-2} and the right elevator is moving upward with acceleration 9.8 ms^{-2} in the space without any gravitational field. Picture (b) presents Einstein's intuition from general relativity by using the strong equivalence principle for the photon experiment.

$$F = m_i a. \tag{2.4}$$

The property of an object that determines how strongly it is pulled on by the force of gravity is equal to the property that determines its resistance to acceleration by any force. Therefore, we can express the *Weak Equivalence Principle* (WEP) as the equality of gravitational and inertial masses.
Also, WEP can be realized in another way. Assume that the Eq. (2.3) shows the gravitational force between the earth and an object. Therefore, by using the Eqs. (2.3) and (2.4), we find

$$a = -\frac{GM_g}{r^2}(\frac{m_g}{m_i}), \tag{2.5}$$

where M_g is the mass of the Earth. Due to the Galileo experiment, the dropped objects from towers acquire the same gravitational acceleration $9.8ms^{-2}$ regardless of the mass and composition of the object. Hence, the above equation reveals WEP.
Let us find out how Einstein devised GR from WEP. Imagine that a person who is in an elevator settled on the earth with gravitational acceleration 9.8 ms^{-2} and another person who is in an elevator moving up with acceleration 9.8 ms^{-2} in the space without any gravitational field as shown in picture (a) of Figure 2.3. If two persons drop an apple in their systems, both can realize that two apples are falling with the same acceleration. The *Strong Equivalence Principle* (SEP) says that two systems are equivalent as a consequence of WEP [16]. Now, assume that we flash a light beam by torch into the second elevator, the person finds out the beam bends downward through acting force on moving photons. Thanks to the STE, we can substitute the mentioned system with the first system and conclude that bending the light beam in a stationary system on the earth can occur only when the path of photons has been curved by the gravitational field (see the picture (b) of Figure 2.3). Einstein's result can be also realized by *Fermat's principle* [17, 18] as a fundamental principle of optics. According to this principle, the light always travels between two points along a path that minimizes the travel time required. In summary, when we study the vacuum case, the spacetime is flat and the shortest path between two points is a straight line. However, in the presence of matter and due to its gravitational effects, the surrounded spacetime or the path of objects will be curved. Hence, the path

taken by light is not a straight line.

2.1.3 General Covariance Principle

According to Special Relativity (SR) [19], the physics laws take the same mathematical form in all inertial reference frames. However, in GR, we extend this principle to all reference frames, whether inertial or non-inertial. In other words, the form of physics laws will be invariant under the arbitrary differentiable coordinate transformations. Hence, to formulate the physical laws, we use the tonsorial language, which is independent of all the reference frames [20].

2.1.4 Correspondence Principle

The correspondence principle was first introduced by Niels Bohr in 1920 to develop his model of the atom [21]. Then, it used in a more general sense to mean the new theories of physics require to explain all the phenomena for which a preceding theory was valid. In other words, the new theory must reproduce the result of the former theory under the corresponded conditions. According to the correspondence principle, GR reduces to SR when the gravity is absent and also it mimics the Newtonian gravity in the limit of weak gravitational fields and low velocities. Moreover, SR reduces to the classical mechanics in the limit of small velocities comparing with light speed.

2.2 The Evidence of General Relativity

Einstein presented a new approach to gravity in large scales in which the spacetime is curved through the gravitational field of a massive object and then the curved spacetime determines how objects move. Like all new theories, the predictions of GR also required to be tested by observational experiments in order to approve the theory. Hence, this section devotes to studying the main observational tests of GR (Note that the first three tests proposed by Einstein [12]).

2.2.1 Perihelion Precession of Mercury

The planets in the solar system are spinning around the sun in an elliptical orbit in which the closest point of the orbit to the sun is called *perihelion*. The first clue of the precession of the perihelion of Mercury's orbit was proposed by Urbain Le Verrier in 1859 [22]. The derivation could be expectable somewhat because the Sun is not a perfect sphere and it is a bit squashed, fatter at the equator, but Le Verrier by looking at 150 years of observations of Mercury's orbit, discovered the perihelion was shifting by 43 arcseconds every century. Einstein's calculations predicted an extra 43 arcseconds in perihelion precession for Mercury [12]. This not only resolved an old mystery in astronomy but strongly proved that Einstein was on the right track.

2.2.2 Gravitational Lensing

One of the most well-known tests of GR is the gravitational deflection of light or gravitational lensing in which the light of a star passing near the sun will bend through the curved spacetime around the sun. Einstein's calculations showed that starlight just grazing the Sun's surface should be deflected by an angle of 1.75 arcsec [22]. Observationally, it could be measurable by looking at the deflection of starlight

during a total solar eclipse. In such a case, the gravitational field of the sun is strong enough to bend the path of light and also stars near the edge of the Sun should be visible since most of the light from the Sun is blocked by the moon. The first realization of this test performed by Arthur Stanley Eddington to observe the total solar eclipse in 1919 [23]. He imaged several stars around the eclipse and confirmed predictions.
After discovering quasars as very distant and bright objects, scientists interested in renewing the gravitational lensing for the light of quasars from massive objects like distant galaxies. The result of lensing was the formation of multiple images of the same galaxy. This occurs because light rays from a distant galaxy that would otherwise diverge may be focused together by lensing. For an observer on the Earth, it looks as if two similar light rays have traveled along straight lines from different parts of the sky.

2.2.3 Gravitational Redshift

Einstein's gravity predicts the wavelength of electromagnetic radiation will lengthen when it climbs out of a gravitational well produced by a massive object. Hence, Photon must disburse energy to escape, but it must always travel at the speed of light, so the missed energy must be found through a decline of frequency or raise of wavelength. This effect is called gravitational redshift and it was first measured on earth in 1960-65 by Pound, Rebka, and Snider, who examined gamma rays emitted and absorbed by atomic nuclei [24].

2.2.4 Gravitational Waves

After discovering GR, Einstein declared that massive accelerating objects such as neutron stars, black holes, stars orbiting each other would disrupt spacetime so that waves of distorted space would radiate from the source like the produced waves due to a stone thrown into a pond [25]. The produced gravitational ripples travel at the speed of light and carry valuable information about the sources. The main sources of gravitational waves are colliding black holes, the collapse of stellar cores, coalescing neutron stars or white dwarf stars, the slightly wobbly rotation of neutron stars that are not perfect spheres. The first observational proof of gravitational waves occurred in 1974 through discovering some interesting results of a binary pulsar by R. A. Hulse and J. H. Taylor [26] and then, it motivated other scientists to study pulsar radio-emissions in order to find some clues of gravitational waves. But, these experiments had always come indirectly and not because of actual physical contact. In 2015, Laser Interferometer Gravitational-Wave Observatory (LIGO) directly detected the distortions in spacetime produced by passing gravitational waves of two colliding black holes nearly 1.3 billion light-years away [27].

2.3 Field Equations

To formulate GR, we apply the action principle, which is a variational method to express a wide range of physical laws. The deduction of equations from physical actions has several advantages. First, it allows the unification with other field theories which are also formulated in terms of physical actions such as Maxwell's theory. Moreover, the action facilitates the identification of the constant quantities through the study of the symmetries of the actions with the Noether theorem.
Let us start with the form of the Einstein-Hilbert action in GR as [28, 29]

$$S = \int \sqrt{-g}\left(\frac{1}{2\kappa^2}(R - 2\Lambda) + \mathcal{L}_M\right)d^4x, \tag{2.6}$$

where $\kappa^2 \equiv 8\pi G = \frac{8\pi}{m_{PL}^2}$ where G and m_{PL} are the gravitational constant and Planck mass, respectively. In the above action, Λ is the cosmological constant, g is the determinant of metric $g_{\mu\nu}$ and R is the Ricci curvature scalar $R \equiv g^{\mu\nu}R_{\mu\nu}$ where the Ricci tensor defines as $R_{\mu\nu} = \partial_\gamma\Gamma^\gamma_{\nu\mu} - \partial_\nu\Gamma^\gamma_{\gamma\mu} + \Gamma^\gamma_{\gamma\lambda}\Gamma^\lambda_{\nu\mu} - \Gamma^\gamma_{\nu\lambda}\Gamma^\lambda_{\gamma\mu}$, where the Christoffel symbol is expressed by $\Gamma^\gamma_{\mu\nu} = \frac{1}{2}g^{\gamma\lambda}(\partial_\nu g_{\lambda\mu} + \partial_\mu g_{\lambda\nu} - \partial_\lambda g_{\mu\nu})$. The first term of the Eq. (2.6) is Einstein-Hilbert's action as the geometrical part of total action and $\mathcal{L}_M$ depicts to the matter sector which determines by the type of component dominated in the universe. By varying the action (2.6) with respect to the metric, we obtain the Einstein field equations as

$$G_{\mu\nu} + \Lambda g_{\mu\nu} \equiv R_{\mu\nu} - \frac{1}{2}Rg_{\mu\nu} + \Lambda g_{\mu\nu} = \kappa^2 T_{\mu\nu}, \tag{2.7}$$

where $G_{\mu\nu}$ is the Einstein tensor and $T_{\mu\nu}$ is the energy-momentum tensor given by

$$T_{\mu\nu} = g_{\mu\nu}\mathcal{L}_M - \frac{2\delta\mathcal{L}_M}{\delta g^{\mu\nu}}. \tag{2.8}$$

We note that the conservation law of the energy-momentum tensor $\nabla^\nu T_{\mu\nu} = 0$ is valid as a direct consequence of the Bianchi identities $\nabla^\nu G_{\mu\nu} = 0$.

2.4 The Solutions of General Relativity

The solutions of Einstein's field equations (2.7) are metrics of spacetime which measure the distance between points in different geometries. By using the metric as the geometrical tool and also the corresponded matter, one can solve Einstein's field equations in order to find the dynamical relations in the context of a cosmological model. A wide range of solutions are proposed in cosmology [30], here we review some crucial metrics of GR.

2.4.1 Friedmann–Lemaître–Robertson–Walker Solution

The Friedmann–Lemaître–Robertson–Walker (FLRW) metric is identified as one of the most distinguished metrics in GR since it forms the structure of the standard cosmological model. Regarding the *cosmological principle* which says the universe is almost homogamous and isotropic in large scale structures, the FLRW metric can be expressed by [31, 32, 33, 34]

$$ds^2 = -dt^2 + a^2(t)\left(\frac{dr^2}{1 - \mathcal{K}r^2} + r^2(d\theta^2 + sin^2\theta d\phi^2)\right), \tag{2.9}$$

where t cosmic time is the time measured by an observer who sees the universe is expanding uniformly around him. Also, r is the comoving radial coordinate, θ and ϕ are the comoving angular coordinates and $a(t)$ is usually a dimensionless factor hinting the expansion of the universe. $\mathcal{K}$ as a constant representing the spatial curvature constant can take two common dimension notations:

- $\mathcal{K}$ with a dimension of length^2. In which case r has a dimension of length and scale factor $a(t)$ is dimensionless.

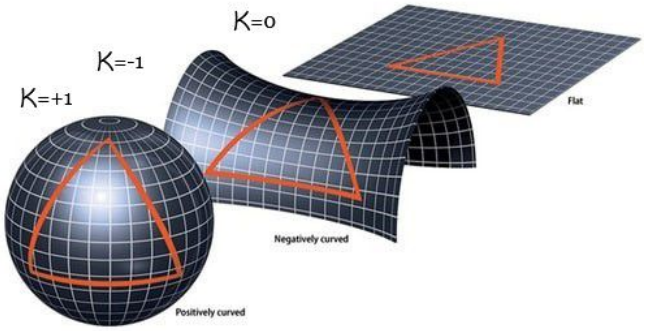

FIGURE 2.4: The values of spatial curvature constant $\mathcal{K}$ can be found as: $\mathcal{K} = +1$ for a closed universe, $\mathcal{K}$=+1 for an open universe and $\mathcal{K} = 0$ is for a flat universe. The recent observations reveal that the universe is spatially flat at present time.

- $\mathcal{K}$ expressed as a set of +1, 0, -1 for negative, zero, and positive curvature, respectively (see Figure 2.4). In which case, r is dimensionless and $a(t)$ has a dimension of length.

The properties of possible spatial curvatures introduced in the second notation can be reviewed as

• **Positive Curvature**. The sum of the three angles of a triangle is more than 180. This case is associated with the curvature constant $\mathcal{K}$ to +1. A 3D space with positive curvature has a structure similar to the 2D surface of a sphere wherein if you travel far enough in any direction, you come back to where you began. Thus space is finite and the universe is closed.

• **Flat space**. The sum of angles of a triangle is exactly 180. The conventional geometry of Euclidean is $\mathcal{K}$ = 0. It can be considered as the limit of the other two cases for an infinite radius of curvature. Since it is balanced between the other two, this is sometimes called a critical universe. For true Euclidean geometry, the topology is also open. It means that space is infinite in all directions. It is also possible to have compact topologies in a flat space, which have a finite volume.

• **Negative Curvature**. The sum of angles of a triangle is < 180. The case of $\mathcal{K}$ = -1 is hard to imagine as it is not even possible to have a 2D surface of constant negative curvature in Euclidean 3D space. 2D surfaces can have local regions of negative curvature. The simplest topological case is when the universe is infinite in all directions, and it is open. In fact, it is more infinite than the Euclidean case.

2.4.2 Black Hole Solution

The Schwarzschild solution describes the gravitational field outside of a mass with spherical symmetry such as a Black Hole (BH) or any object that is asymptotically flat, spherically symmetric and static. The Schwarzschild metric is known as the most straightforward metric of BHs since it is expressed for BHs which are static, chargeless and rotationless. The usual form of Schwarzschild metric is given by [35]

$$ds^2 = -(1 - \frac{2M}{r})dt^2 + \frac{1}{(1 - \frac{2M}{r})}dr^2 + r^2(d\theta^2 + sin^2\theta d^2\phi^2), \tag{2.10}$$

where M is the mass of BH and (t, r, θ, ϕ) are the polar coordinates. Clearly, in far distances when $r \to \infty$, the Schwarzschild metric mimics the Minkowski metric in polar coordinates. It means that the above metric is asymptotically flat. By taking a look at the metric (2.10), one can realize that there are two singularities: $r = 0$ which is a curvature singularity and unavoidable in the BH analysis and $r = 2M$, which is a coordinate singularity and removable by changing coordinates. A Schwarzschild BH can be interpreted with two different regions separated by BH horizon $r = 2M$ is a null hypersurface. The outer region with $r > 2M$ contains the timelike hypersurfaces, which metric becomes flat in very far distances. The inner region with $r < 2M$ includes the spacelike hypersurfaces so that an object falling inside the horizon can only continue moving to decrease values of r until it reaches the curvature singularity $r = 0$.
In order to explain the features of a rotating, stationary, axially symmetric BH, we use the Kerr metric instead of the static Schwarzschild metric. The form of Kerr metric in the polar coordinates (t, r, θ, ϕ) is expressed as [36]

$$ds^2 = -dt^2 + \Sigma(\frac{dr^2}{\Delta} + d\theta^2) + (r^2 + a^2)sin^2\theta d^2\phi^2 + \frac{2Mr}{\Sigma}(asin^2\theta d\phi - dt)^2, \quad (2.11)$$

where

$$\Delta \equiv r^2 - 2Mr + a^2, \qquad \Sigma \equiv r^2 + a^2cos^2\theta. \quad (2.12)$$

In the above expression, M is BH mass and a depicts the rotational feature of BH. Also, analogous with the Schwarzschild metric, the Kerr metric is stationary, axisymmetric and asymptotically flat. We can find two singularities in the Kerr metric: $\Sigma = 0$, which is a curvature singularity and $\Delta = 0$, which is the coordinate singularity and removable. Notice that in the Schwarzschild limit $a = 0$, the Kerr singularities approach the singularities of the Schwarzschild metric (2.10). By the coordinate singularity $\Delta = 0$, we can find that a Kerr BH has two horizons

$$r_+ \equiv M + \sqrt{M^2 - a^2}, \qquad r_- \equiv M - \sqrt{M^2 - a^2}, \quad (2.13)$$

where r_+ and r_- are the outer and inner horizons, respectively. These horizons separate a Kerr BH in three different regions. The region with $r > r_+$, which is included by timelike hypersurfaces wherein the metric becomes flat in the limit of far distances. The region with $r_- < r < r_+$ which contains the spacelike hypersurfaces in which the objects falling inside of outside region can only continue until reaching to the inner horizon. The region with $r < r_-$ which includes the timelike hypersurfaces and also the ring singularity. Notice that the Schwarzschild and Kerr BHs can be generalized to include non-zero electromagnetic charges, non-zero angular momentum and non-zero cosmological constant [37, 38, 39, 40, 41].

2.5 The Standard Model of Cosmology

In this section, we describe the dynamics of an expanding universe based on GR principles and also we investigate the satiation of the cosmos in the presence of different components of matter.

2.5.1 Dynamical Universe

In 1922, Alexander Friedmann first presented a dynamical solution of the field equations (2.7) by using the FLRW metric and the equation of perfect fluid [42]

$$T_{\mu\nu} = \rho u_\mu u_\nu + \frac{p}{a^2} g_{\mu\nu}. \tag{2.14}$$

In the above expression, p and ρ are the pressure and energy density of the perfect fluid, respectively and the indexes μ and ν take the values from 0 to 3 so that zero is the time coordinate and other three values are depended to the space coordinates. Also, u^μ is the four-velocity of a comoving observer for whom space is homogeneous and isotropic. Due to the conservation law of energy-momentum tensor $\nabla^\nu T_{\mu\nu} = 0$, the time component of the energy-momentum tensor can be found as

$$\dot{\rho} + 3H(\rho + p) = 0. \tag{2.15}$$

By using the FRLW metric and the equation of perfect fluid for the field equations (2.7), the dynamical relations of an expanding universe take the following form

$$H^2 \equiv (\frac{\dot{a}}{a})^2 = \frac{\kappa^2}{3}\rho + \frac{\Lambda}{3} - \frac{\mathcal{K}}{a^2}, \tag{2.16}$$

$$\frac{\ddot{a}}{a} = -\frac{\kappa^2}{6}(\rho + 3p) + \frac{\Lambda}{3}. \tag{2.17}$$

The first relation is the Friedmann equation driven from the time component of the field equation [42]. The second is the Raychaudhuri or acceleration equation driven from space part ij of the field equation [43]. In the Friedmann equation, $H \equiv (\frac{\dot{a}}{a})$ is the Hubble parameter and reveals the changes in scale factor in terms of the pressure and energy density of the perfect fluid. Also, $\mathcal{K}$ is spatial curvature constant (observations show $\mathcal{K} = 0$ for the present universe) and Λ is the cosmological constant. From the acceleration equation, one can find the necessary condition to explain inflation and dark energy as the accelerating phase of the universe in early and late times by $\rho + 3p < 0$ when $\Lambda = 0$.
In order to present an exhaustive study of the dynamical universe, it is worth introducing some useful formulas. Let's begin with equation of state $w = \frac{p}{\rho}$ as a dimensionless parameter including $w = 0$ for dust, $w = \frac{1}{3}$ for radiation, $w = -1$ for the cosmological constant and $w = -\frac{1}{3}$ for spatial curvature. By using the equation of state for the Eq. (2.15), we obtain

$$\rho(a) = \rho_0 a^{-3(1+w)} \tag{2.18}$$

assuming we have normalized $a(t_0) = 1$. This relation informs us how the energy density changes in terms of scale factor for different components of the universe. Concerning the above expression for a flat universe ($\mathcal{K} = 0$), the Friedmann equation can be rewritten as

$$a(t) = (\frac{t}{t_0})^{\frac{2}{3(1+w)}} \tag{2.19}$$

where $a_0 = 1$ has used as proper normalization. The above equation expresses the behavior of the scale factor for different components of the universe. Also, we obtain the age of the universe t_0 as

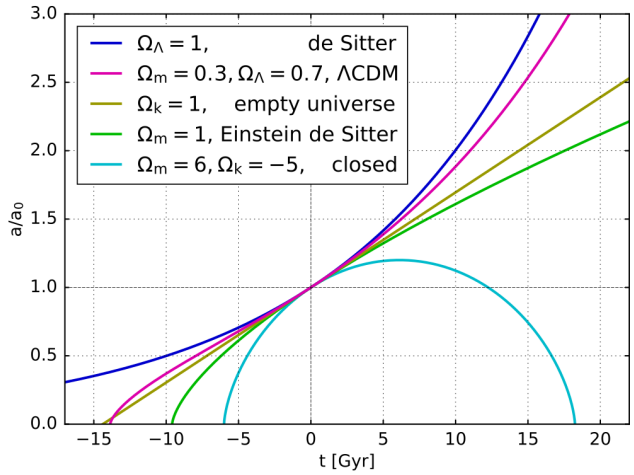

FIGURE 2.5: The rate of expansion of the universe is shown for different single and mixed component universes. The blue line (de Sitter universe) refers to the universe filled only by the cosmological constant and the rate of expansion is exponential. The pink line depicts the present universe occupied by the cosmological constant and cold dark matter. One can find the rate of expansion has decreased rather than the de Sitter universe because of the role of dark matter. The yellow line shows a linear expansion for the Milne universe with the only curvature. The line of Einstein-de Sitter implies the expansion of the universe filled only with matter. The green semicircular presents the closed universe when it is a mixture of matter and curvature.

$$t_0 = \frac{1}{1+w}\left(\frac{4}{3\kappa^2\rho_0}\right)^{\frac{1}{2}} \tag{2.20}$$

and the Hubble constant is expressed by the relation

$$H_0 \equiv \left(\frac{\dot{a}}{a}\right)_{t=t_0} = \frac{2}{3(1+w)}t_0^{-1}. \tag{2.21}$$

We note that the Hubble time $t_H \equiv H_0^{-1}$ can be linked to the age of the universe by

$$t_H = \frac{3(1+w)}{2}t_0. \tag{2.22}$$

Another important cosmological parameter is particle horizon that implies the maximum distance from which light from particles could have traveled to the observer in the age of the universe. In a universe described by the FLRW metric, the current horizon distance is

$$d_{hor}(t_0) = \int_0^{t_0} \frac{dt}{a(t)} \tag{2.23}$$

and for a spatially flat universe, it yields

$$d_{hor}(t_0) = t_0\frac{3(1+w)}{1+3w} = \frac{2}{H_0(1+3w)}. \tag{2.24}$$

By setting the equation of state w of the matter filling the cosmos, we can specify the above dynamical relations for every epoch of the thermal universe.

2.5.2 Single Component Universe

In reality, our universe is a mixture of different components with different values of the equation of state w. However, based on the thermal history of the universe, the role of one component was dominated in every epoch of the universe. Hence, studying the dynamical universe with a single component helps us to have a better insight into the universe.

2.5.2.1 Curvature

As the simplest case, we assume that there is no type of matter (radiation, dust, cosmological constant) and we deal with curvature only. The Friedmann equation for this type of universe, which is known to the *Milne universe*, takes the following form [44]

$$\dot{a}^2 = -\mathcal{K}. \tag{2.25}$$

The above expression for positive curvature $\mathcal{K} = +1$ is an unacceptable solution since it leads to an imaginary value of $\dot{a}$. For flat curvature $\mathcal{K} = 0$, we approach an empty, static and spatially flat universe that recalls us to the Minkowski universe. In other words, in the case of $\mathcal{K} = 0$, all relations of GR are reduced to SR. A negatively curved ($\mathcal{K} = -1$) empty universe is expanding with

$$a_c(t) = \frac{t}{t_0}, \tag{2.26}$$

which is in agreement with Newtonian physics. If there is no gravitational force in the universe, the relative velocity of two points is constant and the scale factor grows linearly with time. Also, the age of this universe is equal to the Hubble time $t_0 = H_0^{-1}$.

2.5.2.2 Radiation

According to the thermal history, the universe was dominated by radiation in very early time through strong interactions of photons with the nuclei of light elements and electrons. For an universe dominated by radiation, the age of the universe is $t_0 = \frac{1}{2H_0}$ and the horizon distance is $d_{hor}(t_0) = 2t_0 = \frac{1}{H_0}$. Also, the energy density changes with the scale factor as $\rho = \rho_0 a^{-4}$ and the rate of expansion of the universe is $a_r(t) = (\frac{t}{t_0})^{\frac{1}{2}}$.

2.5.2.3 Matter

After ending the radiation dominated period, our universe followed by the matter dominated era as the longest stage of the universe and filled with either baryonic and non-baryonic. In such a case, we concentrate on the universe filled with a non-relativistic matter or dust with $w = 0$ which is called *Einstein-de Sitter universe* [45]. The age of such universe $t_0 = \frac{2}{3H_0}$ and the horizon distance is $d_{hor}(t_0) = 3t_0 = \frac{2}{H_0}$. Also, the variation of energy density with the scale factor is $\rho = \rho_0 a^{-3}$ and the universe is expanding as $a_m(t) = (\frac{t}{t_0})^{\frac{2}{3}}$.

2.5.2.4 Cosmological Constant

For the sake of completeness, we consider the *de Sitter universe* referring a universe filled with cosmological constant $w = -1$ [8]. For the age of the universe, we can rewrite the Friedmann equation as

$$\dot{a}^2 = \frac{\kappa^2}{3}\rho_\Lambda a^2, \tag{2.27}$$

which for $w = -1$, we obtain

$$a_\Lambda(t) = e^{H_0(t-t_0)}, \tag{2.28}$$

where $H_0 = (\frac{\kappa^2\rho_\Lambda}{3})^{\frac{1}{2}}$. We note that Figure 2.5 shows the rate of expansion for the mentioned single component universes.

2.5.3 Present Universe

In the previous section, we examined the situation of the universe filled with a single type of component. However, a real universe has formed from different ingredients with different contributions throughout the history of the universe. Now, it is worth studying the constitutive elements of the present universe at the age of of13.7 Gyr. Given high accuracy observations, most of the present universe has been contained by dark energy and dark matter (around %95) and the remained portion (around %5) refers to the ordinary matter as a combination of light elements, stars, neutrinos, and heavy elements (see Figure 2.6) [46]. Let us explain the components, separately.

2.5.3.1 Dark Energy

Dark Energy (DE) is the late time accelerating phase of the universe that two groups of researchers, separately discovered it in 1998 through careful study of supernovae type Ia [47, 48]. What the researchers found was that the Ia supernovae in distant galaxies were fainter than expected from Hubble's law, given the measured redshifts of their host galaxies. The nature of DE is one of the most significant puzzles of modern cosmology. A matter candidate of DE is the cosmological constant representing a constant energy density filling space homogeneously. Quantum mechanics proposes that the source of this vacuum energy might be tiny elementary particles that flicker in and out of existence everywhere throughout the universe. Various attempts have carried out to calculate how big the effects of this vacuum energy should be, but so far these attempts had been unsuccessful. In fact, the order of magnitude of theoretical estimates of the vacuum energy based on the quantum mechanics of matter and the value required to account for the acceleration of the expansion of the universe differ by an incredible factor of at least 10^{120} [49]. Another suggested strategy to illuminate the DE problem is established on modified theories of gravity [50, 51, 52]. Some people believe that one can approach the acceleration phase by assuming some geometrical modifications in the heart of the Einstein gravity instead of adding the cosmological constant to the content of the universe. There are a wide range of modified gravity models among the cosmological literature such as $f(R)$ gravity which considers a general function of Ricci scalar R instead of R expressed in the action of GR [53, 54] or Braneworld gravity in which gravity is an interaction in higher dimensions [55]. Regarding the observations, DE contains around %70 of the present universe [46].

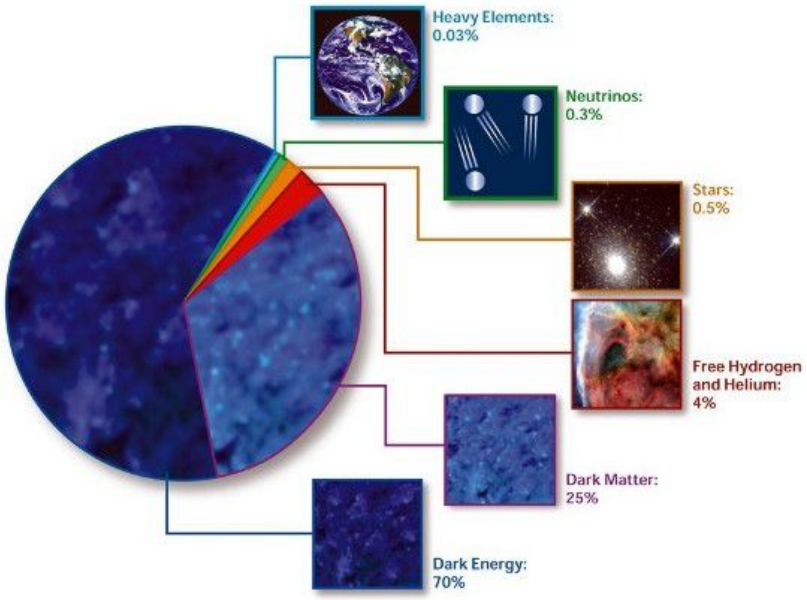

FIGURE 2.6: The current content of the universe is formed from Dark Energy, Dark Matter and ordinary matter, including light elements, stars, neutrinos, and heavy elements.

2.5.3.2 Dark Matter

After DE, Dark Matter (DM) forms the majority portion of the universe (around %25) [46]. DM is a mass that does not emit or absorb or reflect electromagnetic radiation and only can be detected through its gravitational effects. The main observational evidence of DM is detecting the emitted X-rays or gamma rays radiation from the gas filling the space between galaxies in the clusters [56]. The nature of DM is unknown for scientists, but there are some candidates to explain what is DM?. The stellar remnants such as white dwarfs, neutron stars and massive black holes are addressed as DM. Moreover, a brown dwarf can be a suitable candidate for DM since it is too low in mass in order to occur nuclear fusion in their cores. The most important candidate is Weakly Interacting Massive Particles (WIMPs) which are theoretically proposed in some extensions of the standard model of particle physics [57]. WIMPs are massive particles that interact like neutrinos only through weak nuclear and gravitational forces. The main problem of WIMPs is that they have not been detected yet.

2.5.3.3 Light Elements

As a consequence of the Big Bang nucleosynthesis period, the universe is full of light elements such as Hydrogen and Helium. In fact, they are the main source of nuclear fusion in the core of stars. Moreover, they exist in the space intergalactic and usually emit in the range of X-ray or infrared. They form the most measurable mass of the universe (around %4) [46].

2.5.3.4 Stars

Star is a huge ball of gas (Hydrogen and Helium) held together by gravity. The central core of a star is extremely hot and produces energy by the nuclear fusion process. Some of the released energy is spent to makes the star glow and part is for

the temperature of the star surface. Stars form around %0.5 of the content of the universe [46].

2.5.3.5 Neutrinos

The neutrinos accumulate around %0.3 of the present universe [46]. These particles are usually released during the nuclear fusion process in stars and because of low mass, interact weakly with other particles through gravity and weak nuclear forces [58]. Also, cosmic neutrino background comes from the decoupling of the neutrinos from hadrons, when the universe had been cold sufficiently [59].

2.5.3.6 Heavy Elements

The least portion of the universe is formed by heavy elements around %0.03 [46]. As we know, the energy of stars comes from the combining of light elements into heavier elements in a nuclear fusion process. It is generally believed that most of the elements in the universe heavier than helium are created, or synthesized, in stars when lighter nuclei fuse to make heavier nuclei. The process is called stellar nucleosynthesis. It requires a high-speed collision, which can only be achieved at a very high temperature. The minimum temperature required for the fusion of hydrogen is 5 million degrees. Elements with more protons in their nuclei require still higher temperatures. Most of the heavy elements, from oxygen up through iron, are thought to be produced in stars that contain at least ten times as much matter as our Sun. After the hydrogen in the core of a star is exhausted, the star can burn helium to form progressively heavier elements, carbon and oxygen and so on until iron and nickel are formed. Up to this point, the process releases energy. The formation of elements heavier than iron and nickel requires the input of energy. During the explosive nucleosynthesis process, supernova explosions result when the cores of massive stars have exhausted their fuel supplies and burned everything into iron and nickel. The nuclei with mass heavier than nickel are thought to be formed during these explosions [60].
Now that we know all elements of the universe, it is worth to apply the Friedmann equation for the present universe. From the general form of the Friedmann equation, we have

$$H(t)^2 = \frac{\kappa^2}{3}\rho(t) - \frac{\mathcal{K}}{a(t)^2}, \tag{2.29}$$

where $\rho(t)$ is the energy density contributed by all components of the universe, including the cosmological constant. Let us introduce the density parameter Ω as

$$\Omega \equiv \frac{\rho}{\rho_{critical}}, \tag{2.30}$$

where $\rho_{critical} \equiv \frac{3H(t)^2}{\kappa^2}$ is the energy density of a spatially flat universe. By using the Eqs. (2.29) and (2.30) at present time, one can find

$$\mathcal{K} = H_0^2(\Omega_0 - 1). \tag{2.31}$$

Now we can rewrite the Eq. (2.29) as

$$H(t)^2 = \frac{\kappa^2}{3}\rho(t) - \frac{H_0^2}{a(t)^2}(\Omega_0 - 1). \tag{2.32}$$

Dividing by H_0^2, this becomes

$$\frac{H(t)^2}{H_0^2} = \frac{\rho(t)}{\rho_{critical,0}} + \frac{1-\Omega_0}{a(t)^2}. \tag{2.33}$$

In the previous sections, we found the energy density of radiation as $\rho_r = \rho_{r,0}/a^{-4}$, matter as $\rho_m = \rho_{m,0}/a^{-3}$ and cosmological as $\rho_\Lambda = \rho_{\Lambda,0}$=*constant* based on current evidence. Eventually, the Friedmann equation (2.33) takes the following form

$$\frac{H(t)^2}{H_0^2} = \frac{\Omega_{r,0}}{a^4} + \frac{\Omega_{m,0}}{a^3} + \Omega_{\Lambda,0} + \frac{1-\Omega_0}{a^2}, \tag{2.34}$$

where $\Omega_{r,0} = \rho_{r,0}/\rho_{critical,0}$, $\Omega_{m,0} = \rho_{m,0}/\rho_{critical,0}$, $\Omega_{\Lambda,0} = \rho_{\Lambda,0}/\rho_{critical,0}$ and $\Omega_0 = \Omega_{r,0} + \Omega_{m,0} + \Omega_{\Lambda,0}$.

2.6 Thermal History of the Universe

Since the Big Bang, the universe has passed through different epochs. Due to the extreme conditions and the violence of its very early stages, it arguably saw more activity and change during the first second than in all the billions of years since.

2.6.1 Age of the Universe

Before starting to survey the thermal history of the universe from the Big Bang to the present time, that would be nice to describe how scientists estimated the age of the universe. Let's begin with an approximative approach. We know that the Hubble parameter reveals the rate of universe expansion and its associated time, which is called the Hubble time, can be a good approximation of the age of the universe. The Hubble constant in the present time is $H_0 = 70$ kms^{-1}Mpc^{-1}, then the Hubble time t_H is around 14 Gyr. This is the simplest estimation and there is uncertainty in obtaining the value of the Hubble constant. On the other hand, the high accuracy observations accomplished for the oldest objects in the universe show that the age of the cosmos is between 10-13 Gyr, roughly. This observational fact tells us that we should be suspicious about the time determined by the Hubble parameter. Now, we attempt to understand the age of the universe theoretically. Since the longest period of the universe was dominated by matter, we start with a universe filled by matter. Then, the rate of expansion in this universe is $a(t) = (\frac{t}{t_0})^{\frac{2}{3}}$ and from the Eq. (2.22), the age is linked to the Hubble time as $t_0 = \frac{2}{3}H_0^{-1} = 9.3$ Gyr. The obtained result is not delicious to us compared with the observational evidence. The key to solving the problem is referred to Λ as the cosmological constant since we are trying to estimate the age of the present universe. Hence, we must add the role of DE to our calculations.
By assuming a spatially flat universe in the presence of Λ, we can access the age of the universe around 13.7 Gyr which has good agreement with observations of the oldest stars in the universe [46].

2.6.2 Universe Stages

Let's review what has happened since the Big Bang to now (see Figure 2.7):

• $\mathbf{t < 10^{-43}}s, \mathbf{T > 10^{32}}K$. Immediately after Big Bang, the universe followed by the Planck era. During this too short period, the temperature, pressure, and energy were

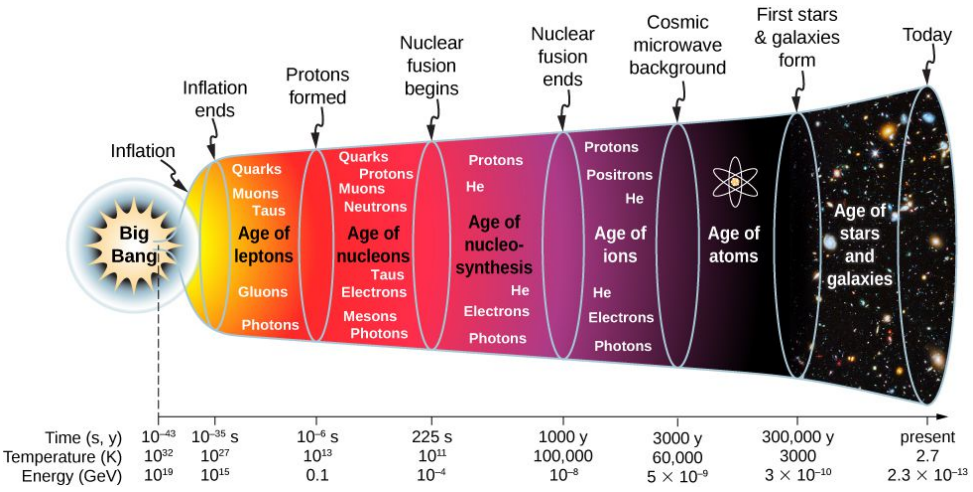

FIGURE 2.7: The thermal history of the universe is classified into four main epochs in terms of time, temperature and energy (e.g. Planck era, radiation dominated, matter-dominated and DE dominated).

extremely high. Also, the unification or Theory of Everything (TOE) between four fundamental forces of nature was valid through the critical condition in this epoch. Moreover, the GR is unable to explain gravity dominated in this period and we require to build a gravitational theory in the context of quantum mechanics. Such a theory is known as Quantum Gravity which is unknown for us yet.

• $\mathbf{t < 10^{-36}}s, \mathbf{T > 10^{29}}K$. As a result of universe expansion, the temperature dropped and the universe became a bit cold. Therefore, the required conditions of unification were not valid and the gravity force took part from the other three forces through breaking symmetries. This era is called the Grand Unification Theory (GUT) era.

• $\mathbf{t < 10^{-32}}s, \mathbf{T = 10^{28} \sim 10^{22}}K$. Through more expansion, the universe became colder and the nuclear force took part from two remained forces. Inflaton as scalar field driving Inflation, created by the breaking symmetries, happened in this period. According to cosmic inflation, the universe experienced a very huge and short expansion by a factor of the order of 10^{26}. As a consequence of cosmic inflation, the temperature of the universe declined sharply from about 10^{27} down to 10^{22} kelvins. By decaying inflaton at the end of the inflation or reheating process, the universe started to expand normally.

• $\mathbf{t = 10^{-12} \sim 10^{-6}}s, \mathbf{T > 10^{12}}K$. In $10^{-12}s$ after Big Bang, the third breaking symmetries occurred through taking part electromagnetic and weak nuclear forces [61, 62, 63, 64, 65, 66, 67]. In this period, the temperature of the universe was high and free quarks couldn't form the neutrons and protons. However, the universe was filled by quark-gluon plasma through the reheating of cosmic inflation.

• $\mathbf{t = 10^{-6} \sim 1}s, \mathbf{T > 10^{10}}K$. Because of expansion and then dropping the temperature, free quarks could form the neutrons and protons [68, 69, 70, 71, 72, 73].

• $\mathbf{t = 1}s, \mathbf{T = 10^{10}}K$. In one second after starting the universe, background neutrinos released or decoupled from the baryonic matter. In other words, the matter became transparent for Cosmic Neutrino Background (CNB) analogous to the much later cosmic microwave background released during recombination, around 380,000

years after the Big Bang. Since neutrinos interact weakly with matter, they can travel freely to reach to us.

• $\mathbf{t = 1 \sim 10}s, \mathbf{T = 10^{10} \sim 10^{9}}K$. The majority of hadrons and anti-hadrons annihilate each other at the end of the hadron epoch and left leptons (such as the electron, muons and certain neutrinos) and anti-leptons. The lepton epoch follows a similar path to the earlier hadron epoch. Initially, leptons and anti-leptons are produced in pairs. About 10 seconds after the Big Bang, the temperature of the universe falls to the point at which new lepton/anti-lepton pairs are no longer created and most remaining leptons and anti-leptons quickly annihilate each other, giving rise to pairs of high energy photons.

• $\mathbf{t = 10 \sim 10^{3}}s, \mathbf{T = 10^{9} \sim 10^{7}}K$. The Big Bang Nucleosynthesis (BBN) as one of the most significant stages of the universe that occurred during this period [74, 75, 76, 77]. By dropping the temperature and pressure, protons and neutrons started to combine and formed the nuclei of light elements such as Hydrogen and Helium through the nuclear fusion process. The abundance of light elements in the present universe is referred to as such this era.

• $\mathbf{t = 10 \sim 380}kyr, \mathbf{T = 10^{9} \sim 4000}K$. The Radiation dominated era happened in this period. The universe was full of electrons, nuclei, and high energy photons. The electrons were not able to join to the nuclei to form atoms since the high energy photons interacted hardly with the matter.

• $\mathbf{t = 380}kyr, \mathbf{T = 4000}K$. In 380,000 years after Big Bang, the universe became enough cold and then the energy of photons decreased dramatically. Electrons could combine with nuclei and first atoms formed in the universe. Also, the cosmic microwave background photons decoupled from the matter at the last scattering surface and the matter became transparent for photons [78].

• $\mathbf{t = 380}kyr \sim \mathbf{150}Myr, \mathbf{T = 4000 \sim 60}K$. The period after the formation of the first atoms and before the first stars is sometimes referred to as the Dark Age. Although photons exist (the cosmic background photons released during decoupling and photons occasionally released by neutral hydrogen atoms, known as the 21 cm spin line of neutral hydrogen), the universe at this time is literally dark, with no star or galaxy. The activity in the universe has declined dramatically, with very low energy levels and very large time scales and the universe is dominated by mysterious DM.

• $\mathbf{t = 250}Myr \sim \mathbf{1 - 10}Gyr, \mathbf{T = 60}K$. The first quasars form from gravitational collapse, and the intense radiation emitted by them, reionizes the surrounding universe. This is the second of two major phase changes of hydrogen gas that happened in the universe (the first was at the Recombination period). Hence, most of the universe goes from being neutral back to being composed of ionized plasma [79, 80, 81].

• $\mathbf{t = 300 - 400}Myr \sim \mathbf{10}Gyr, \mathbf{T = 60 \sim 19}K$. Gravity reinforces slight disorders in the density of the primordial gas and they become more and denser so that the universe continues to expand rapidly. These small, dense clouds of cosmic gas start to collapse under their gravity and become hot enough to nuclear fusion reactions between hydrogen atoms in order to create the first stars. The first stars or metal-free stars are short-lived supermassive stars (hundred times the mass of the Sun).

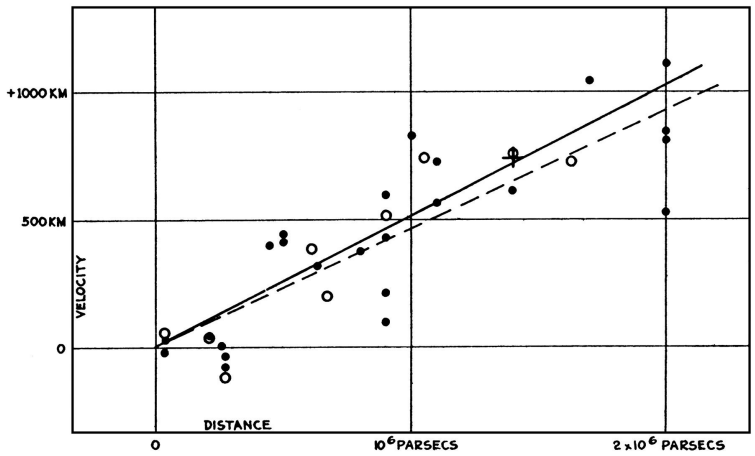

FIGURE 2.8: Edwin Hubble's original diagram in which the vertical and horizontal axes refer to the velocity and distance of galaxies from the observer.

Eventually, through stellar and explosive nucleosynthesis, stars begin to form the material from previous rounds of star-making. Larger stars burn out quickly and explode in massive supernova events, their ashes going to form subsequent generations of stars. Large volumes of matter collapse to form galaxies and gravitational attraction pulls galaxies towards each other to form clusters and superclusters.

• $\mathbf{t = 8.5}Gyr \sim \mathbf{13.7}Gyr, \mathbf{T = 19} \sim \mathbf{2.7}K$. The farthest observable photons are the cosmic background photons. The expansion of the universe and the recycling of star materials into new stars are becoming prevalent. Furthermore, matter density declines relative to DE density, and expansion of the universe begins to accelerate [47, 48].

2.7 Hot Big Bang Theory

The standard model of cosmology has been established on the Hot Big Bang (HBB) theory which states the universe began to expand by a huge explosion when the temperature and energy were extremely high at the early time. Although the Big Bang theory is the most convenient picture in cosmology to start the universe, it has to be in good agreement with observations. Hence, it is worth to survey the strengths and weaknesses of the HBB theory.

2.7.1 Proofs of HBB Theory

First, let us explain some observations that verify the Big Bang theory.

2.7.1.1 An Expanding Universe

Our knowledge from a sky object comes from analyzing the electromagnetic radiation of that object. In fact, the wavelengths of emitted radiation contain various information about the source. Let's begin with redshift as an essential observational parameter

$$z \equiv \frac{\lambda_{ob} - \lambda_{em}}{\lambda_{em}}, \tag{2.35}$$

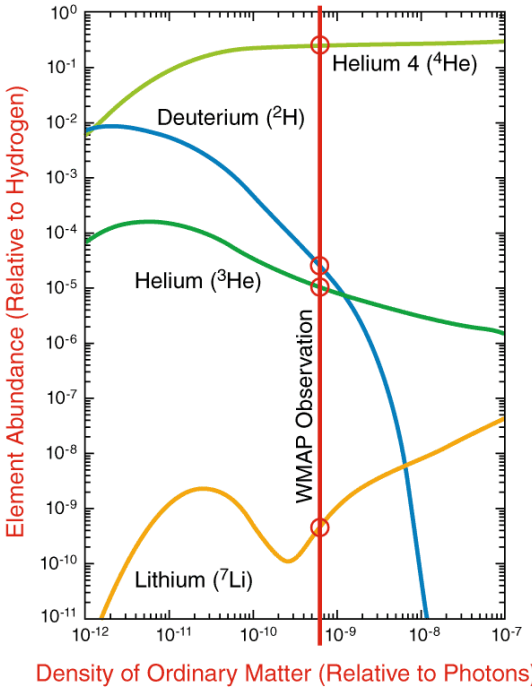

FIGURE 2.9: The predicted abundance of the BBN from light elements when the energy density of the ordinary matter varies. One can understand that the abundance of Helium is relatively insensitive to the abundance of ordinary matter, above a certain threshold.

where λ_{em} is a particular absorption line measured in the lab and λ_{ob} is the measured wavelength of the same absorption line from a sky object. If $z < 0$, the object is closing to us as an observer and it means there is a blueshift instead of redshift and for positive values $z > 0$, the object is faring away from us through a redshift tilt. The mentioned analysis can be understood in the light of the Doppler effect in which there is an increase in frequency for observers towards whom the source is approaching and a decrease in frequency for observers from whom the source is receding.
In 1929, Edwin Hubble measured the redshift of some galaxies and then estimated their distances from us. Then, by plotting the redshift versus distance as presented in Figure 2.8, he found a linear connection between two parameters as [82]

$$z = \frac{H_0}{c} r, \tag{2.36}$$

where H_0 is Hubble constant. Also, by using the non-relativistic relation of Doppler effect $z = \frac{v}{c}$, the above relation takes the following form

$$v = H_0 r, \tag{2.37}$$

where v is the velocity of the galaxy and r is the distance to us as an observer. From the previous section, the value of Hubble constant depends on the age and the matter filling the universe. For the present mixture of matter and at time 13.7 Gyr, the Hubble constant is $H_0 = 70\ \mathrm{kms}^{-1}\mathrm{Mpc}^{-1}$ [46]. When Hubble measured the redshift of galaxies, he found that the majority of them show a redshift rather than blueshift. Thanks to the Doppler effect, they are receding us and this is meaningful only in an expanding universe not static case. The Hubble expansion can be identified as

observational evidence of HBB theory which believes the universe began to grow from a highly dense and pressure state.

2.7.1.2 Abundance of Light Elements

As we know, the ordinary matter makes around %5 content of the universe in which light elements with %4 has the most significant role at present. The light elements are known as the main fuel in the core of stars in order to occur the nuclear fusion. Also, they are in stellar and galactic spaces and usually emit in the range of X-rays or gamma rays through the gravitational effects of DM. The abundance of the light elements e.g. Helium, Deuterium, and Lithium comes back to the BBN era in which protons and neutrons combined and released energy by nuclear fusion activities. The Big Bang theory predicts that the mass of the universe has been formed by around %75 Hydrogen, %25 Helium, %0.01 deuterium and smaller quantities of lithium. The predicted abundance of light elements depends on the density of ordinary matter in the early universe and also the combination of elements might be changed during the evaluation of the matter. Since Helium neither decays nor combines effortlessly to form more massive nuclei, it is relatively insensitive to the abundance of ordinary matter as presented in Figure 2.9. Hence, we expect that the measured plenty of Helium at present be the same with theoretical predictions carried out by HBB theory. Recent observations show that the abundance of Helium in the universe has a good agreement with the HBB prediction [2]. This reality is recognized as one of the most important observational probes of the HBB theory.

2.7.1.3 Cosmic Microwave Background

The most important evidence of Big Bang theory is detecting cosmic microwave background as the relic photons of the Big Bang explosion when the universe was critical in temperature and pressure [78]. According to the history of the universe, in radiation dominated era, photons were highly energetic and interacted dramatically with matter so that electrons could not join to nuclei to form atoms. After a while, because of more expansion, the universe became colder and photons were not able to interact with the matter. As a result of this, the cosmic background photons released at the last scattering surface and the first atoms formed through combining the electrons with nuclei. Now, in 13.7 Gyr after Big Bang, the background photons are in the range of microwave and low temperature roughly 2.72 Kelvin degrees. Let us explain the history of cosmic microwave background discovery briefly. Cosmologist George Gamow and his collaborators (Ralph Alpher and Robert Herman) first predicted the cosmic background photons in 1948 [83, 84, 85, 86]. They were doing research related to Big Bang nucleosynthesis, or the production of elements in the universe besides the lightest isotope of hydrogen. But the cosmic background photons first found by accident. In 1965, two researchers with Bell Telephone Laboratories (Arno Penzias and Robert Wilson) were creating a radio receiver and were confused by the noise it was picking up, so that came uniformly from all directions of the sky. The unknown noise was cosmic background photons and Penzias and Wilson received the Noble prize in 1978 because of their discovery [78]. In order to present more precise analysis, the COBE satellite engaged in detecting the cosmic background photons in 1990 [87, 88]. COBE measured the temperature of background photons around 2.72 Kelvin degree and showed the received spectrum of the cosmic microwave background is similar to black body radiation. Additionally, it detected the first acoustic peak, acoustical oscillations in the plasma which corresponds to large-scale density variations in the early universe created by gravitational

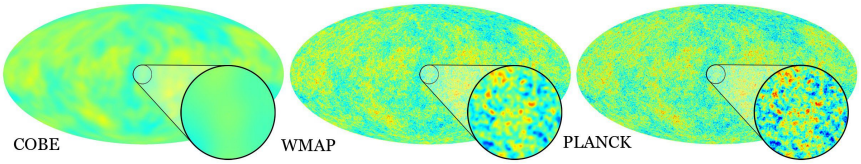

FIGURE 2.10: Comparison of the obtained results from COBE , WMAP and Planck.

instabilities. The second acoustic peak and even the third were detected by WMAP deployed in 2001 [89]. After the retirement of WMAP in 2010, the third main mission carried out by PLANCK satellite in 2009 through precise measurements at the small angular scales up to now (see Figure 2.10). Also, multiple missions have been monitoring the cosmic microwave background to provide improved measurements of the polarization of cosmic background photons by BICEP2 mission [90]. Detailed information about CMB and its experiments related to inflation will be presented in chapter 4.

2.7.2 Shortcomings of HBB Theory

Now that we know the strength of HBB theory, it is time to review the defects of the theory e.g. Flatness, horizon and monopole problems.

2.7.2.1 Flatness Problem

As we expressed in the previous sections, the spatial curvature of the universe can take three different forms in which $\mathcal{K} = -1$ for an open universe, $\mathcal{K} = +1$ for a closed universe and $\mathcal{K} = 0$ for a flat universe. The very precise observations reveal that the present universe is so flat ($\Omega \simeq 1$) and the present energy density is almost equal to its critical value. Since the total density departs rapidly from the critical value over cosmic time, the early universe must have had a density even closer to the critical density. The flatness problem says that the HBB theory can not present a clear explanation for this amount of flatness. We can also state the flatness problem by asking the question that How the universe fines tune the energy density of the universe to be flat during all time?
Now, let us express the flatness problem by appropriated relations. By using the definition of the density parameter Eq. (2.30), the Friedmann equation can be rewritten as

$$1 - \Omega(t) = -\frac{\mathcal{K}}{a(t)^2 H(t)^2}. \tag{2.38}$$

The above relation at the present time takes the following form

$$1 - \Omega_0 = -\frac{\mathcal{K}}{H_0^2}, \tag{2.39}$$

where used the proper normalization $a(t_0) = 1$. The observations of Ia supernova and cosmic background anisotropy disclose $|1 - \Omega_0| \leq 0.2$. This means that the present universe is so flat and the energy density is almost equal to the critical value. Let's see what happened at an earlier time. By combining the Eqs. (2.38) and (2.39), we find the following equation

$$1 - \Omega(t) = \frac{H_0^2(1-\Omega_0)}{a(t)^2 H(t)^2}. \tag{2.40}$$

When the universe is dominated by radiation and matter, the Eq. (2.34) can be given as

$$\frac{H^2(t)}{H_0^2} = \frac{\Omega_{r,0}}{a^4} + \frac{\Omega_{m,0}}{a^3}. \tag{2.41}$$

By using the above relation and the Eq. (2.40), we have

$$1 - \Omega(t) = \frac{(1-\Omega_0)a^2}{\Omega_{r,0} + a\Omega_{m,0}}. \tag{2.42}$$

Now, it is worth to investigate the above expression for different eras of the universe. During matter dominated era $|1-\Omega(t)|_m \propto t^{\frac{2}{3}}$, radiation dominated era $|1-\Omega(t)|_r \propto t$, at the time of radiation-matter equality $|1-\Omega(t)|_{rm} \leq 2 \times 10^{-4}$, big bang nucleosynthesis era $|1-\Omega(t)|_{BBN} \leq 3 \times 10^{-14}$ and Planck era $|1-\Omega(t)|_{pl} \leq 1 \times 10^{-60}$.
The above values in different epochs of the universe show that when we go backward in cosmic time, we access more flatness than the present time and this result is exactly what that we name flatness problem [91, 92].

2.7.2.2 Horizon Problem

Due to the thermal history of the universe, the cosmic background photons decoupled from the matter in 380,000 years after Big Bang at the last scattering surface and today we are receiving the photons in 2.72 Kelvin degree. Also, we know the cosmic photons are not completely isotropic since there is a temperature difference between some cosmic background photons. To explain the horizon problem, let's consider an observer on the earth who is receiving two isotropic cosmic background photons from the last scattering surface separated by 180° distance (see the left circle of Figure 2.11). Also, assume the distance of each photon is a little smaller than horizon distance (the most distance traveled by a photon in a proper cosmic time in which the causality principle be valid) related to the proper time. Two photons are isotropic and this means that they had the chance to exchange the information in order to be in a thermal balance. The horizon problem says that two photons can not be in thermal equilibrium. Because, if they want to meet each other to exchange their information, each of them must travel a distance around twice the horizon distance in the present proper time and it breaks the
causality principle. The horizon problem can be more interesting when we condemn ourselves to the proper time at the last scattering surface. At that time, the horizon distance take the following form

$$d_{hor}(t_{ls}) = \frac{2}{H(t_{ls})}. \tag{2.43}$$

Since the Hubble distance at last scattering surface was 0.2 Mpc, we have $d_{hor}(t_{ls}) \approx$ 0.4 Mpc. Hence, points more than 0.4 Mpc apart at the time of last scattering surface were not in causal connection. Also, we can express this result in terms of angular separation as

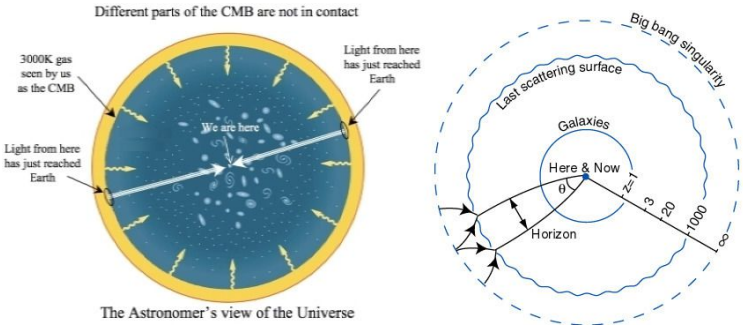

FIGURE 2.11: Two cosmic background photons separated by 180° which can not be causally connected (see the left circle). Two background photons separated by an angles small as were out of contact with each other at the last scattering surface (see the right circle).

$$\theta_{hor} = \frac{d_{hor}(t_{ls})}{d_A} \approx 0.03 rad \approx 2^\circ, \tag{2.44}$$

where used the angular diameter distance to the last scattering surface $d_A \approx 13$ Mpc. The above relation states that the points on the last scattering surface separated by an angles small as $\sim 2^\circ$ were out of contact with each other (see the right circle of Figure 2.11) [93, 94].

2.7.2.3 Monopole Problem

The monopole problem is known as a problem connecting cosmology and particle physics. In the very early universe, there was a unification between four fundamental forces e.g. gravity, electromagnetic, strong and weak nuclear through the crucial conditions of the universe. Since the universe started to expand and became colder, the forces took part in each other step by step. Gravity was the first force separated from the unification and the universe experienced the phase transition from TOE to the GUT. As a result of the phase transition, the symmetries broke and topological defects created in the universe. Monopoles are known as one of these defects created in the GUT era [95, 96]. The number density of magnetic monopoles, at the time of their creation, would be

$$n_M(t_{GUT}) \sim \frac{1}{(2ct_{GUT})^3} \sim 10^{82} m^{-3}. \tag{2.45}$$

The monopole problem says that although the produced monopoles in the GUT era had high number density, today no monopole has ever been observed [97, 98, 99, 100, 101].

Chapter 3

Cosmic Inflation

As we expressed in the previous chapter, the HBB theory suffers from some ambiguities including flatness, horizon and monopole problems. In fact, the standard cosmology can not present a clear explanation for the mentioned shortcomings. In 1981, A. H. Guth introduced the idea of cosmic inflation in order to remove the HBB problems in which the universe experienced a vast and rapid expansion at the early time [102]. Discovering inflation opened a new window in modern cosmology via its role in structure formation of the universe by scalar perturbations generated during the inflationary era. Also, the produced tensor perturbations are the main responsible for creating the primordial gravitational waves at the early time. Hence, the whole chapter is dedicated to investigating the standard modeling of inflation which is further discussed in a wide range of cosmological textbooks [5, 11, 103, 104, 105, 106, 107].

3.1 Solution of HBB Problems

For the first section of the present chapter, let's see how inflation can solve the problems of HBB theory.

3.1.1 Flatness Problem

Based on the flatness problem, the HBB theory can not explain the extreme flatness of the early universe. To describe the inflationary solution, consider an ant on the surface of a balloon. When the balloon is small, it would be obvious that the ant is standing on a two-dimensional curved surface. Now imagine the balloon is expanding sharply, the ant will see the surface is flat, even though it is actually curved if it could be seen from large enough distance. Now, if we extend this example to a small universe inflated by a significant amount, that part of the universe you can observe, appears to be nearly flat. Let us show the solution by appropriated relations. The equation

$$|1-\Omega(t)| = \frac{1}{a(t)^2 H(t)^2} \tag{3.1}$$

is the Friedmann equation rewritten by using the definition of density parameter $\Omega(t)$ (2.30) for any universe which is not perfectly flat (only the case of $\mathcal{K} = -1$). By using the Hubble parameter as $H \propto t^{-1}$ and the Eq. (2.19) which states the rate of expansion of the universe in the presence of different components of the universe when $w \neq 1$, the above equation takes the following form

$$|1-\Omega(t)| \propto t^{\frac{2(1+3w)}{3(1+w)}}. \tag{3.2}$$

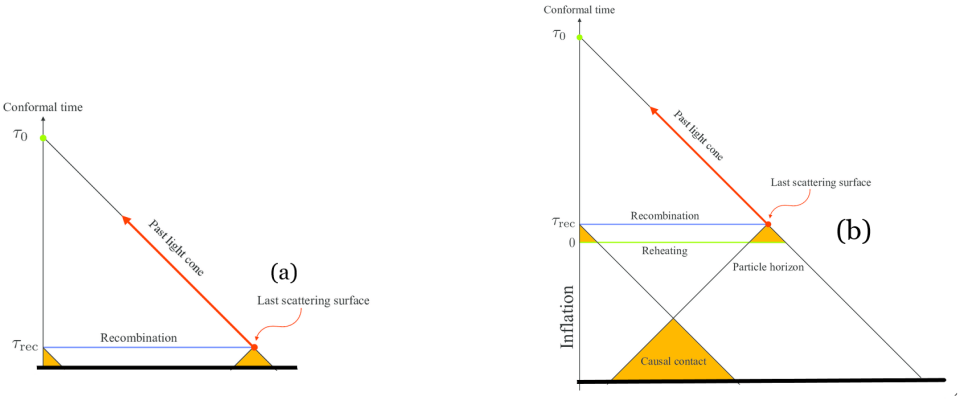

FIGURE 3.1: Without inflation, since the cosmic background photons were not connected causally, they could not be in the thermal equilibrium (the left picture). With inflation, the horizon distance increased sharply and the photons linked each other to form isotropic radiation (the right picture).

On the other hand, if we consider an exponential expansion for the inflationary era, for the start of inflation we have

$$|1 - \Omega(t)| \propto e^{-2H_{ini}t} \tag{3.3}$$

and for the end of inflation

$$|1 - \Omega(t_{end})| = e^{-2N}|1 - \Omega(t_{ini})|. \tag{3.4}$$

Notice that the above relation is obtained by using $t_{end} = t_i + \frac{N}{H_i}$ as a direct result of the definition of the number of e-folds by

$$e^N \equiv \frac{a(t_{end})}{a(t_{ini})}. \tag{3.5}$$

If we suppose that the universe was extremely curved before starting inflation $|1 - \Omega(t_{ini})| \sim 1$, the Eq. (3.4) can be found by

$$|1 - \Omega(t_{end})| \sim e^{-2N}. \tag{3.6}$$

Based on inflationary observations, if we consider very large e-folds around 70 for standard inflation, we have

$$|1 - \Omega(t_{end})| \sim e^{-140} \sim 10^{-60}. \tag{3.7}$$

This is the required amount of flatness for the early universe discussed in the previous chapter and means that cosmic inflation by an exponential expansion can describe the extreme flatness of the universe [102].

3.1.2 Horizon Problem

The horizon problem says that the CMB photons decoupled from the last scattering surface, could not be in thermal equilibrium because the horizon distance in the last scattering surface was so small and they were not connected causally (see picture (a) of Figure 3.1).

Thanks to the idea of inflation, the horizon distance in the last scattering surface increased significantly and almost whole CMB photons could exchange their thermal information (see picture (b) of Figure 3.1). Now, it is worth to show the result by the appropriate relations. Since before inflation, the universe was dominated by radiation, the horizon distance at the beginning of inflation is given by

$$d_{hor}(t_{ini}) = ca_{ini}\int_0^{t_{ini}} \frac{dt}{a_{ini}(\frac{t}{t_{ini}})^{\frac{1}{2}}} = 2ct_{ini} \tag{3.8}$$

and for the end of inflation

$$d_{hor}(t_{end}) = ca_{ini}e^N\left(\int_0^{t_{ini}} \frac{dt}{a_{ini}(\frac{t}{t_{ini}})^{\frac{1}{2}}} + \int_{t_{ini}}^{t_{end}} \frac{dt}{a_{ini}e^{H_{ini}(t-t_{ini})}}\right), \tag{3.9}$$

where used $e^N = \frac{a(t_{end})}{a(t_{ini})}$. For large values of number of e-folds, the above relation takes the following form

$$d_{hor}(t_{end}) = ce^N(2t_{ini} + H_{ini}^{-1}). \tag{3.10}$$

If we assume the inflation occurred around 10^{-36}s after Big Bang, the horizon distance at the start of inflation was $\approx 10^{-28}$m and for very large e-folds $N = 100$, the horizon distance at the end of inflation (3.9) was $\approx 10^{16}$m≈ 0.8 pc. By comparing the horizon distances at the start and end of inflation, one can understand that inflation boosted the horizon distance dramatically from small scales to very large scales and it could be stretched to the post-inflationary universe in particular at the time of last scattering [102, 108].

3.1.3 Monopole Problem

As we learned before, the standard model of cosmology can not answer why there is no monopole in the present universe despite its abundance in the early universe. The prescription of inflation to remove the monopole problem is that monopoles as a type of topological defects created at the time of GUT and then disappeared during the inflationary period through a large amount of expansion. In other words, if we determine the number density of monopoles at the time of GUT as $n(t_{GUT}) \approx 10^{82}\text{m}^{-3}$, then after around 100 e-folding of inflation, the number density of monopoles would be declined significantly as $n(t_{end}) = e^{-300}n(t_{GUT}) \approx 10^{-49}\text{m}^{-3}$. Because of this reason, the probability of finding monopoles is very low in the present universe.

3.2 Single Field Model

The most convenient model of cosmic inflation has been established on a single scalar field, which is called *inflaton* as the sole component of the universe during the inflationary era. In particle physics, a scalar field is an unavoidable part of spontaneous symmetry breaking whose value varies as a function of position and time. For example, inflaton created as a product of GUT symmetry breaking or Higgs boson created as a result of ElectroWeak (EW) symmetry breaking. To formulate cosmic inflation, let's begin with writing the form of the Lagrangian for a scalar field whose behaves similar to a classical particle by

$$\mathcal{L}_M = \frac{1}{2}g^{\mu\nu}\partial_\mu\varphi\partial_\nu\varphi - V(\varphi). \tag{3.11}$$

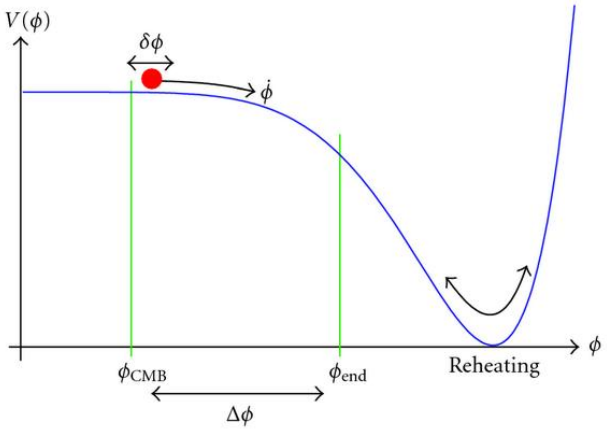

FIGURE 3.2: In the reheating process as the final step of inflation, inflaton rolls slowly down to the minimum point of potential and starts to oscillate around this point. Then, it decays to the standard particles.

By varying the above expression respect to the metric (2.8) and using the energy-momentum tensor of perfect fluid (2.14), one can find the energy density and pressure of inflaton by

$$\rho = \frac{1}{2}\dot{\varphi}^2 + V(\varphi), \qquad P = \frac{1}{2}\dot{\varphi}^2 - V(\varphi), \tag{3.12}$$

where the first term is the kinetic energy and $V(\varphi)$ is the energy potential that would be fixed by an inflationary model. The dynamical equations (2.16) and (2.17) are given by

$$H^2 = \frac{\kappa^2}{3}\left(\frac{1}{2}\dot{\varphi}^2 + V(\varphi)\right), \qquad \frac{\ddot{a}}{a} = -\frac{\kappa^2}{3}\left(\dot{\varphi}^2 - V(\varphi)\right) \tag{3.13}$$

and the Klein-Gordon equation can be driven by variation of the action (2.6) respect to the scalar field as

$$\ddot{\varphi} + 3H\dot{\varphi} = -\frac{dV(\varphi)}{d\varphi}. \tag{3.14}$$

Also, the necessary condition to occur cosmic inflation $\rho + 3p < 0$ can be rewritten as

$$\dot{\varphi}^2 < V(\varphi) \tag{3.15}$$

which means during inflation, the potential of the inflaton dominates its kinetic energy. Also, this shows that the inflationary potential must be sufficiently flat which is difficult to obtain in a realistic situation [109]. Let's take a look at the Klein-Gordon equation (3.14). It presents the equation of motion of a scalar field accelerated by a force proportional $-\frac{dV(\varphi)}{d\varphi}$ and prevented by a frictional force proportional $3H\dot{\varphi}$ through the expansion of the universe. By this simulation, inflaton rolls *slowly* down from the top of potential to the minimum point so that the acceleration condition (3.15) merges to

$$\dot{\varphi}^2 \ll V(\varphi). \tag{3.16}$$

Moreover, in order to have a specific amount of expansion during the inflationary epoch, we set

$$\ddot{\varphi} \ll 3H\dot{\varphi}. \tag{3.17}$$

The two above conditions are known as the conditions of the *slow-roll approximation* which let us construct analytical solutions, both for the background and the perturbations. The slow-roll approximation is usually described by the slow-roll parameters [110]

$$\epsilon_V \equiv \frac{1}{2\kappa^2}\left(\frac{V'(\varphi)}{V(\varphi)}\right)^2, \qquad \eta_V \equiv \frac{1}{\kappa^2}\left(\frac{V''(\varphi)}{V(\varphi)}\right), \qquad \zeta_V \equiv \frac{1}{\kappa^2}\left(\frac{V'(\varphi)V'''(\varphi)}{V^2(\varphi)}\right)^{1/2}, \tag{3.18}$$

where the prime denotes to derivation respect to the φ. The two quantities ϵ_V, η_V and ζ_V are referred to as the Potential Slow-Roll (PSR) parameters. It would be obvious that setting the slow-roll conditions (3.16) and (3.17) leads to $\epsilon_V \ll 1$ and $\eta_V \ll 1$. However, the opposite is not valid because the smallness of ϵ_V and η_V is only necessary conditions not sufficient to take place inflation. As an alternative formalism, we can work with the more rigorous approach based on the Hubble parameter as the Hubble Slow-Roll (HSR) parameters. The slow roll parameters in this picture can be expressed as [111, 112]

$$\epsilon_H = -\frac{\dot{H}}{H^2}, \qquad \eta_H = \epsilon_H - \left(\frac{\dot{\epsilon_H}}{2H\epsilon_H}\right), \tag{3.19}$$

where dot implies to time derivative. We note that if $\epsilon_H \ll 1$ and $\eta_H \ll 1$, surely the slow-roll conditions (3.16) and (3.17) are true and in such case, the HSR approximation implies the PSR approximation.
By setting the slow-roll conditions, the Friedmann and Klein-Gordon equations take the following form

$$H^2 \simeq \frac{\kappa^2}{3}V(\varphi), \qquad 3H\dot{\varphi} \simeq -\frac{dV(\varphi)}{d\varphi}. \tag{3.20}$$

Also, the energy density and pressure of inflaton are given as $\rho \simeq V(\varphi)$ and $p \simeq -V(\varphi)$ with the equation of state $w \simeq -1$. In other words, the inflationary era mimics the de Sitter universe when the slow-roll approximation is engaged for the inflationary analysis.
Now that we understood the slow-roll approximation, it is easy to express the number of e-folds between the start and end of inflation as

$$N \equiv \int_{t_{ini}}^{t_{end}} H dt = -\sqrt{\frac{\kappa^2}{2}} \int_{\varphi_{ini}}^{\varphi_{end}} (\epsilon_V)^{-\frac{1}{2}}, \tag{3.21}$$

where φ_{ini} and φ_{end} are the values of inflaton at the start and end of inflation, respectively.

3.3 Reheating Process

We learned that inflation takes place when the scalar field rolls slowly down from the top of the potential to the minimum point of potential (3.16) and also the scale

factor grows for the specific value of the number of e-folds (3.17). Now, it is worth introducing the reheating process as the final stage of inflation. When inflation ended, the universe became supercooled through the huge and rapid expansion. Therefore, it required to acquire energy in order to continue the normal expansion. Let's see how it could occur in the standard formalism. Inflation ended when the slow-roll conditions were broken or inflaton approached the minimum point of potential. In such a case, inflaton started to oscillate around the minimum point and decayed to particles of the standard model [113, 114, 115, 116, 117, 118, 119, 120, 121]. This is the process which is called reheating (see Figure 3.2) [122, 123, 124, 125, 126]. The next stage of reheating was thermalization in which the particles generated during the first stage, interacted with each other and came to a state of thermal equilibrium with the reheating temperature T_r. We note that almost all matters filling the universe at the subsequent radiation-dominated stage created during this process. Let us describe the process by appropriated relations.

3.3.1 Evaluation of Inflaton

In order to present a more satisfying explanation of the reheating process, we consider the chaotic inflation $V(\varphi) = \frac{1}{2}m^2\varphi^2$ where m is the mass of scalar field, during the following analysis. The dynamical equations are given by

$$\ddot{\varphi} + 3H\dot{\varphi} + m^2\varphi = 0, \tag{3.22}$$

$$H^2 = \frac{\kappa^2}{6}(\dot{\varphi}^2 + m\varphi^2). \tag{3.23}$$

By parameterizing the Eq. (3.23) in terms of two independent variables e.g., the Hubble parameter H and the angular variable θ, we find

$$\dot{\varphi} = \sqrt{\frac{6}{\kappa^2}}H\sin\theta, \qquad m\varphi = \sqrt{\frac{6}{\kappa^2}}H\cos\theta \tag{3.24}$$

and by using the Klein-Gordon equation (3.22), we obtain the dynamics of two independent parameters as

$$\dot{H} = -3H^2\sin^2\theta, \tag{3.25}$$

$$\dot{\theta} = -m - \frac{3}{2}H\sin 2\theta. \tag{3.26}$$

By setting the condition at the end of inflation $mt \gg 1$, the second term of the Eq. (3.26) can be neglected and inflaton oscillates with a frequency of $w \simeq m$. Also, by solving the Eq. (3.25) for the Hubble parameter, we obtain

$$H = \frac{2}{3t}(1 - \frac{\sin(2mt)}{2mt})^{-1}, \tag{3.27}$$

where the second term represents the oscillation of inflaton and is small compared to unity. Now, by using the Eq. (3.24), the evaluation of the scalar field can be interpreted by

$$\varphi(t) \simeq \Phi(t)\cos(mt)\left(1 + \frac{\sin(2mt)}{2mt}\right), \tag{3.28}$$

where the amplitude of oscillations is provided by

$$\Phi(t) = \sqrt{\frac{8}{3\kappa^2}}\frac{1}{mt}. \tag{3.29}$$

Notice that the behaviour of scale factor can be found from the Eq. (3.27) as

$$a(t) \propto t^{\frac{2}{3}}. \tag{3.30}$$

This shows that the energy density of inflaton declines analogous with the energy density of non-relativistic particles of mass m e.g., a^{-3}.

In summary, we can state that:

The oscillations of inflaton can be explained as a collection of scalar particles, independent from each other, oscillating coherently at the same frequency m.

For time intervals larger than the oscillating period, the energy and number densities are related to the amplitude Φ as

$$\rho_\varphi = \frac{1}{2}m^2\Phi^2, \qquad n_\varphi = \frac{1}{2}m\Phi^2. \tag{3.31}$$

In fact, reheating takes place when the amplitude of oscillations of the inflaton declines much faster than (3.28) and the energy density is converted to the energy density of other particles and fields.

3.3.2 Decay of Inflaton

By assuming the interaction of inflaton φ with a field χ and a spinor field ψ, the corresponded Lagrangian can be written by

$$L = \frac{1}{2}\partial_i\varphi\partial^i\varphi - V(\varphi) + \frac{1}{2}\partial_i\chi\partial^i\chi - \frac{1}{2}m_\chi^2(0)\chi^2 + \bar{\psi}(i\gamma^i\partial_i - m_\psi(0))\psi - \frac{1}{2}g^2\varphi^2\chi^2 - h\bar{\psi}\psi\varphi. \tag{3.32}$$

where g, h and ξ are small coupling constants, R is Ricci scalar as the spacetime curvature and $V(\varphi)$ is the effective potential of the inflaton. Also, we suppose that the potential has a minimum when $\varphi = \sigma$ and is quadratic in φ.

$$V(\varphi) \sim \frac{1}{2}m^2(\varphi - \sigma)^2. \tag{3.33}$$

By setting the shift $\varphi - \sigma \to \varphi$ as a result of spontaneous symmetry breaking, the effective potential takes the familiar form $\frac{1}{2}m^2\varphi^2$ and the Lagrangian acquires the interaction terms related linearly to the inflaton φ as

$$\Delta\mathcal{L} = -g^2\sigma\varphi\chi^2 - h\bar{\psi}\psi\varphi. \tag{3.34}$$

This eventually lead to decaying inflaton to a pair of scalar χ-particles or spinor ψ-particles

$$\Gamma(\varphi \to \chi\chi) = \frac{g^4\sigma^2}{8\pi m}, \qquad \Gamma(\varphi \to \bar{\psi}\psi) = \frac{h^2 m}{8\pi}. \tag{3.35}$$

where $\Gamma = \Gamma(\varphi \to \chi\chi) + \Gamma(\varphi \to \bar{\psi}\psi)$ is the total decay rate of φ-particles.
To present the effects of particle production, we can consider the equation of motion of inflaton in the presence of the non-gravitational quantum corrections as

$$\ddot{\varphi} + 3H(t)\dot{\varphi} + (m^2 + \Pi(w))\varphi = 0, \tag{3.36}$$

where $\Pi(w)$ is the flat space polarization operator with 4-momentum $k = (w = m, 0, 0, 0)$ for inflaton. By overlooking the time dependance of H and ImΠ, Eq. (3.36) takes the following solution

$$\varphi(t) \approx \Phi(t)\sin(mt), \tag{3.37}$$

where

$$\Phi(t) \approx \Phi_0 \exp\Big(-\frac{1}{2}(3H + \frac{\mathrm{Im}\Pi(m)}{m})t\Big). \tag{3.38}$$

In the case of $m \gg min(2m_\chi, 2m_\psi)$, $\Pi(w)$ has an imaginary part which can identify with the decay width thanks to the optical theorem through unitarity:

$$\mathrm{Im}\Pi(w) = m\Gamma_\varphi. \tag{3.39}$$

The amplitude of the oscillations of the field φ decreases as

$$\Phi(t) = \Phi_0 \exp(-\frac{1}{2}(3H + \Gamma)t) \tag{3.40}$$

due to the universe expansion as well as due to particle production.

In summary, we can state that:

The amplitude of inflaton oscillations decreases due to particle production which occurs during the decay of the inflaton field.

Let us show the result in another way. The inflaton amplitude $\Phi(t)$ obeys the equation

$$\frac{1}{a^3}\frac{d}{dt}(a^3\Phi^2) = -\Gamma\Phi^2. \tag{3.41}$$

By multiplying the latter by m, one can obtain the following equation for the number density

$$\frac{d}{dt}(a^3 n_\varphi) = -a^3 n_\varphi \Gamma. \tag{3.42}$$

The above expression implies the Boltzmann equation and shows that the comoving number density of φ particles exponentially decreases with the decay rate of Γ.

3.3.3 Reheating Temperature

During the oscillating phase, the universe behaves in the same way as if it was dominated by non-relativistic particles of mass m : $H(t) \sim \frac{2}{(3t)}$. The inflaton energy density is then transferred to the relativistic decay products, the energy density of which decreasing much faster than the energy of the oscillating field φ. The reheating process eventually ends when $H < \Gamma_\Phi$. The *reheating time* is defined as the time at which the transition between these two regimes occurs: $t_r \simeq \frac{2}{(3\Gamma_\varphi)}$. By equating the inflaton energy density

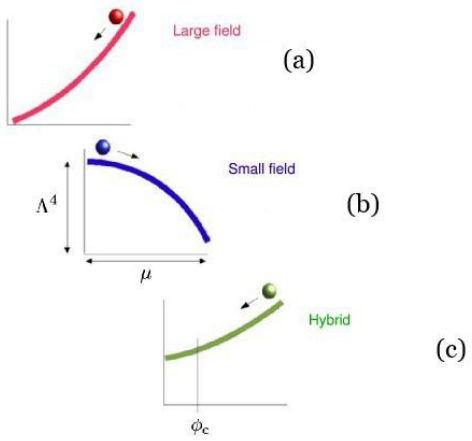

FIGURE 3.3: The behavior of potential in three main classes of single field model. The large field case in which inflaton rolls down from the top of the potential with a large value and reach to the minimum point with a small value. The small field case in which inflaton starts with a small value and reaches to the large value at the minimum point. The hybrid case in which inflation ends in the presence of an auxiliary field at a critical point.

$$\rho_\varphi = \frac{4}{3\kappa^2 t_r^2} \tag{3.43}$$

with the one of a thermal bath

$$\rho_{rad} = \frac{\pi^2}{30} N(T_r) T_r^4 \tag{3.44}$$

one can obtain the reheating temperature as [1]:

$$T_r \simeq 0.2\sqrt{\Gamma_\varphi m_{PL}}. \tag{3.45}$$

It is remarkable that t_r does only depend on the particle theory parameters and not on the initial value of φ.
Notice that some inflationary models consider a *preheating* stage before the reheating process so that first, the classical inflaton decays into massive bosons (in particular, into φ-particles) due to an extremely rapid and broad parametric resonance. Then, these particles decay to the standard particles and eventually, it follows by a thermalization stage for the produced particles.

3.4 Some Inflationary Models

Now that we explained the standard mechanism of cosmic inflation, it would be worth to survey the common inflationary models. There are many inflationary models proposed in the cosmological literature and it is not possible to cover all in this

[1] where $N(T_r)$ is the number of relativistic degrees of freedom at the temperature T so that one should take 1 for each scalar, 2 for each massless vector particle, etc. Notice that in the realistic models, one may expect $N(T_r) \equiv 10^2 - 10^3$.

thesis even briefly. Hence, we restrict ourselves to some models with a good community among inflationary papers. Before moving on the models, let us present a quick review of the properties of a successful inflationary model.

- **A Graceful Entry and Exit.** Inflation as an artificial theory patched to the standard model, must have a successful entry from the Planck period to the inflationary era and also a graceful exit from the inflationary era to radiation dominated epoch. Our knowledge from the start of inflation is not enough compared to the end of inflation since inflation has emerged from the Planck era where is the realm of gravity in the context of quantum mechanics.
- **Number of e-folds.** As we learned, cosmic inflation first presented for removing the HBB problems through a specific amount of expansion in the early universe. A unique inflationary model has to offer an acceptable value of the number of e-folds in a good agreement with observations.
- **Perturbations.** The most significant part of inflation has been related to the role of the perturbations generated during the inflationary era so that the scalar and tensor perturbations are the main responsible for structure formation of the universe and primordial gravitational waves, respectively.
- **Reheating Process.** At the end of inflation, inflaton decays to the standard particles to reheat the supercooled universe. The process is called reheating discussed in the previous section. The inflationary model should be able to suggest the reheating mechanism.

3.4.1 Basic Inflationary Models

The single field models are classified into the three following categories due to the form of inflationary potential [127, 128].

3.4.1.1 Large Field Potentials

In this model, inflaton rolls down slowly with a large value from the top of the potential and reach to the minimum point of potential with a small value (see the picture (a) of Figure 3.3). The main generic form of large field models is the polynomial potentials $V(\varphi) = V_0\varphi^p$ in which $p = 2$ implies to the chaotic inflation $V(\varphi) = \frac{1}{2}m^2\varphi^2$ where m is the mass of inflaton [129] and $p = 4$ is associated to the quartic potential $V(\varphi) = \lambda\varphi^4$ as a self-interacting potential. Another widely-noted generic form of large field case is exponential potential $V(\varphi) = \Lambda^4 \exp(\frac{\varphi}{\mu})$ which has the useful property that both the background evolution and the perturbation equations are exactly solvable. Large field models are typically specified by a red spectral index $n_s < 1$ and a tensor-to-scalar ratio ~ 0.1.

3.4.1.2 Small Field Potentials

This class of models comes from naturally from spontaneous symmetry breaking and pseudo Nambu-Goldstone modes in which inflaton starts to roll down from an unstable point $V'(\varphi) = 0$ to the minimum point with a large value of inflaton (see the picture (b) of Figure 3.3). The generic forms of potential are expressed as $V(\varphi) = \Lambda^4(1 + \cos(\frac{\varphi}{\mu}))$ for natural inflation [130] or $V(\varphi) = \lambda\varphi^4 \ln(\varphi)$ for Weinberg-Coleman potential [131]. Small field models show the very small tensor-to-scalar ratio $r \leq 0.01$ with a red spectral index $n_s < 1$.

3.4.1.3 Hybrid Potentials

The hybrid model frequently raises when we describe inflation in the context of supersymmetry and supergravity [132, 133, 134, 109]. Based on the model, there is a remained vacuum energy in the minimum point of potential and it means that inflation will continue forever. An assistant field is engaged to terminate the inflationary era in a point near the minimum of potential and also to prepare a reheating mechanism (see the picture (c) of Figure 3.3). Although the auxiliary field is unstable at a critical field value φ_c, it is stable at large φ. Notice that the only inflaton φ is the dynamical scalar field and the assistant field is used only for ending inflation at the critical point. Hence, the hybrid model is an effective form of single field potentials. This class of models is characterized by a blue spectral index $n_s > 1$ and a very small scalar-to-tensor ratio $r \ll 0.01$ which are not in good agreement with observations.

3.4.2 Inflation in Modified Theories of Gravity

After discovering the late time acceleration or DE in 1998 [47, 48], people realized that the standard model is not able to explain the nature of DE. Hence, two main approaches proposed to overcome the issue. The first was adding the cosmological constant Λ to the right-hand side of the Eq. (2.7) [49] and the second was assuming some modifications in the geometry of the universe on the left-hand side of the Eq. (2.7) which led to introducing the modified theories of gravity [50, 51, 52]. Some of these modifications are classical and some of them are based on quantum theories such as string theory. In this section, we introduce some of these theories which have been widely discussed among cosmological literature and also show how inflation operates in the context of such theories.

3.4.2.1 *f(R)* Gravity

The simplest geometrical modification of GR is replacing R with a general function of the Ricci scalar $f(R)$ in the Einstein-Hilbert action (2.6) by [53, 54]

$$S = \int \sqrt{-g}\left(\frac{f(R)}{2\kappa^2} + \mathcal{L}_M\right) d^4x \tag{3.46}$$

where the Einstein-Hilbert action is recovered for $f(R) = \frac{R}{2}$ and also, the vacuum solution can be found for the zeroth order of R. Generally, there are two formalisms in deriving field equations from the action (3.46). The first is the standard metric formalism in which the field equations are obtained by varying the action with respect to the metric. In this formalism, the Christoffel symbol $\Gamma^{\gamma}_{\mu\nu}$ depends on the metric $g_{\mu\nu}$. The second approach is the Palatini formalism in which metric and the Christoffel symbol are expressed as independent variables. Although these two approaches lead to different field equations for a non-linear Lagrangian density in R, they are identical to each other for the GR action.
Despite the regular inflationary models based on scalar fields, $f(R)$ gravity attempts to describe inflation without any type of matter and only by considering some appropriate geometrical modifications. The treatment is similar to the DE case in which $f(R)$ gravity explains DE by changes in geometry instead of adding the cosmological constant to the matter content of the universe. The simplest inflationary model in $f(R)$ gravity proposed by A. A. Starobinsky in 1980 as [108]

$$S = \int \sqrt{-g}\left(\frac{(R + \frac{\alpha R^2}{2})}{2\kappa^2} + \mathcal{L}_M\right) d^4x, \tag{3.47}$$

where $\alpha > 0$. We note that the reheating process in such models is supported by the oscillating phase of the Ricci scalar. Although the R^2 inflation is useful to clarify inflation and DE, it suffers from some problems when it is inquired by high precision observational datasets. This motivates us to consider the general form of the model as R^{2p} in the Einstein frame used the conformal transformation in order to find small derivations from the R^2 model. This case will be treated completely in chapter 6.

3.4.2.2 Scalar-Tensor Gravity

Another simple extension of Einstein's gravity is the scalar-tensor theory in which an additional spin-0 (scalar) degrees of freedom is considered in additions to the spin-2 (tensor) degrees of freedom. Therefore, the form of action in GR (2.6) is modified to [135, 136, 137]

$$S_J = \int \sqrt{-g}\left[\frac{1}{2\kappa^2}\left(\varphi R - \frac{w(\varphi)}{\varphi}\partial_\mu\varphi\partial^\mu\varphi - 2\Lambda(\varphi)\right) + \mathcal{L}_M(\chi, g_{\mu\nu})\right]d^4x, \tag{3.48}$$

where $\mathcal{L}_M(\chi, g_{\mu\nu})$ implies to the Lagrangian of other matters fields minimally coupled to the metric and $w(\varphi)$ and $\Lambda(\varphi)$ are free functions. Since working in the Jordan frame is very difficult through the non-minimal connection of gravity and scalar field, it is worth to engage the conformal transformation in order to map the Jordan frame to the Einstein frame as an easier frame. By using the conformal transformation $g_{\mu\nu} = e^{2\Gamma(x)}\bar{g}_{\mu\nu}$ and corresponding relations, the form of action in the Jordan frame (3.48) is turned to the action in the Einstein frame as

$$S_E = \int \sqrt{-\bar{g}}\left[\frac{1}{\kappa^2}\left(\frac{\bar{R}}{2} - (\frac{1}{2}\bar{\partial}_\mu\psi\bar{\partial}^\mu\psi + V(\psi))\right) + e^{4\Gamma(\psi)}\mathcal{L}_M(\chi; g_{\mu\nu})\right]d^4x, \tag{3.49}$$

where the new form of scalar field $\psi(\varphi)$ and its potential $V(\psi)$ take the following forms

$$\frac{\partial\Gamma(\varphi)}{\partial\psi} = -\frac{1}{2}\frac{\partial\ln(\varphi)}{\partial\psi} = (2(3+2w(\varphi)))^{-\frac{1}{2}}, \qquad V(\psi) = e^{4\Gamma}\Lambda(\varphi(\psi)). \tag{3.50}$$

It is easy to find that the action (3.48) depicts the action in GR when gravity and the new scalar field are minimally connected. Notice that for the case of $w = constant$ and $\Lambda = constant$, the scalar-tensor theory reduces to the Brans-Dicke theory. Also, the standard mechanism of inflation in the context of the scalar-tensor theories is based on inflaton as the matter section of the action (3.48). One of the fields might roll quickly to the minimum of its potential and then the problem reduces to single-field inflation, either the familiar chaotic inflation in general relativity when $\psi = 0$ or old extended inflation in Brans-Dicke when inflation disappears [137].

3.4.2.3 Braneworld Gravity

One of the most elegant applications of string theory in cosmology is Braneworld gravity or extra dimensions theory in which our 4D universe, which is called *brane*, is embedded in extra dimensions, which are called *bulk* [55]. The additional dimensions are compact and spatial. Through such theory, gravity is intrinsically an interaction associated with the bulk since the graviton is the sole particle formed by

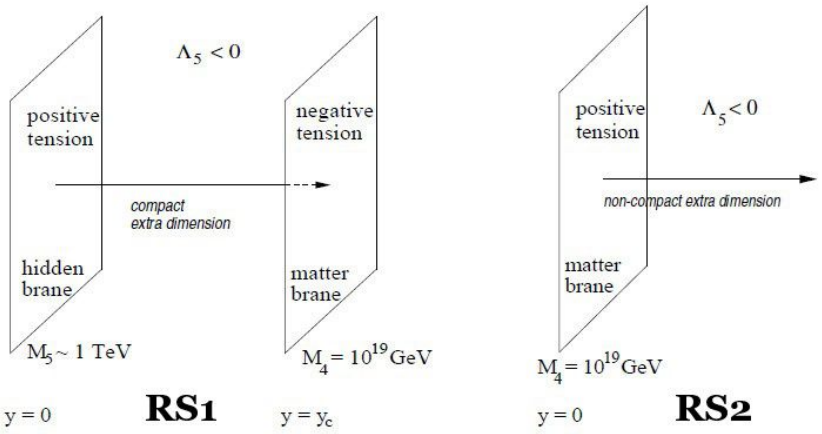

FIGURE 3.4: The RS1 diagram displays that our universe as matter brane with a negative tension is located at $y = y_c$ and the hidden brane on the bulk is located at $y = 0$ with a positive tension. The gap between branes is occupied by an extra spatial dimension as a warped bulk with a negative cosmological constant. In the RS2 model, the hidden brane is sent to infinity and our brane is located at $y = 0$ with positive tension. Also, the bulk is warped and equipped with the negative cosmological constant.

the closed strings. Therefore, the GR can be modified by rewriting the action in the context of extra dimensions. Among the cosmological literature, there are two main braneworld models. One is the RS1 and RS2 models proposed by L. Randall and R. Sundrum in 1999 [138, 139] and the other is the DGP model proposed by G. Dvali, G. Gabadadze and M. Porrati in 2000 [140]. Let us introduce two models, briefly. In the RS1 model, Our brane as matter brane has a negative tension and one can measure the Planck mass as 10^{-19} GeV on matter brane. The large distance between the hidden brane as electroweak scale (TeV) and the matter brane as Planck scale, can be explained to be an effect of the curvature of the Anti-De sitter bulk. The extra-dimensional coordinate is $0 \leq y \leq y_c$ where $y = R_c\theta$. Our visible world locates at the extra dimension coordinate $y_c = L$ and the hidden brane with positive tension is situated at $y = 0$. The extra dimension has Z2 symmetry about $y = 0$ and $y = L$. We note that a positive tension brane is a place where gravity is stronger than our brane (see the left diagram of Figure 3.4). The action of the RS1 model is expressed by

$$S_{RS1} = S_{Gravity} + S_{MB} + S_{HB}, \tag{3.51}$$

where

$$S_{Gravity} = \frac{M_5^2}{2} \int d^4x \int_{-y_c}^{y_c} dy \sqrt{g_5}(R_5 + 2\Lambda_5), \tag{3.52}$$

$$S_{MB} = \int d^4x \sqrt{-g_{MB}}\lambda_{MB} \tag{3.53}$$

and

$$S_{HB} = \int d^4x \sqrt{g_{HB}}\lambda_{HB}, \tag{3.54}$$

where the subscribe "MB" and "HB" denote to matter brane and hidden brane, respectively. Also, λ is the brane tension. In the RS2 model, there is only one brane as matter brane at $y = 0$ with positive tension and the hidden brane at y_c is sent to infinity (see the right diagram of Figure 3.4). The form of action in this model is the same as the previous model without S_{HB}.
Let's turn to the DGP model. The model has one brane like RS2, but the main difference of the model with RS models is that the bulk is Minkowski (flat) not warped and also without the cosmological constant. Hence, there is no tension on the brane. Conventional 4D gravity is recovered on scales smaller than a crossover scale. The form of action in the DGP model is expressed by

$$S_{DGP} = \frac{M_5^3}{2}\int d^4x \int dy\sqrt{g_5}R_5 + \frac{M_4^2}{2}\int d^4x\sqrt{-g}R + \int d^4x\mathcal{L}_M. \tag{3.55}$$

Notice that the second term of the above action is the induced gravity on the brane through the interaction of bulk gravitons and brane matter.
Since the interaction of the bulk with our brane produces some effects on our 4-D universe, we can expect some interesting consequences from extra dimensions in cosmology. For instance, in order to describe inflation, we can consider a scalar field on the bulk so that its effects on brane can play the role of inflaton in our universe [141, 142].

3.4.3 Eternal Inflation

Despite the conventional approach to inflation, eternal inflation remarks that inflation doesn't require to be held all at once. Instead, little bubbles of space could have randomly stopped inflating, or come into trajectories which would lead to the end of inflation. The inside of bubbles would be in a lower energy state and since they are in an energetically favorable state, they would expand into the inflating outside. If the universe were not expanding, or if it were expanding slowly, each bubble would eventually fall into another bubble and the whole universe would be converted to the lower vacuum energy. But, in a rapidly expanding universe, the space between bubbles is growing even as the bubbles are themselves growing into that space. If the expansion is fast enough, the growth of inflating space will be faster than its conversion into lower-energy bubbles and inflation will never end [143, 106].
How can we inquire about the theory?. Most pairs of bubble universes will never collide with each other. They are too far apart and the space between them is expanding too fast, but some pairs will form close enough together that they will meet. The ensuing collision will disturb the space-time inside each bubble so that perturbation may be visible today as a small temperature anisotropy in cosmic microwave background [144, 145, 146, 147, 148].

3.5 Inflationary Perturbations

As we have seen in the previous sections, the early universe became flat and nearly uniformed through a vast and rapid expansion as cosmic inflation. However, one should be careful about the word "nearly" used in the above expression. In fact, the homogeneity of the early universe has been affected by the presence of primordial perturbations generated during the inflationary era. The origin of structure formation of the universe is referred to small seed perturbations which over time, grew

to become all of the structure we observe. The appearance of the primordial inflationary perturbations is also confirmed by detailed measurements of the CMB anisotropic so that the scalar perturbations are the main responsible for the observed anisotropy of CMB photons at last scattering time. Moreover, the tensor perturbations produced during inflation, generate the primordial gravitational waves that are observed through the magnetic polarization of CMB photons. The above considerations about the perturbations, motivate us to devote the present section to explain the inflationary perturbations which can be found among the great inflationary reviews [149, 150, 151, 152, 153, 154, 155].

3.5.1 Metric Perturbations

To formulate the inflationary perturbations, we consider a linear perturbation in scalar field

$$\varphi = \varphi_0(t) + \delta\varphi(t,x), \tag{3.56}$$

where $\delta\varphi(t,x)$ is a generated perturbation in the scalar field through quantum fluctuations. Since inflaton is the sole component of the universe during inflation, the perturbations in the energy density of inflaton will lead to perturbations in energy-momentum tensor. Also, the perturbations in energy-momentum tensor imply to the perturbations in geometry or the Einstein tensor and metric through the form of the field equation (2.7). Let's start with the perturbed FRW metric with the line element

$$ds^2 = -(1+2A)dt^2 + 2a(\partial_i B - S_i)dx^i dt + a^2[(1-2\psi)\delta_{ij} + 2\partial_{ij}E + 2\partial_{(i}F_{j)} + h_{ij}]dx^i dx^j, \tag{3.57}$$

where ∂_i depicts the spatial partial derivative $\frac{\partial}{\partial x^i}$. We will use lower case Latin indices to refer to the 3 spatial coordinates. It will be extremely useful to perform a Scalar-Vector-Tensor (SVT) decomposition of the perturbations that lead to the linearization of equations of the scalar, vector, and tensor modes, separately (see [156] for the second order of perturbations). In summary, we will mostly be concerned about scalar fluctuations and the associated density perturbations due to their role for structure formation and anisotropy of cosmic microwave background. Vector perturbations would decay quickly with the expansion of the universe. Tensor perturbations are a major prediction of inflation through the generation of the primordial gravitational waves.

3.5.1.1 Scalar Perturbations

The four perturbed terms of scalar part A, $\partial_i B$, $\psi\delta_{ij}$ and $\partial_{ij}E$ are constructed from 3-scalars, their derivatives, and the background spatial metric. The intrinsic Ricci scalar curvature of constant time hypersurfaces can be given by

$$R = \frac{4}{a^2}\nabla^2\psi, \tag{3.58}$$

where $\nabla^2 \equiv \delta^{ij}\partial_{ij}$ is the spatial Laplacian and hence, we refer to ψ as the curvature perturbation. Since the metric perturbations are not uniquely defined, we can define the new coordinates or the gauge choice. In particular, when we deal with the perturbed metric, we implicitly choice a specific time-slicing of the spacetime

and defined specific spatial coordinates on these time slices. Under such a scalar coordinate/gauge transformation, we have

$$t \longrightarrow t + \delta t, \qquad x^i \longrightarrow x^i + \delta^{ij}\partial_j \delta x, \tag{3.59}$$

where δt and δx define the time slicing and the spatial threading, respectively. Then, the scalar metric perturbations are transformed as

$$A \longrightarrow A\dot{\delta t}, \quad B \longrightarrow B + a^{-1}\delta t - a\dot{\delta x}, \quad E \longrightarrow E - \delta x, \quad \psi \longrightarrow \psi + H\delta t. \tag{3.60}$$

We can build a variety of gauge-invariant combinations of the scalar metric perturbations. The longitudinal gauge corresponds to a specific gauge-transformation to a (zero-shear) frame such that $E = B = 0$, leaving the gauge-invariant variables

$$\Phi \equiv A - \frac{d}{dt}[a^2(\dot{E} - \frac{B}{a})], \qquad \Psi \equiv \psi + a^2 H(\dot{E} - \frac{B}{a}). \tag{3.61}$$

Matter perturbations are also gauge-dependent and hence the scalar field, density, and pressure perturbations follow the transformation relation

$$\delta\rho \longrightarrow \delta\rho - \dot{\rho}\delta t. \tag{3.62}$$

By definition of the adiabatic pressure perturbation as

$$\delta P_{ad} \equiv \frac{\dot{P}}{\dot{\rho}}\delta\rho \tag{3.63}$$

the non-adiabatic part of the pressure perturbation, or entropy perturbation, is a gauge-invariant perturbation

$$\delta P_{nad} = \delta P - \frac{\dot{P}}{\dot{\rho}}\delta\rho. \tag{3.64}$$

The scalar part of the 3-momentum is defined by $\partial_i \delta q$ and this momentum potential transforms as

$$\delta q \longrightarrow \delta q + (\rho + P)\delta t. \tag{3.65}$$

Thus, we can obtain the gauge-invariant comoving density perturbation as [157, 158, 159, 160]

$$\delta\rho_m = \delta\rho - 3H\delta q. \tag{3.66}$$

Since we can construct the gauge-invariant combinations of perturbations, we make two further combinations in terms of matter and metric perturbations. Hence, the curvature perturbation on uniform density hypersurfaces and the comoving curvature perturbation are given by [161, 162]

$$-\zeta \equiv \psi + \frac{H}{\dot{\rho}}\delta\rho, \qquad \mathcal{R} \equiv \psi - \frac{H}{(\rho + P)}\delta q. \tag{3.67}$$

The difference between the two curvature perturbations R and -ζ is proportional to the comoving density perturbation

$$-\zeta = \mathcal{R} + \frac{H}{\dot{\rho}}\delta\rho_m. \tag{3.68}$$

For single field inflation with $\delta q = -\dot{\varphi}\delta\varphi$, we have

$$\mathcal{R} \equiv \psi + \frac{H}{\dot{\varphi}}\delta\varphi. \tag{3.69}$$

Under the slow-roll approximation, single-field inflation, we obtain $\frac{\delta\rho}{\dot{\rho}} \simeq \frac{\delta\varphi}{\dot{\varphi}}$ and hence $\delta\rho_m \simeq 0$ and these two curvature perturbations, i.e., R and $-\zeta$, would be matched together. Another variable used to describe scalar perturbations is the field perturbation in the spatially flat gauge (where ψ=0) that is gauge invariant

$$\delta\varphi_\psi \equiv \delta\varphi + \frac{\dot{\varphi}}{H}\psi. \tag{3.70}$$

For single field inflation, this shows a rescaling of the comoving curvature perturbation R in (3.67). We see that what appears as a field perturbation in one gauge is a metric perturbation in another gauge and vice versa.

3.5.1.2 Vector Perturbations

The vector perturbations S_i and F_i are distinguished from scalar perturbations through their divergence-free feature, i.e., $\partial^i S_i = 0$. Under the following gauge transformation

$$x^i \longrightarrow x^i + \delta x^i \tag{3.71}$$

the vector metric perturbations transform as

$$S_i \longrightarrow S_i + a\dot{\delta x}_i, \qquad F_i \longrightarrow F_i - \delta x_i \tag{3.72}$$

and the combination $\dot{F}_i + \frac{S_i}{a}$ is the vector shear perturbation which is gauge-invariant.

3.5.1.3 Tensor Perturbations

Since the tensor perturbations h_{ij} are transverse $\partial^i h_{ij} = 0$ and trace-free $\delta^{ij}h_{ij} = 0$, they are independent of coordinate gauge transformations. These are referred to as gravitational waves as they are the free part of the gravitational field and evolve independently of linear matter perturbations. We will decompose arbitrary tensor perturbations into eigenmodes of the spatial Laplacian, with comoving wavenumber k, and scalar amplitude $h(t)$

$$h_{ij} = h(t)e_{ij}^{(+,\times)}(x) \tag{3.73}$$

with two possible polarisation states, $+$ and *times*.

3.5.2 Field Equations

Now, let's obtain the field equations of perturbations.

3.5.2.1 Scalar Perturbations

The perturbed Einstein equations $\delta G_{\mu\nu} = \kappa^2\delta T_{\mu\nu}$ connects the metric perturbations to matter perturbations via the energy and momentum as [163]

$$3H(\dot{\psi} + HA) + \frac{k^2}{a^2}[\psi + H(a^2\dot{E} - aB)] = -\frac{\kappa^2\delta\rho}{2}, \tag{3.74}$$

$$\dot{\psi} + HA = -\frac{\kappa^2 \delta q}{2}. \tag{3.75}$$

These can be combined to give the gauge-invariant generalisation of the Poisson equation

$$\frac{k^2}{a^2}\Psi = -\frac{\kappa^2 \delta \rho_m}{2} \tag{3.76}$$

relating the longitudinal gauge metric perturbation (3.61) to the comoving density perturbation (3.66). The Einstein equations also yield two evolution equations for the scalar metric perturbations

$$\ddot{\psi} + 3H\dot{\psi} + H\dot{A} + (3H^2 + 2\dot{H})A = \frac{\kappa^2}{2}(\delta P - \frac{2}{3}k^2\delta\Pi), \tag{3.77}$$

$$(\dot{E} - \frac{B}{a}) + 3H(\dot{E} - \frac{B}{a}) + \frac{(\psi - A)}{a^2} = \kappa^2\delta\Pi, \tag{3.78}$$

where the scalar part of the anisotropic stress is given by

$$\delta\Pi_{ij} = [\partial_i\partial_j + (\frac{k^2}{3})\delta_{ij}]\Pi. \tag{3.79}$$

Equation (3.79) can be written in terms of the longitudinal gauge metric perturbations Φ and Ψ (3.61) by

$$\Psi - \Phi = \kappa^2 a^2 \delta\Pi \tag{3.80}$$

where we have $\Psi = \Phi$ in the absence of anisotropic stresses. The energy-momentum conservation law gives evolution equations for the perturbed energy and momentum as

$$\delta\dot{\rho} + 3H(\delta\rho + \delta P) = \frac{k^2}{a^2}\delta q + (\rho + P)[3\dot{\psi} + k^2(\dot{E} + \frac{B}{a})], \tag{3.81}$$

$$\dot{\delta}q + 3H\delta q = -\delta P + \frac{2}{3}k^2\delta\Pi - (\rho + P)A. \tag{3.82}$$

By rewriting the energy conservation equation (3.81) in terms of the curvature perturbation on uniform-density hypersurfaces ζ expressed in (3.67), we obtain

$$\dot{\zeta} = -H\frac{\delta P_{nad}}{(\rho + P)} - \Sigma, \tag{3.83}$$

where δP_{nad} is the non-adiabatic pressure perturbation, defined in (3.64). Also, Σ is the scalar shear along comoving worldlines [159] which can be given relative to the Hubble rate as

$$\frac{\Sigma}{H} \equiv -\frac{k^2}{3H}\left[\dot{E} - \frac{B}{a} + \frac{\delta q}{a^2(\rho + P)}\right] = -\frac{k^2}{3H^2a^2}\zeta - \frac{k^2\Psi}{3a^2H^2}\left[1 - \frac{2\rho k^2}{9(\rho + P)a^2H^2}\right]. \tag{3.84}$$

Thus ζ is constant for adiabatic perturbations on super-Hubble scales ($\frac{k}{aH} \ll 1$), so long as Ψ remains finite, in which case the shear of comoving worldlines can be neglected. If we consider N scalar fields with Lagrangian density

$$\mathcal{L} = -V(\varphi_1, ..., \varphi_N) - \frac{1}{2}\sum_{I=1}^{N} g^{\mu\nu}\varphi_{I,\mu}\varphi_{I,\nu} \tag{3.85}$$

which are minimally coupled to gravity, then the total energy, pressure and momentum perturbations are obtained by

$$\delta\rho = \sum_I [\dot{\varphi}_I(\dot{\delta}\varphi_I - \dot{\varphi}_I A) + V_I\delta\varphi_I], \tag{3.86}$$

$$\delta P = \sum_I [\dot{\varphi}_I(\dot{\delta}\varphi_I - \dot{\varphi}_I A) - V_I\delta\varphi_I], \tag{3.87}$$

$$\delta_{q,i} = -\sum \dot{\varphi}_I \delta\varphi_{I,i}, \tag{3.88}$$

where $V_I \equiv \frac{\partial V}{\partial \varphi_I}$. The above relations give the gauge-invariant comoving density perturbation as

$$\delta\rho_m = \sum_I [\dot{\varphi}_I(\dot{\delta}\varphi_I - \dot{\varphi}_I A) - \ddot{\varphi}_I\delta\varphi_I]. \tag{3.89}$$

The comoving density is sometimes used to represent the total matter perturbation, but for a single scalar field it is proportional to the non-adiabatic pressure (3.64)

$$\delta P_{nad} = -\frac{2V_{,\varphi}}{3H\dot{\varphi}}\delta\rho_m. \tag{3.90}$$

From the Einstein constraint equation (3.76), the above expression will vanish on large scales ($\frac{k}{aH} \longrightarrow 0$) if Ψ remains finite. Hence, single scalar field perturbations become adiabatic in the large scales limit.
The anisotropic stress, $\delta\Pi$, vanishes to linear order for any number of scalar fields minimally coupled to gravity. The first-order scalar field perturbations obey the wave equation

$$\ddot{\delta}\varphi_I + 3H\dot{\delta}\varphi_I + \frac{k^2}{a^2}\delta\varphi_I + {}_J\, V_{IJ}\delta\varphi_J = -2V_I A + \dot{\varphi}_I[\dot{A} + 3\dot{\psi} + \frac{k^2}{a^2}(a^2\dot{E} - aB)]. \tag{3.91}$$

3.5.2.2 Vector Perturbations

The divergence-free part of the 3-momentum follows the momentum conservation

$$\dot{\delta}q_i + 3H\delta q_i = k^2\delta P i_i, \tag{3.92}$$

where the vector part of the anisotropic stress is given by $\delta\Pi_{ij} = \partial_{(i}\Pi_{j)}$. The gauge-invariant vector metric perturbation is then linked to the divergence-free part of the momentum by the constraint equation

$$k^2(\dot{F}_i + \frac{S_i}{a}) = 2\kappa^2\delta q_i. \tag{3.93}$$

Thus the Einstein equations constrain the gauge-invariant vector metric perturbation to vanish in the presence of only scalar fields, for which the divergence-free momentum necessarily vanishes.

Eq. (3.93) shows that vector metric perturbations can be supported only by divergence-free momenta, but even then eq. (3.92) shows that the vector perturbations are redshifted away by the Hubble expansion on large scales unless they are driven by anisotropic stress.

3.5.2.3 Tensor Perturbations

Since there is no constraint equation for the tensor perturbations, these are the free gravitational degrees of freedom which refer to the gravitational waves. The spatial part of the Einstein equations implies to a wave equation for the amplitude of the tensor metric perturbations (3.73)

$$\ddot{h} + 3H\dot{h} + \frac{k^2}{a^2}h = 0. \tag{3.94}$$

This is similar to the wave equation of a massless scalar field (3.91) in an unperturbed FRW metric.

3.5.3 Primordial Power Spectra

Around the epoch of BBN, the universe is dominated by radiation composed of photons and 3 species of relativistic neutrinos. Moreover, there are non-relativistic baryons coupled tightly to the photons, and the coupled cold dark matter. There is probably also some form of vacuum energy, or dark energy, which eventually comes to dominate the energy density of the universe at present. All of these different components may have different density perturbations $\delta\rho_i$ which can be characterized by the gauge-invariant curvature perturbations

$$\zeta_i \equiv -\psi - \frac{H}{\dot{\rho}_i}\delta\rho_i \tag{3.95}$$

for each component. These individual ζ_i remain constant on large scales [155] as a consequence of local energy-conservation for all components and hence $\delta P_{nad,i} = 0$. Even when energy is not separately conserved for each component, it may still be possible to define a conserved perturbation on large scales concerning some other locally conserved quantity such as the baryon number so long as the net baryon number is conserved [164]. Perfect fluid models of non-interacting DE will also have ζ_{DE} = constant on large scales, but scalar field models of dark energy do not, in general, have a well-defined equation of state and hence ζ_{DE} = is not necessarily constant on large scales.
The total curvature perturbation ζ (3.67) is obtained by the weighted sum of the individual curvature perturbations

$$\zeta = \sum_i \frac{\dot{\rho}_i}{\dot{\rho}}\zeta_i. \tag{3.96}$$

This is often referred to as the adiabatic density perturbation, while the difference determines the isocurvature density perturbations

$$\mathcal{S}_i \equiv 3(\zeta_i - \zeta_\gamma). \tag{3.97}$$

By convention, the isocurvature perturbations are defined relative to the photons. Hence, these are also referred to as entropy perturbations. The factor of 3 arises so that $\mathcal{S}_B$ coincides with the perturbation in the local baryon-photon ratio

$$\mathcal{S}_B = 3(\zeta_B - \zeta_\gamma) = \frac{\delta(\frac{n_B}{n_\gamma})}{(\frac{n_B}{n_\gamma})}. \tag{3.98}$$

As a consequence of the conservation of the individual ζ_i, the relative isocurvature perturbation $\mathcal{S}_i$ remains constant on large scales. The total curvature perturbation only remains constant on large scales as the universe evolves from radiation to matter domination for adiabatic perturbations with $\mathcal{S}_i = 0$, in agreement with Eq. (3.83). The primordial power spectrum of density perturbations in the radiation-dominated era is given in terms of either $\zeta \simeq \zeta_\gamma$ or the comoving curvature perturbation $\mathcal{R}$ (3.67). By Combination of Eqs. (3.76) and (3.68), we obtain

$$\mathcal{R} = -\zeta - \frac{2\rho}{9(\rho + P)}(\frac{k}{aH})^2\Psi. \tag{3.99}$$

Notice that $\mathcal{R}$ and -ζ coincide on large scales. The power on a given scale is given by the k-space weighted contribution of modes with given wavenumber. Thus the power spectrum of scalar curvature perturbations, $\mathcal{R}$, is commonly given as

$$\mathcal{P}_\mathcal{R} \equiv \frac{4\pi k^3}{(2\pi)^3}|\mathcal{R}^2|. \tag{3.100}$$

An alternative notation widely used for the scalar power spectrum is the fractional density perturbation when adiabatic density perturbations re-enter the Hubble scale during the matter-dominated era

$$\delta_H^2 \equiv A_S^2 \equiv \frac{4}{25}\mathcal{P}_\mathcal{R}. \tag{3.101}$$

An isocurvature power spectrum is naturally defined as

$$\mathcal{P}_\mathcal{S} \equiv \frac{4\pi k^3}{(2\pi)^3}|\mathcal{S}^2|. \tag{3.102}$$

The cross-correlation between adiabatic and isocurvature perturbations can be given in terms of a correlation angle of Δ

$$\mathcal{C}_{\mathcal{RS}} \equiv \mathcal{R}_\mathcal{R}^{\frac{1}{2}}\mathcal{P}_\mathcal{S}^{\frac{1}{2}}\cos\Delta. \tag{3.103}$$

The tensor power spectrum is denoted by

$$\mathcal{P}_T \equiv 2\frac{4\pi k^3}{(2\pi)^3}|h^2|, \tag{3.104}$$

where the additional factor of 2 comes from adding the 2 independent polarizations of the graviton. Again there is an alternative notation also widely used [11, 153]

$$A_{GW}^2 \equiv \frac{1}{100}\mathcal{P}_T. \tag{3.105}$$

The scale dependence of the scalar power spectrum is given by the logarithmic derivative of the power spectrum

$$n_\mathcal{R} - 1 \equiv \left.\frac{d\ln\mathcal{P}_\mathcal{R}}{d\ln k}\right|_{k=aH} \tag{3.106}$$

which is evaluated at Hubble-radius crossing, $k = aH$. Notice that $n_\mathcal{R} = 1$ for a scale-invariant spectrum by convention. Also, the isocurvature spectrum is defined

$$n_{\mathcal{S}} \equiv \left.\frac{d\ln \mathcal{P}_{\mathcal{S}}}{d\ln k}\right|_{k=aH} \tag{3.107}$$

where $n_{\mathcal{S}} = 0$ for a scale-invariant spectrum. Similarly $n_T = 0$ for a scale-invariant tensor spectrum.

3.5.4 The Power Spectra in Single Field Inflation

In this section, we investigate the spectra of scalar and tensor perturbations for single field models. By writing the perturbed scalar field equation of motion (3.91) for a single scalar field in the spatially flat gauge (where $\psi = 0$) and also using the Einstein constraint equation, we obtain

$$\ddot{\delta}\varphi_\psi + 3H\dot{\delta}\varphi_\psi + \left(\frac{k^2}{a^2} + V_{\varphi\varphi} - \frac{\kappa^2}{a^3}\frac{d}{dt}\left(\frac{a^3\dot{\varphi}^2}{H}\right)\right)\delta\varphi_\psi = 0, \tag{3.108}$$

where $\delta\phi_\psi$ is gauge-invariant and defined by the Eq. (3.70). By introducing the new variables $v = a\delta\phi_\psi$ and $z = \frac{a\dot{\phi}}{H}$, the above relations reduces to [163, 162]

$$v'' + (k^2 - \frac{z''}{z})v = 0, \tag{3.109}$$

where a prime denotes a derivative with respect to conformal time $\tau \equiv \int a^{-1}dt$. The term of effective mass $\frac{z''}{z}$ can be expressed by [165, 163, 166]

$$\frac{z''}{z} = (aH)^2(2 + 5\epsilon - 3\eta + 9\epsilon^2 - 7\epsilon\eta + \eta^2 + \zeta^2) \tag{3.110}$$

where

$$\epsilon \equiv -\frac{\dot{H}}{H^2}, \qquad \eta \equiv 2\epsilon - \frac{\dot{\epsilon}}{2H\epsilon}, \qquad \zeta^2 \equiv \left(2\epsilon - \frac{\dot{\eta}}{H\eta}\right)\eta. \tag{3.111}$$

By neglecting the time-dependence of the slow-roll parameters and other terms of second and higher order in the slow-roll expansion, we have

$$\tau \simeq -\frac{1}{(1-\epsilon)aH}, \qquad \frac{z''}{z} = \frac{\nu_{\mathcal{R}}^2 - (\frac{1}{4})}{\tau^2}, \tag{3.112}$$

where $\nu_{\mathcal{R}} \simeq \frac{3}{2} + 3\epsilon - \eta$. Then, the general solution of Eq. (3.109) is expressed as a linear combination of Hankel functions

$$v \simeq \frac{\sqrt{\pi|\tau|}}{2} e^{i(1+2\nu_R)\pi/4}\left(c_1 H^1_{\nu R}(k|\tau|) + c_2 H^2_{\nu R}(k|\tau|)\right). \tag{3.113}$$

The power spectrum of scalar field perturbations is found by

$$\mathcal{P}_{\delta\varphi} \equiv \frac{4\pi k^3}{(2\pi)^3}|\frac{v}{a}|^2. \tag{3.114}$$

The power spectrum on small scales ($k \gg aH$) and large scales ($k \gg aH$) are found respectively by

$$\mathcal{P}_{\delta\phi} \simeq (\frac{k}{2\pi a})^2, \qquad \mathcal{P}_{\delta\phi} \simeq \left((1-\epsilon)\frac{\Gamma(\nu_R)H)}{\Gamma(3/2)2\pi}\right)^2 \left(\frac{|k\tau|}{2}\right)^{3-2\nu_{\mathcal{R}}}, \tag{3.115}$$

where we used the relation $H^1_\nu(k|\tau|) \to -(i/\pi)\Gamma(\nu)(k|\tau|/2)^{-\nu}$ when $k\tau \to 0$ and $\Gamma(3/2) = \sqrt{\pi}/2$. Also, for a massless field in de Sitter (where ϵ=η=0 and $\nu_R = 3/2$), we mimic the familar following relations

$$\mathcal{P}_{\delta\phi} \to (\frac{H}{2\pi})^2 \qquad for \qquad \frac{k}{aH} \to 0. \tag{3.116}$$

For the comoving curvature perturbation (3.67), we have $R = \frac{H}{\dot\phi}\delta\phi_\psi$ and the equation of motion (3.108) can be written as

$$\frac{1}{a^3\epsilon}\frac{d}{dt}(a^3\epsilon\dot{\mathcal{R}} + \frac{k^2}{a^2}\mathcal{R}) = 0. \tag{3.117}$$

For the large-scale limit ($k \to 0$), we obtain the solution

$$\mathcal{R} = C_1 + C_2 \int \frac{dt}{a^3\epsilon}, \tag{3.118}$$

where C_1 and C_2 are integration constants. In the majority of single-field inflationary models, the second term can be identified as a decaying mode and rapidly becomes negligible after the Hubble exit. Hence, the curvature perturbation becomes constant on super-Hubble scales. Then, by using Eq. (3.115) to set the initial amplitude shortly after Hubble-exit, we have

$$\mathcal{P}_{\mathcal{R}} = \left(\frac{H}{\dot\varphi}\right)^2 \mathcal{P}_{\delta\varphi} \simeq (\frac{H^2}{2\pi\dot\varphi})^2_{k=aH} \tag{3.119}$$

to leading order in slow-roll parameters. This can be written in terms of the value of the potential energy and its first derivative at Hubble-exit as

$$\mathcal{P}_{\mathcal{R}} = \left(\frac{\kappa^6}{12p^2}\frac{V^3}{V_\varphi^2}\right)_{k=aH}. \tag{3.120}$$

Since the curvature perturbation would be conserved on large scales in a single field model, one can rewrite the above relation at the first Hubble radius crossing with the one at the second Hubble radius crossing. The energy scale of inflation can be determined by the COBE normalization $\mathcal{P}_{\mathcal{R}} \simeq 2 \times 10^9$ for about 60 e-folds [167]. The spectral index, n_R, is given by

$$n_{\mathcal{R}} - 1 = 3 - 2\nu_{\mathcal{R}}. \tag{3.121}$$

To leading order in the slow-roll parameters we have

$$n_{\mathcal{R}} - 1 = -6\epsilon + 2\eta. \tag{3.122}$$

Since the parameters ϵ and η are much smaller than unity during slow-roll inflation, scalar perturbations generated in standard inflation are close to scale-invariant ($n_R \simeq 1$). For $n_R < 1$ and $n_R > 1$, the power spectrum refers to the spectrum red or blue tilt, respectively. Also, the running spectral index is defined as

$$\alpha_{\mathcal{R}} \equiv \frac{d\ln_{\mathcal{R}}}{d\ln k}|_{k=aH} \tag{3.123}$$

and is written in terms of the slow-roll parameters as

$$\alpha_{\mathcal{R}} = 16\epsilon\eta - 24\epsilon^2 - 2\zeta^2. \tag{3.124}$$

Since the tensor perturbations describe the propagation of gravitational waves, the wave equation for tensor perturbations can be written in terms of $u = ah/2\sqrt{\kappa}$, where h is the amplitude of the gravitational (3.73)

$$u'' + (k^2 - \frac{a''}{a})u = 0, \tag{3.125}$$

where

$$\frac{a''}{a} = (aH)^2(2-\epsilon). \tag{3.126}$$

In terms of the slow-roll parameters, we have

$$\frac{a''}{a} \simeq \frac{\nu_T^2 - (1/4)}{\tau^2}, \tag{3.127}$$

where $\nu_T \simeq \frac{3}{2} + \epsilon$. Similar to the curvature perturbation, by neglecting the time dependence of slow-roll parameter ϵ and using the same vacuum normalization (3.115) for small-scale modes in the asymptotic past, we obtain the tensor power spectrum (3.104) on large scales as

$$\mathcal{P}_T \simeq 8\kappa^2\left((1-\epsilon)\frac{\Gamma(\nu_T)}{\Gamma(\frac{3}{2})}\frac{H}{2\pi}\right)^2\left(\frac{|k\tau|}{2}\right)^{3-2\nu_T}. \tag{3.128}$$

Also, we can use the exact solution to the wave equation (3.94) in the long wavelength limit

$$h = D_1 + D_2\int\frac{dt}{a^3}, \tag{3.129}$$

where the constant amplitude D_1 on super-Hubble scales is determined by Eq. (3.128) shortly after Hubble-exit. Hence, to leading order in slow-roll, we have

$$\mathcal{P}_T \simeq 8\kappa^2\left(\frac{H}{2\pi}\right)^2_{k=aH} \simeq \frac{2}{3}\left(\frac{V\kappa^4}{\pi^2}\right)_{k=aH}. \tag{3.130}$$

The spectral index of tensor perturbations $n_T \equiv \frac{d\ln\mathcal{P}_T}{d\ln k}$ is obtained as

$$n_T = -2\epsilon \tag{3.131}$$

which is a red spectrum. Also, the running of the tensor tilt defined as $\alpha_T \equiv \frac{dn_T}{dlnk}$, is given by

$$\alpha_T = -4\epsilon(2\epsilon - \eta). \tag{3.132}$$

Another important inflationary parameters is the tensor-to-scalar ratio which is obtained as

$$r \equiv \frac{\mathcal{P}_T}{\mathcal{P}_R} \simeq 16\epsilon. \tag{3.133}$$

Finally, by combing the Eqs. (3.131) and (3.133), the consistency relation is given by [163]

$$r = -8n_T. \tag{3.134}$$

Notice that the strategy presented for a single field can be used for different inflationary models.

Chapter 4

Cosmic Microwave Background

No doubt discovering Cosmic Microwave Background (CMB) is one of the most significant achievements of the human throughout the history of cosmology. CMB photons are the relic photons of big bang when the universe had a critical condition in temperature, energy, and pressure. Now, after around 14 Gyr, we are receiving the photons even very low in temperature and energy. A CMB photon is like a traveler who has started a very long journey since the big bang and has traversed through all stages of the universe. Now, he has arrived at us with a backpack filled with valuable information from different scales of the universe. In this thesis, we devote the present chapter to explain some important features of CMB since it is recognized as the main source of inflationary effects. In other words, CMB observations aid us to perform a better judgment among inflationary models proposed in inflationary literature.

4.1 Discovery and Detection

After discovering Hubble expansion in 1930 [82], nuclear physicist George Gamow with Ralph Alpher and Robert Herman started to engage the idea of the hot big bang to explain the abundances of all elements in the universe [83, 84, 85, 86]. Later in 1948, Adler and Herman published a paper that predicted the temperature of the bath of relic photons of the big bang is around 5 Kelvin degrees. But, they did not present any mechanism to detect this temperature. In the early 1960s, when two American engineers (Arno Penzias and Robert Wilson) were testing their microwave detector at Bell laboratory, they experienced a specific and unexpected noise in the received signal that was identical in all directions of the sky. They were not able to describe what is the source of this unknown noise. After a while, Penzias explained the story of the mysterious noise to a radio astronomer Bernie Burke. Later, Burke heard about a talk by James Peebles describing how Robert Dicke's group was gearing up to measure radiation left from the early universe. Burke explained Penzias's discovery to Dicke and immediately, Dicke called with Penzias to acquire more information about the received noise. The noise was exactly the relic photons of the big bang what Dicke's group was seeking it. Eventually, in 1987, Penzias and Wilson received the Nobel prize physics because of their accidental discovery [78]. Discovering CMB photons is considered as one of the most significant observational proofs of HBB theory, as we discussed in the last section of chapter 2.
According to the thermal history of the universe presented in chapter 2, photons in radiation-dominated time were highly energetic and interacted hardly with matter so that electrons could not join to nuclei to form atoms. Later, the universe became colder and photons were not able to interact with the matter and the CMB photons released from the last scattering surface. At present, the CMB photons are low in energy and temperature.

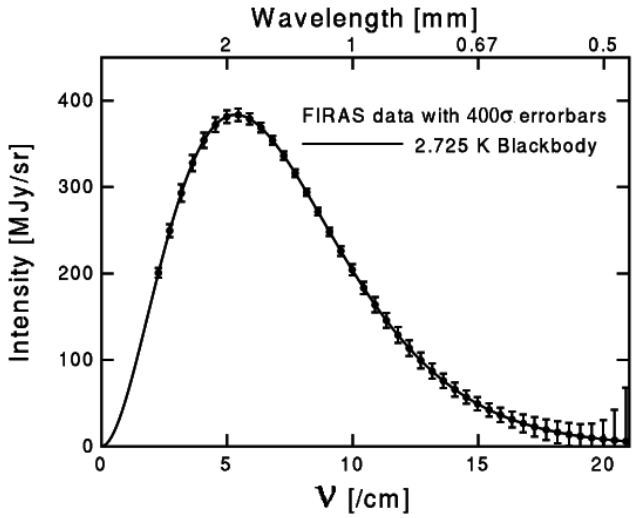

FIGURE 4.1: The CMB spectrum measured by the FIRAS instrument of the COBE satellite. The plot reveals that the CMB spectrum is very similar to a blackbody spectrum and the measured temperature of CMB is around 2.725 Kelvin degrees.

Let's review the main accomplished experiments on CMB to now. Between 1965 and 1990, the carried out measurements showed that the spectrum of CMB photons is almost similar to a blackbody spectrum and also, there were some measurements in high frequencies that seemed to indicate as infrared excess. In 1990, NASA launched the COsmic Background Explorer (COBE) satellite to investigate CMB and inferred background radiation. The measurements of the Far Infrared Absolute Spectrophotometer (FIRAS) instrument of the COBE confirmed that the CMB spectrum is exactly similar to a blackbody spectrum and also the temperature of CMB photons is around 2.72 Kelvin degrees. Moreover, the Differential Microwave Radiometer (DMR) instrument of the COBE approved the existence of tiny anisotropies in CMB photons (see Figure 4.1) [87, 88]. Two main researchers of CMB measurements, George Fitzgerald Smoot and John Cromwell Mather, received the Nobel Prize in Physics for their attempts on CMB discovery in 2006. Based on the achievements of COBE, many experiments performed to illuminate dark points of CMB. The main goal of these experiments was measurements of the acoustic picks of CMB anisotropies. The first pick detected by measurements of Balloon Observations Of Millimetric Extragalactic Radiation ANd Geophysics (BOOMERANG) and Millimeter Anisotropy eXperiment IMaging Array (MAXIMA) [168, 169, 170]. The first pick showed that our universe has a spatial curvature nearly flat rather than curved [171]. The next main experiment accomplished by Wilkinson Microwave Anisotropy Probe (WMAP) satellite to detect the second and even the third acoustic picks of CMB anisotropies [89]. Today, the Background Imaging of Cosmic Extragalactic Polarization (BICEP2) satellite has been engaged to detect the B-mode polarized photons generated during the inflationary era and Planck satellite is the main responsible for distinguishing B-mode polarized CMB photons from other polarized photons produced by different mechanisms [90]. In the following sections, we will present more information about the mentioned effects on CMB.

4.2 CMB Power Spectrum

The fundamental visible parameter of CMB is the intensity of radiation per unit frequency per polarization at each point of the sky. The polarization state of the radiation in a direction of sky denoted $\hat{n}$ is described by the intensity matrix $\langle E_i(\hat{n})E_j^*(\hat{n})\rangle$ where E is the electric field vector and the brackets denote time averaging.
The performed experiments on CMB reveal that the spectrum of received photons is analogous with the spectrum of isotropic blackbody radiation with an average temperature of $T = 2.725$ Kelvin degrees [172] across the sky at the 10^{-5} level and fractional polarization at the 10^{-6} level. The observables can be described by a temperature fluctuation matrix decomposed in the Pauli basis [173, 174]

$$P = C\langle E(\hat{n})E^{\dagger}(\hat{n})\rangle \tag{4.1}$$

or

$$P = \Theta(\hat{n})I + Q(\hat{n})\sigma_3 + U(\hat{n})\sigma_1 + V(\hat{n})\sigma_2 \tag{4.2}$$

where the Stokes parameters (Θ,Q,U,V) are dimension-less. Note that the circular polarization V is absent cosmologically and under a counterclockwise rotation of the coordinate axes by ψ, $Q \pm iU \longrightarrow e^{\mp 2i\psi}(Q \pm iU)$. The temperature and polarization fields are decomposed as [175, 176]

$$\Theta_{lm} = \int d\hat{n} Y^*_{lm}(\hat{n})\Theta(\hat{n}) \tag{4.3}$$

or

$$E_{lm} \pm iB_{lm} = -\int d\hat{n}\, {}_{\pm 2}Y^*_{lm}(\hat{n})[Q(\hat{n}) \pm iU(\hat{n})] \tag{4.4}$$

in terms of the complete and orthogonal set of spin harmonic functions, ${}_sY_{lm}$, which are eigenfunctions of the Laplace operator on a rank s tensor [177]. For small sections of sky, the spin-harmonic expansion becomes a Fourier expansion with $Y_{lm} \longrightarrow e^{il.\hat{n}}$ and ${}_{\pm}Y_{lm} \longrightarrow -e^{\mp 2i\phi_l}e^{il.\hat{n}}$, where ϕ_l is the azimuthal angle of the Fouier wavevector l. Note that the E and B modes are then simply the Q and U states in the coordinate system defined by l [178], i.e. B-modes have a polarization orientation at 45° to the wavevector. $E(\hat{n}) = \sum E_{lm}Y_{lm}(\hat{n})$ and $B(\hat{n}) = \sum B_{lm}Y_{lm}(\hat{n})$ describe scalar and pseudoscalar fields on the sky.
The main observable of CMB spectrum is the two point correlation between fields X,$X' \in \{\Theta, E, B\}$

$$\langle X^*_{lm}X'_{l'm'}\rangle = \delta_{ll'}\delta_{mm'}C_l^{XX'} \tag{4.5}$$

and are described by power spectra C_l as long as the fields are statistically isotropic. If parity is also conserved then B has no correlation with Θ or E. Also, the power spectra contain all of the statistical information about the fields when the fluctuations are Gaussian distributed.

4.3 Primary CMB Anisotropies

Now, we focus on the primary factors of temperature and polarization anisotropies of CMB photons.

4.3.1 Temperature Anisotropy

The results of COBE confirmed the temperature anisotropies of CMB photons in large angular scales in addition to proving the fact that the CMB spectrum is similar to a blackbody with the average temperature around T=2.72 Kelvin degrees. The next balloons and satellites engaged in clarifying the physics of CMB anisotropies and their effects on large scale structure. The most part of temperature anisotropy produced on the last scattering surface at decoupling time through the adiabatic density perturbations of the inflationary epoch. According to the thermal history of the universe presented in chapter 2, before the recombination era and CMB decoupling, the universe is filled by the photon-baryon fluid along with DM interacting only through gravity and weak nuclear activities not electromagnetic. The density perturbations produced during the inflationary epoch in DM are grown due to the expansion of the universe and then the gravitational effect is resisted by the pressure of photons in the fluid collapse of the photon-baryon fluid. The pressure acts as a restoring force. In other words, as an overdensity fluid, the fluid felt into the potential well of DM is compressed until the collapse is stopped by the photon pressure and then rebounds until the expansion is blocked by the weight of fluid and the gravity of DM as a rarefaction fluid. The strife between the gravity of DM and the pressure of photon in the fluid can be simulated as a harmonic oscillator that produces acoustic or sound waves in the fluid. In some scales where the last scattering of CMB photons occurs in the sound waves horizon, the oscillation is dragged into the last scattering surface and CMB photons with different modes acquire different phases of oscillation. The CMB photons in the overdensity or rarefaction modes are associated with the peak of the CMB spectrum and behave differently in temperature while the troughs correspond to maximum veracity where the compression is neutral. In compression mode, the hot CMB photons release energy through the asserted resistance force against the gravity of DM and turn to the cold spots. In contrast, the hot CMB photons in rarefaction mode do not require to lose as much energy in climbing out of a shallower potential well and are known as the hot spots. Let us explain the phenomenon with more details.

4.3.1.1 Cosmological Parameters

We begin with a review of the cosmological parameters presented in chapter 2 and expressed in this chapter. The expansion of the universe is described by the scale factor $a(t)$, close to unity at present, and the Hubble constant $H_0 \approx 70\ h$ km sec^{-1} Mpc^{-1}. The mean densities of different components of the universe control $a(t)$ and are typically expressed today in units of the critical density Ω_i, with an evolution $\rho_i \propto a^{-3(1+w_i)}$, where $w_i = p_i/\rho_i$ with p_i is the pressure. In particular the CMB photons have $w_\gamma = 1/3$ and so $\rho_\gamma \propto a^{-4}$ or $T \propto a^{-1}$. The quantities $\Omega_i h^2$ are proportional to the physical density of the species today. We will be interested in the baryonic component $\Omega_b h^2$ and the total non-relativistic matter $\Omega_m h^2$, where the difference is made up of cold dark matter. We also search for a dark energy [179, 180] component Ω_e, with an equation of state parameter w_e considered as a cosmological constant (Ω_Λ, $w_\Lambda = -1$). We represent the total density as $\Omega_{tot} = \sum_i \Omega_i$.

4.3.1.2 Sound Waves

By expansion of the universe, CMB photons start to become cold and eventually they no longer have sufficient energy to overcome the binding energy of hydrogen $B = 13.6$ eV to keep the medium ionized. Then, CMB photons are released and travel

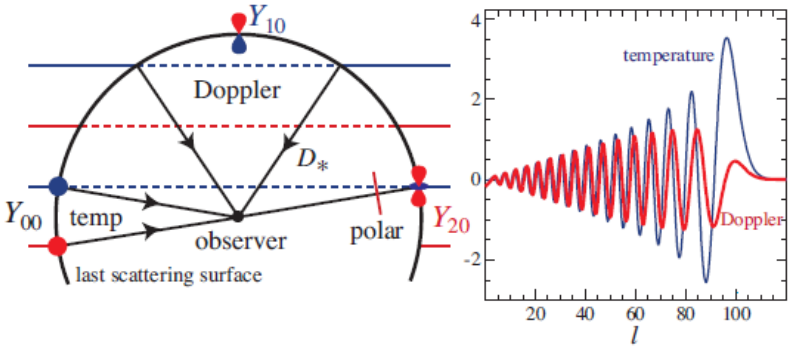

FIGURE 4.2: Left: the main sources of anisotropy are the effective local temperature with a monopole structure (Y_{00}), the Doppler effect with a dipole structure (Y_{10}) and the quadrupole source of polarization (Y_{20}) decomposed into plane waves. Right: the projection of the sources involves a coupling of the plane wave angular dependence or momenta with that of the source.

to the observer. This era is called recombination and is occurred rapidly around $a_* \approx 10^{-3}$ at an energy scale of $\sim 1/3$ eV as can be seen by the equilibrium Saha equation

$$\frac{x_e^2}{1-x_e} = \frac{n_e n_p}{n_H n_b} = \frac{1}{n_b}\left(\frac{m_e T}{2\pi}\right)^{3/2} e^{-B/T} \tag{4.6}$$

or

$$\approx 3\times 10^{15}\left(\frac{\Omega_b h^2}{0.02}\right)^{-1}\left(\frac{B}{T}\right)^{3/2} e^{-B/T} \tag{4.7}$$

where x_e is the ionization fraction of hydrogen and we have neglected a small contribution from helium. Notice that the low T/B of the transition, mainly caused by the low baryon-photon ratio of the universe, is sufficient that photons in the tail of the blackbody distribution be energetic enough to ionize hydrogen.
The properties of the baryon-photon plasma on the last scattering surface, where CMB photons are released from matter, directly translate into the observable primary temperature and polarization anisotropies in the CMB. These properties are handled by Thomson scattering of photons off of free electrons with a differential cross-section of

$$\frac{d\sigma}{d\Omega} = \frac{3}{8\pi}|\hat{E}'.\hat{E}|^2\sigma_T \tag{4.8}$$

where $\sigma_T = 8\pi\alpha^2/3m_e$ is the Thomson cross section, $\hat{E}'$ and $\hat{E}$ denote the incoming and outgoing directions of the electric field or polarization vector. By considering polarization and incoming angle, the comoving mean free path of a photon in the electrons is

$$\dot{\tau}^{-1} = \frac{1}{n_e\sigma_T a} \approx 2.5\left(x_e\frac{\Omega_b h^2}{0.02}\right)^{-1}\left(\frac{a_*}{10^{-3}}\right)^2 Mpc \tag{4.9}$$

which is relatively small by cosmological standards. Overdots here and below represent derivatives with respect to conformal time. Electrons are coupled to baryons

by Coulomb interactions and the scales larger than $\dot{\tau}^{-1}$, the photon-baryon plasma can be considered a nearly perfect fluid [181]. In particular, rapid scattering keeps the photons isotropic in the baryon rest frame and so sets its dipole moment equal to the baryon velocity.
Regarding the tight coupling approximation, the CMB is described by the local temperature or monopole, in space $\Theta_{00}(x)$, the dipole $\Theta_{lm}(x)$ and a residual quadrupole moment $\Theta_{2m}(x)$. Besides, the photons experience a gravitational redshift from gravitational potentials and gravitational waves.
Now, let us consider the spatial temperature perturbation $\Theta(x) \equiv \sqrt{4\pi}\Theta_{00}(x)$, where the normalization convention reflects that of Y_{lm}, on a last scattering surface considered to be infinitely sharp at a comoving distance D_* (see Figure 4.2). In a flat universe, the spatial field may be represented by its Fourier harmonics

$$\Theta(\hat{n}) = \int dD\Theta(x)\delta(D - D_*) \tag{4.10}$$

$$= \int \frac{d^3k}{(2\pi)^3}\Theta(k)e^{ik.D_*\hat{n}} \tag{4.11}$$

In an spatially curved universe, the plane waves must be replaced by the eigenfunctions of the Laplace operator to account for a change in the relationship between distance and angle that we discuss below. Also to achieve high precision in the predictions, the delta function must be replaced by the visibility function $\dot{\tau}e^{-\tau}$, the probability of a photon last scattering in a distance interval dD to account for the finite duration of recombination. By expanding the plane waves spherical harmonics, we obtain

$$\Theta_{lm} = \int \frac{d^3k}{(2\pi)^3}\Theta(k)4\pi i^l j_l(kD_*)Y_{lm}(\hat{k}) \tag{4.12}$$

The power spectrum of the local temperature anisotropy governed by the spatial temperature field at recombination, can be expressed by

$$\langle\Theta^*(k)\Theta(k') \equiv (2\pi)^3\delta(k - k')P_T(k)\rangle \tag{4.13}$$

so that

$$C_l^{\Theta\Theta} = 4\pi \int \frac{dk}{k} j_l^2(kD_*)\frac{k^3P_T(k)}{2\pi^2} \tag{4.14}$$

Note that the quantity $k^3P_T/2\pi^2$ is the contribution per log interval to the variance of the temperature $\sigma^2 = \int d^3k/(2\pi)^3P_T$. For a slowly-varying log power, the integral in Eq. (4.14) can be performed analytically

$$\frac{(l(l+1))}{2\pi}C_l^{\Theta\Theta} \equiv \left(\frac{\Delta_T^2}{T^2}\right) \approx \frac{k^3P_T(k)}{2\pi^2}|_{k=l/D_*} \tag{4.15}$$

and so it is convenient to represent the anisotropy by the rms temperature contribution per log interval Δ_T . It is also the contribution to the anisotropy variance per log interval in l for $l \gg 1$. We also define the analogous quantities to describe the polarization fields (Δ_P) and the temperature-polarization cross correlations $(l(l+1))C_l^{\Theta E}/2\pi)$.

4.3.1.3 Fluid Dynamics

As we learned from the previous section, the critical variables are the monopole or temperature fluctuation $\Theta(k) \equiv \sqrt{4\pi}\Theta_{00}(k)$, the dipole or bulk velocity $v_\gamma(k) = -i\sqrt{4\pi/3}\Theta_{10}(k)$, and the quadrupole or anisotropic stress $\pi_\gamma(k) = -(12/5)\sqrt{4\pi/5}\Theta_{20}(k)$. For convenience we have chosen the coordinate system in which $z \| k$ so that the plane waves are azimuthally symmetric and stimulate only the $m = 0$ mode (see Fig. 4.2). Likewise, we have suppressed the vector dependence of the bulk velocity by the same assumption $v_\gamma = -iv_\gamma\hat{k}$. The analogous quantities for the baryons are the density perturbation δ_b and bulk velocity v_b. For gravity, we choose a conformal Newtonian representation (see e.g. [182]) where the gravitational potential perturbations are defined by the Newtonian potential Ψ (time-time metric fluctuation) and the curvature fluctuation Φ (space-space metric fluctuation $\approx -\Psi$).
Covariant conservation of energy and momentum requires that the photons and baryons satisfy separate continuity equations

$$\dot{\Theta} = -\frac{k}{3}v_\gamma - \dot{\Phi}, \qquad \dot{\delta}_b = -kv_b - 3\dot{\Phi} \tag{4.16}$$

and coupled Euler equations

$$\dot{v}_\gamma = k(\Theta + \psi) - \frac{k}{6}\pi_\gamma - \dot{\tau}(v_\gamma - v_b) \tag{4.17}$$

$$\dot{v}_b = -\frac{\dot{a}}{a}v_b + k\Psi + \dot{\tau}(v_\gamma - v_b)/R \tag{4.18}$$

where $R = (p_\rho + \rho_b)/(p_\gamma + \rho_\gamma) \approx 3\rho_b/4\rho_\gamma$ is the photon-baryon momentum density ratio. We have neglected a small correction to the anisotropic stress term in a curved universe.
The Eqs. (4.16) represent particle number conservation. For the baryons, $\rho_b \propto n_b$. For the photons, $T \propto n_\gamma^{1/3}$, which explains the $1/3$ in the velocity divergence term. The $\dot{\Phi}$ terms come from the fact that Φ is a perturbation to the scale factor and so they are the perturbative analogues of the cosmological redshift and density dilution from the expansion. The Euler equations have similar interpretations. The expansion makes particle momenta decay as a^{-1}. The cosmological redshift of T accounts for this effect in the photons. For the baryons, it becomes the expansion drag on v_b ($\dot{a}/a$ term). Potential gradients $k\Psi$ generate potential flow. For the photons, stress gradients in the fluid, both isotropic ($k\delta p_\gamma/(p_\gamma + \rho_\gamma) = k\Theta$) and anisotropic ($k\pi_\gamma$) counter infall. Thomson scattering exchanges momentum between the two fluids ($\dot{\tau}$ terms).
For scales much larger than the mean free path $\dot{\tau}^{-1}$, the Euler equation may be expanded to leading order in $k/\dot{\tau}$, such that the photons are isotropic in the baryon rest frame $v_\gamma = v_b$ and so the joint Euler equation becomes

$$\frac{d}{d\eta}[(1+R)v_\gamma] = k[\Theta + (1+R)\Psi] \tag{4.19}$$

Combining this with the Eqs. (4.16) leads to the oscillator equation [183]

$$\frac{d}{d\eta}[(1+R)\dot{\Theta}] + \frac{k^2}{3}\Theta = -\frac{k^2}{3}(1+R)\Psi - \frac{d}{d\eta}[(1+R)\dot{\Phi}] \tag{4.20}$$

and a small residual anisotropic stress or quadrupole that tracks the evolution of the fluid velocity [184]

$$\pi_\gamma = \frac{32k}{15\dot{\tau}} v_\gamma \tag{4.21}$$

This dependence reflects the fact that a local quadrupole can arise from a gradient in the velocity field, for example as photons from two hot crests of a plane wave fluctuation meet at the trough in between (see Figure 4.2 left), but is suppressed by scattering.
Eq. (4.20) is the fundamental relation for acoustic oscillations. The change in the momentum of the photon-baryon fluid is determined by a competition between the pressure restoring and gravitational driving forces which causes the system to oscillate around its equilibrium. Note that the frequency of the oscillation

$$w^2 = \frac{k^2}{3(1+R)} = c_s^2 k^2 \tag{4.22}$$

where c_s is the sound speed of the fluid.

4.3.1.4 Initial Conditions

The simplest inflationary models make a set of definite predictions for the initial conditions of the acoustic oscillations and hence their successful observation provides strong support for the inflationary paradigm. Quantum fluctuations in the scalar field that drives inflation imprints a nearly spectrum of Gaussian curvature (potential) fluctuations $k^3 P_\Phi / 2\pi^2 \propto k^{n-1}$ where $n \approx 1$ [185, 186, 187] on a spatially flat background metric. Gravitational infall into these initial potentials eventually generates all of the structure in the universe. Quantum fluctuations in the gravitational wave degrees of freedom also produce a nearly scale-invariant spectrum of fluctuations whose power depends on E_i^4 where E_i is the energy scale of inflation [188, 189].
A Newtonian gravitational potential $\Psi \approx -\Phi$ necessarily imparts an initial temperature perturbation since Ψ represents a spatially varying time-time perturbation to the metric away from coordinates where the temperature is homogeneous. The perturbation is equivalent to a change in the scale factor since

$$a \propto t^{2/3(1+p/\rho)} \tag{4.23}$$

which then produces a change in the temperature perturbation from the cosmological redshift $T \propto a^{-1}$ of

$$\Theta = -\frac{2}{3(1+p/\rho)} \Psi \tag{4.24}$$

or $-\psi/2$ in the radiation dominated era [190, 191]. We call $\Theta + \Psi$ the effective temperature since it also accounts for the redshift a photon experiences when climbing out of a potential well, also known as the Sachs-Wolfe effect [192]. In the matter dominated epoch, $\Theta + \Psi = \Psi/3$.
There are three important aspects of these results. First, inflation sets the temporal phase of all wavemodes by starting them all at the initial epoch. We shall see that this predicts a coherent set of peaks in the CMB spectrum with a definite phase. Cosmological defect models predict a more random distribution of acoustic phases which produces incoherent acoustic phenomena [193, 194, 195]. Defects can be now be ruled out as a primary mechanism for structure formation in the universe. More

generally, without inflation or some other modification to the matter-radiation dominated universe, curvature perturbations cannot be generated outside the apparent horizon and so build up only by the causal motion of matter. This generally entails at least a delay in temporal phase of the oscillations which is not observed.
Secondly, since the power spectrum of the effective temperature is directly related to scale-invariant curvature fluctuations from inflation, Eq. (4.15) implies the acoustic oscillations should also be approximately scale invariant in amplitude in the tight coupling regime. Observations are in excellent agreement with this fundamental prediction with tight constraints on the index $n = 0.94^{+0.11}_{-0.04}$ (see [196, 197, 198]). We will therefore base the discussion of the acoustic phenomenology on models with nearly scale-invariant initial curvature fluctuations as predicted by inflation.
Finally, the scale-invariant gravitational wave background leads to a quadrupolar distortion in the CMB temperature field just like its effect on a ring of test masses. Because the quadrupole axes lie in the plane transverse to the wavevector, this quadrupole anisotropy leads to B-mode polarization as the tight coupling approximation breaks down. A measurement of B-modes from gravitational waves would determine the energy scale of inflation E_i but its strong scaling with E_i implies that it can only open a relatively small window between a few 10^{15} – few 10^{16} GeV for possible detection [199].

4.3.1.5 Silk Damping

The photon diffusion or diffusion damping is a process reducing the anisotropies in CMB temperature in the early universe and was first proposed by Joseph Silk in 1968. Therefore sometimes it is called *Silk damping*. As we learned from the last section, the CMB photons would be specified as hot and cold spots when the acoustic waves of photon-baryon fluid created by the gravitational collapse of primordial density perturbations have been dragged into the last scattering surface. Hence, the CMB photons with maximum compression are known as cold modes through losing energy and those with maximum rarefaction are entitled as hot modes. Silk damping says that when the photons in the fluid transit from the overdense point (maximum compression) to the underdense (maximum rarefaction), they push electrons along and these, in turn, pulls on protons by the Coulomb force. Hence, the Silk damping process acts as a frictional force for the photons and wastes their energy. It means that the temperature difference between CMB photons in overdense and underdense points is decreased by the viscosity of the photon-baryon fluid.

4.3.1.6 Acoustic Peaks Information

Now, let's review the physical information of acoustic peaks.

- **First Peak**

  The reason for the first peak is that sound waves of the right frequency would have had just enough time to reach maximum compression when the universe became transparent. The angle we see on the sky depends only on the angular diameter distance to the surface of last scattering. In turn, the angular diameter distance depends on how light rays converge or diverge: in a spatially closed universe ($\Omega_k < 0$) they converge, and in a spatially open universe they diverge, relative to a flat universe. Now, consider two rays that i) both terminate at one point at redshift $z = 0$ and ii) end on either side of a region of fixed size at redshift $z \approx 1100$, then compared to a flat universe, a closed universe will

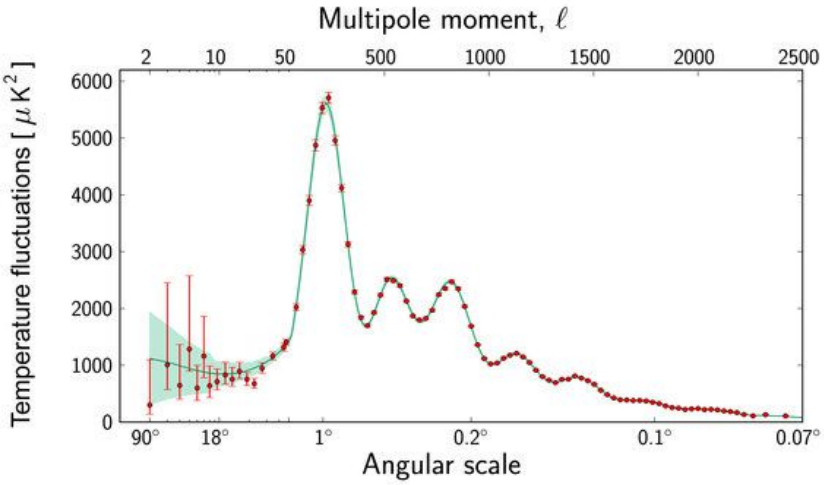

FIGURE 4.3: The main features of the temperature power spectrum including the first 5 acoustic peaks and damping tail have been measured.

give a larger apparent angle, and an open universe will give a smaller apparent angle. This means that the primary information coming from the angular location of the first acoustic peak reveals some realities about the geometry of the universe.

- **Second Peak**

  The second peak is much lower the first. To understand this, consider a potential well with masses and springs. In this case, we consider the "springs" as the pressure and the "masses" as provided by the baryons. The maximum compression achieved by the masses at the bottom of the potential well depends on the pressure and the mass and is larger for larger mass. In contrast, the maximum rarefaction is independent of the masses. This implies that if we were to fix everything but increase the baryon density, the compression peaks (first, third, fifth, etc.) would increase in height relative to the rarefaction peaks (second, fourth, sixths, etc.). As a result, the ratio of second to first peak amplitude tells us about Ωb, which is the ratio of the baryon density to the critical closure density.

- **Higher Peaks**

  In a universe filled with only radiation, when a perturbation reached maximum compression, as it expanded out the photons would continue to redshift with the universe, hence the gravitational potential would decay away. This would allow the temperature perturbation to be much greater than it would otherwise, and hence would enhance the peaks. In contrast, non-relativistic matter does not redshift and this lead to relatively smaller fluctuations and smaller peaks.
  In the presence of radiation and matter, specially at smaller scale factor, radiation becomes relatively more important. Therefore, higher frequencies (and thus higher multipoles) should have an enhancement in amplitude. That is not to say that higher harmonics should have larger amplitudes in an absolute sense, just that the strength is relatively increased. The actual dependence

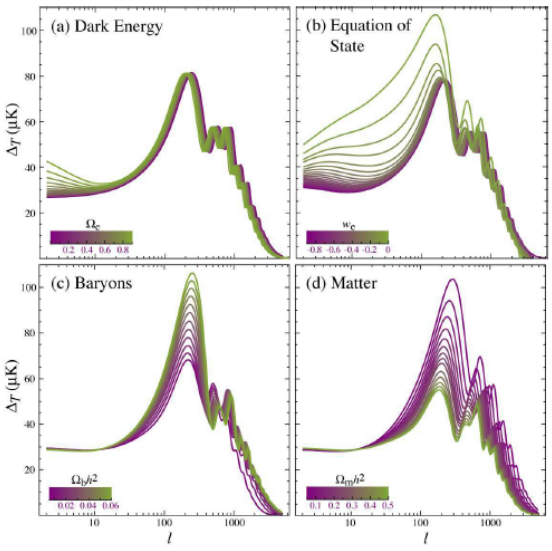

FIGURE 4.4: The temperature power spectrum versus the cosmological parameters, including the energy density of the dark energy today Ωe in units of the critical density, the equation of state parameter of the dark energy w_e, the physical baryon density $\Omega_b h^2$ and the physical matter density $\Omega_m h^2$.

of amplitude on multiple is therefore a measure of the total density of non-relativistic matter in the universe, since that quantity affects the transition between radiation domination and matter domination. The multipoles of the peaks are also affected because as you recall the expansion rate of the universe is different in the relativistic regime (where $a \propto t^{1/2}$) from the non-relativistic regime (where $a \propto t^{2/3}$). This also affects the angular size of the universe (as we see it) for a given physical size or time after the Big Bang.

4.3.2 Polarization Anisotropy

Besides temperature fluctuations, the CMB photons are described with polarization anisotropies generated by both scalar and tensor perturbations of the inflationary era. The E-mode polarization (a divergence-free mode) of CMB is created by Thompson scattering of the CMB photons from free electrons in a heated plasma at last scattering time and the B-mode polarization (a curl-free mode) is normally produced by the gravitational waves generated during cosmic inflation.
The main source of E-mode polarization of CMB can be addressed to the recombination era through Thompson scattering of CMB photons from free electrons at that time. Let's see how could it happen. The primary anisotropy of CMB occurred in the last scattering surface when the created acoustic oscillation in the photon-baryon fluid due to scalar perturbations stretched to the recombination era. Therefore, some of the photons had the opportunities to catch the oscillation and turned to the hot and cold spots on the last scattering surface. Based on the Thompson scattering, a photon colliding with a free electron can be E-mode polarized due to the interaction of the electric component of the incoming photon with the electron. Then, the vibrating electron, in turn, emits radiation in all directions with the frequency of the inbound photon. Now, consider that two isotropic CMB photons interacting with a free electron are E-mode polarized by Thompson scattering at last scattering

time. Then, the product radiation remains unpolarized since the isotropic orthogonal polarizations balance each other. However, in the presence of a quadrupole anisotropy for incoming CMB photons, linear polarization is generated by Thompson scattering. An additional mechanism to produce E-mode polarization of CMB can be found in the reionization epoch where the photons emitted from the first stars ionize the hydrogen atoms wherein the CMB photons are E-mode polarized by Thomspon scattering from the liberated electron.
The produced tensor perturbations during the inflationary epoch as the main responsible for the primary gravitational waves can create B-mode polarization of CMB photons in addition to E-mode polarization. Hence, they are known as one of the most important probes of cosmic inflation in modern cosmology. Notice that the B-mode polarized CMB photons are contaminated by some large scale factors as foreground effects and this is a great challenge in CMB data analysis. One of these effects is the gravitational lensing of E-mode polarized photons wherein the polarization of photons crossing from the gravitational well of a massive object, changes from E-mode to B-mode.

4.4 Secondary CMB Anisotropies

Here, we review some secondary factors of temperature anisotropies of CMB photons.

4.4.1 Reionization Era

One of the most significant factors of the late time anisotropies occurred during the ionization era of the universe through the Thompson scattering of CMB photons by the released electrons from the ionization process of hydrogen. First, let's review what happened during the ionization period. As we studied before, in the recombination era, the CMB photons were not able to interact with free electrons due to losing the energy in an expanding universe and then the electrons found the opportunity to combine with the hydrogen and helium nuclei generated during BBN epoch in order to form the atoms of the light elements. After the decoupling of the CMB photons in the last scattering surface, the universe entered the dark age where was unobservable across much of the electromagnetic spectrum and any short wavelength radiation that might have been emitted was quickly absorbed by the atomic gas. Gradually, the gravitational collapse of overdense regions on the medium filled with the light elements caused to form the first sky objects like stars, galaxies, and quasars. Then, the high energy photons emitted from these structures ionized the present hydrogen atoms and as a result, electrons released. This process continued until the bulk of the universe was ionized completely and the light at many wavelengths could escape from the early galaxies and quasars, revealing the distant universe that we see today with optical and infrared telescopes. The secondary anisotropy of CMB happened by Thompson scattering of CMB photons from the free electrons liberated during the ionization epoch and it created two effects on CMB. First was erasing the temperature anisotropies occurred in small scales and the second was inducing the polarization anisotropies on large scales.

4.4.2 Sunyaev-Zel'dovich Effect

The Sunyaev–Zel'dovich (SZ) effect was first introduced by Rashid Sunyaev and Yakov B. Zel'dovich in 1969 as a large scale effect producing anisotropies on CMB

due to the scattering of CMB photons by rapidly moving electrons in the hot gas in clusters of galaxies. The SZ factor can distort the CMB photons by two main processes, including thermal and kinetic effects. In thermal case, the gas falling into the gravitational potential well of the galaxy clusters is ionized by increasing the temperature and then CMB photons passing through the plasma are inverse Compton scattered by high energy electrons. The kinetic effect is caused by the motion of the galaxy clusters concerning the rest frame of the CMB. The motion of the high energy electrons in the hot intercluster plasma induces a Doppler shift to the scattered photons.

4.4.3 Integrated Sachs-Wolfe Effect

Proposed by Rainer K. Sachs and Arthur M.Wolfe in 1967, the Integrated Sachs-Wolf (ISW) effect is known as a large scale factor for CMB anisotropy through the presence of the gravitational well created from supermassive objects in the late time universe. Based on GR principles, the gravitational field of supercluster contained from the numerous galaxies curves the surrounded spacetime significantly. Hence, the CMB photons crossing through the supercluster are constrained to path this gravitational well and get a boost in energy when entering the well. Naturally, the photons would lose that extra energy as they climb back out of the well. In other words, by crossing the CMB photons through such structure, they are blue and redshifted when they respectively enter and exit the gravitational potential well. The net effect is zero except in the case of a non-static universe. If we restrict our attention to the late time universe dominated by DE, we can realize that the gravitational well of the supercluster would be stretched gradually by the late-time acceleration of the universe. Hence, the CMB photons existing from the well lose less energy than the value they gained in entering the well and their temperature would be raised than other CMB photons.

Chapter 5

Non-Minimal Large Field Inflationary Models

As we learned, the standard inflationary models based on the scalar field can be classified into three main types, including Large field, small field, and hybrid models. Among these models, the large field case in which inflaton rolls down slowly with a large value from the top of the potential and approaches to the minimum point of potential with a small value has been investigated in a wide range of cosmological literature [200, 201, 202, 203, 204, 205, 206, 207] since it has only one free parameter to be fixed compared to the other two inflationary models with additional parameters and also it shows the comparable values of the scalar-to-tensor with observations. On the other hand, the idea of Non-Minimal Coupling (NMC) between gravity and a scalar field in many cosmological scenarios has been considered as an unavoidable part of the gravitational theory in particular in the presence of some quantum corrections in curved spacetime and even it is necessary at the classical level for renormalization of gravity [208, 209, 210]. Hence, the large field inflationary models in the context of NMC idea have been investigated in many inflationary papers [211, 212, 213, 214, 215, 216, 217, 218, 219, 220, 221, 222, 223, 224, 225, 226, 227, 228, 229, 230, 231, 232, 233, 234, 235, 236, 237, 238, 239, 240]. In this chapter, we provide constraints from CMB anisotropies data on the coupling constant ξ in the context of inflationary models with a power-law potential as a generator form of large filed models. Notice that the chapter is based on our research paper published on the Physics of Dark Universe Journal.

5.1 NMC Idea

Before starting the analysis of our model, let us devote the present section to introduce the idea of NMC. Due to cosmic inflation, the universe experienced a rapid and huge expansion in early time in which the generated scalar and tensor perturbations are responsible for structure formation of the universe and primordial gravitational waves, respectively. The standard formalism of inflation in GR is established on a scalar field (inflaton) as the sole component of the universe driven inflation and it decays at the end of inflation to other particles to take place the reheating process. The form of inflationary action in GR is given by

$$S = \int d^4x\sqrt{-g}\left(\frac{R}{2\kappa^2} - \frac{1}{2}g^{\mu\nu}\partial_\mu\varphi\partial_\nu\varphi - V(\varphi)\right), \tag{5.1}$$

where $V(\varphi)$ is the potential of the inflaton. In the above expression, there is a minimal coupling between the Ricci scalar R as the gravitational sector and scalar field φ as the matter sector. However, according to the NMC idea, we are forced to examine

the interaction of these two fields in particular when quantum corrections in curved space-time are considered [241] and even at the classical level, it seems that NMC idea plays a great role for renormalization of gravitational theory [242, 243, 244]. The effect of NMC can be considered by the term of $\frac{1}{2}\xi\varphi^2 R$ in the form of inflationary action as

$$S = \int d^4x\sqrt{-g}\left(\frac{R}{2\kappa^2} - \frac{1}{2}g^{\mu\nu}\partial_\mu\varphi\partial_\nu\varphi - V(\varphi) + \frac{1}{2}\xi\varphi^2 R\right), \tag{5.2}$$

where ξ is the coupling constant and its value deeply affects the validity of inflationary models [213, 245, 246, 208]. Let's take a look at the action (5.2) to realize the critical role of the NMC term in the inflationary analysis. The present form of NMC term $\frac{1}{2}\xi\varphi^2 R$ is very conventional among classical theories of φ and metric theories of gravity, but sometimes it can be distractive for inflationary scenario especially when a mass term for inflaton as $\frac{1}{2}m^2\varphi^2$ is assumed in the form of action. In such a condition, the NMC term plays the role of an effective mass for inflaton and leads to some derivations from slow-rolling down behavior of inflaton [247, 213, 248, 208].
As we pointed out the viability of an inflationary model is strongly affected by bearing of NMC term and in particular by the values of the coupling constant ξ in which usually the NMC makes it harder to reach inflation with typical potentials used in the case of minimal coupling [247, 213, 215]. To verify this claim, we can refer to the role of the NMC term as an effective mass of inflaton when the mass term of inflaton $\frac{1}{2}m^2\varphi^2$ is considered in the form of action since it can distort the slow-rolling down of inflaton in our inflationary model. Another reason to support our statement is corresponded to counting the coupling constant as a free parameter in our investigation. The very common attitude to ξ is that it can be found as a fine-tuning parameter restricted by observations in order to achieve an inflationary solution. The results show that for a particular potential, in some range of ξ, we access to inflation and for other values, we lose the inflationary solution. Although having such a viewpoint to the coupling constant is beneficial in our model, it can be problematic when some potentials with constant parameters are considered in the study. The fine-tuning of ξ by observational datasets to achieve inflation leads to the fine-tuning of the constant parameters of the potential under consideration and then these parameters might take the values which are not consistent with their predictions from particle physics. As an example, we can refer to the self-counting constant in chaotic inflationary potential $V = \lambda\varphi^4$ wherein the constraint coming from observations is $\lambda < 10^{-12}$, but the energy scale predicted by particle physics is much higher. In fact, the constraint on λ is reduced by fine-tuning coupling constant ξ [216, 249, 245, 246, 250]. Hence, besides the fine-tuning approach to the coupling constant, one can find some prescriptions of ξ fixed by particle physics. In such a viewpoint, the value of ξ depends on the nature of the scalar field and the gravitational theory under investigation [208]. Notice that the first attitude to ξ will be used when there is no fixed value from theoretical predictions. In the next sections, we present the inflationary paradigm in the Jordan frame as the non-minimal frame and also in the Einstein frame as the conformal frame by using the conformal transformation discussed in the appendix A.

5.2 The Inflationary Analysis in Jordan Frame

Now let us introduce the formulation of the inflationary analysis with NMC. We can start with varying the form of the action (5.2) with respect to the metric $g_{\mu\nu}$ as

$$(1-\kappa^2\xi\varphi^2)G_{\mu\nu}=\kappa^2T_{\mu\nu}(\varphi), \tag{5.3}$$

where

$$T_{\mu\nu}(\varphi)=\partial_\mu\varphi\partial_\nu\varphi-\frac{1}{2}g_{\mu\nu}\partial^\gamma\varphi\partial_\gamma\varphi-V(\varphi)g_{\mu\nu}+\xi\left(g_{\mu\nu}\Box\varphi^2-\partial_\mu\partial_\nu\varphi^2\right) \tag{5.4}$$

and by varying the action with respect to the scalar field φ, we obtain the Klein-Gordon equation as the motion equation of inflaton by

$$\ddot{\varphi}+3H\dot{\varphi}+\xi R\varphi+\frac{dV}{d\varphi}=0. \tag{5.5}$$

Clearly, in the case of minimal coupling $\xi=0$, the above expressions reduce to the familiar forms of GR. The field equations (5.3) can be rewritten to three different approaches. First, one can transfer the term of $\xi\varphi^2G_{\mu\nu}$ to the right-hand side and make the typical form of the Einstein equations as

$$G_{\mu\nu}=\kappa^2\bar{T}_{\mu\nu}(\varphi), \tag{5.6}$$

where

$$\bar{T}_{\mu\nu}(\varphi)=T_{\mu\nu}(\varphi)+\xi\varphi^2G_{\mu\nu}. \tag{5.7}$$

In the second approach, we deal with a φ-dependent gravitational constant as

$$G_{eff}\equiv\frac{G}{1-\kappa^2\xi\varphi^2} \tag{5.8}$$

then the field equation (5.3) takes the following form

$$G_{\mu\nu}=\kappa^2_{eff}T_{\mu\nu}(\varphi), \tag{5.9}$$

where

$$\kappa^2_{eff}\equiv 8\pi G_{eff} \tag{5.10}$$

Another possibility for the field equation is counting the gravitational constant as a φ-independent coupling. Then, the field equation is given by

$$G_{\mu\nu}=\kappa^2\hat{T}_{\mu\nu}(\varphi), \tag{5.11}$$

where

$$\hat{T}_{\mu\nu}(\varphi)=\frac{T_{\mu\nu}(\varphi)}{1-\kappa^2\xi\varphi^2}. \tag{5.12}$$

By taking a look at the field equations in two approaches (5.9) and (5.11), one can find there two singularities for a scalar field in the case of $\xi<0$ by

$$\pm\,\varphi_{critical}=\pm\frac{1}{\kappa\sqrt{|\xi|}}. \tag{5.13}$$

These critical values are known as barriers which the scalar field can not cross. Notice that by restricting ourselves to the form of (5.3), we can escape from the singularities and all values of the scalar field are approachable in our analysis.
Let's check the validity of the conservation law for the energy-momentum tensor when the NMC term. For the field equation (5.11), the conservation law $\nabla^{\nu}\hat{T}_{\mu\nu} = 0$ is consistent as a consequence of the contracted Bianchi identities $\nabla^{\nu}G_{\mu\nu} = 0$. However, for the first form of the field equations (5.3), the contracted Bianchi identities leads to

$$\nabla^{\nu}T_{\mu\nu} = -\frac{2\kappa^2\xi\varphi}{1-\kappa^2\xi\varphi^2}T_{\mu\nu}\nabla^{\nu}\varphi. \tag{5.14}$$

One can find that the conservation law can be valid when the scalar field φ takes the constant value.
Now that we studied the role of NMC in the inflationary paradigm, it would be nice to investigate the appropriated dynamical equations. By using the spatially flat FLRW metric (2.9) and then solving the field equation (5.11) for the scalar field as perfect fluid matter, we obtain the energy density and pressure of inflaton expressed in the Eqs. (2.16) and (2.17) by

$$\rho = \frac{1}{(1-\kappa^2\xi\varphi^2)}\left(\frac{\dot{\varphi}^2}{2} + V(\varphi) + 6\xi H\varphi\dot{\varphi}\right), \tag{5.15}$$

$$P = \frac{1}{(1-\kappa^2\xi\varphi^2)}\left(\frac{\dot{\varphi}^2}{2} - 2\xi\dot{\varphi}^2 - V(\varphi) - 2\xi\varphi\ddot{\varphi} - 4\xi H\varphi\dot{\varphi}\right). \tag{5.16}$$

When $\xi = 0$, the above expressions are reduced to the Eq. (3.13). In such a case, the acceleration condition $\rho + 3P < 0$ is given as

$$(1-3\xi)\dot{\varphi}^2 - V(\varphi) - 3\xi\varphi(\ddot{\varphi} + H\dot{\varphi}) < 0 \tag{5.17}$$

and by using the Klein-Gordon equation (5.5), one can find

$$(1-3\xi)\dot{\varphi}^2 - V(\varphi) + 3\xi^2R\varphi^2 + 6\xi H\varphi\dot{\varphi} + 3\xi\varphi\frac{dV}{d\varphi} < 0. \tag{5.18}$$

To present a better analysis, we focus on the case of $\xi \leq \frac{1}{6}$ which covers many prescriptions proposed by particle physics. Then, the above condition is diminished to

$$V - \frac{3\xi\varphi}{2}\frac{dV}{d\varphi} > 0. \tag{5.19}$$

In order to apply the slow-roll approximation (3.16) and (3.17) for the model in Jordan frame, we use the HSR parameters (3.19). Also, the number of e-folds can be found by the Eq. (3.21).

5.3 The Inflationary Analysis in Einstein Frame

By using the conformal transformation (A.1) for the action (5.2) with $\Omega^2 = 1+\kappa^2\xi\varphi^2$, the form of action in the Einstein frame is given by

$$S_E = \int d^4x\sqrt{-\hat{g}}\left(\frac{\hat{R}}{2\kappa^2} - \frac{1}{2}F^2(\varphi)\hat{g}^{\mu\nu}\partial_{\mu}\varphi\partial_{\nu}\varphi - \hat{V}(\hat{\varphi})\right). \tag{5.20}$$

Also, the redefined scalar field $\hat{\varphi}$ in the Einstein frame is connected to inflaton as

$$F^2(\varphi) \equiv \left(\frac{d\hat{\varphi}}{d\varphi}\right)^2 \equiv \frac{1+\kappa^2\xi\varphi^2(1+6\xi)}{(1+\kappa^2\xi\varphi^2)^2} \tag{5.21}$$

and we deal with an effective potential

$$\hat{V}(\hat{\varphi}) \equiv \frac{V(\varphi)}{(1+\kappa^2\xi\varphi^2)^2}. \tag{5.22}$$

When considering the Einstein frame, we need to transform our coordinate system using,

$$dT = \sqrt{\Omega}dt, \qquad \hat{a} = \sqrt{\Omega}a \tag{5.23}$$

to obtain the metric in the FRW form. By considering the FRW metric $d\hat{s}^2 = dT^2 - \hat{a}^2(T)\delta_{ij}dx^i dx^j$, the field equations in the Einstein frame take the form

$$\hat{H}^2 = \frac{\kappa^2}{3}\left[\frac{1}{2}\left(\frac{d\hat{\varphi}}{dT}\right)^2 + \hat{V}(\hat{\varphi})\right], \quad \frac{\ddot{\hat{a}}}{\hat{a}} = -\frac{\kappa^2}{3}\left[\left(\frac{d\hat{\varphi}}{dT}\right)^2 - V(\varphi)\right], \quad \frac{d^2\hat{\varphi}}{dT^2} + 3\hat{H}\frac{d\hat{\varphi}}{dT} + \frac{d\hat{V}}{d\hat{\varphi}} = 0. \tag{5.24}$$

Then the slow-roll conditions can straightforwardly written as,

$$\dot{\hat{\varphi}}^2 \ll \hat{V}, \qquad \ddot{\hat{\varphi}} \ll 3\hat{H}\dot{\hat{\varphi}} \tag{5.25}$$

and the slow-roll parameters are defined accordingly

$$\hat{\epsilon} \equiv \frac{1}{2\kappa^2}\frac{\hat{V}'(\hat{\varphi})^2}{\hat{V}(\hat{\varphi})}, \quad \hat{\eta} \equiv \frac{1}{\kappa^2}\frac{\hat{V}''(\hat{\varphi})}{\hat{V}(\hat{\varphi})}, \quad \hat{\zeta} \equiv \frac{1}{\kappa^2}\left(\frac{\hat{V}'(\hat{\varphi})\hat{V}'''(\hat{\varphi})}{\hat{V}^2(\hat{\varphi})}\right)^{1/2}, \tag{5.26}$$

where primes now imply a derivative with respect to the redefined scalar field $\hat{\varphi}$. Since we will calculate the inflationary parameters up to the first order of slow-roll parameters, we can be assured that the conformal transformation is valid and two frames provide the same results. Consequently, for the following analysis, we use the Einstein frames instead of the Jordan frame in order to escape the difficulties of the NMC term.

5.4 Large Field Potential

The large field models referred to as chaotic inflation, are characterized by the monomial potential $V(\varphi) = c\varphi^n$ wherein the number n is usually a positive integer (it was realized in [251] that this type of scenario can emerge in the context of supergravity). One can find that the majority of inflationary models with power-law potential consider integer powers to investigate the inflationary phase (see the references in the preface of this chapter). Another possibility to fix n is some interesting fractional values corresponded to axion monodromy inflation [252, 253, 254, 255, 256, 257]. The microphysical structure of string theory provides a rather simple and general mechanism for large field inflation, monodromy, in which an underlying periodicity of the theory ensures that as the inflaton field traverses many cycles with sub-Planckian period $2\pi f \ll M_P$, the potential energy increases over each cycle, but much of the remaining physics essentially repeats itself. We point out that the chaotic inflationary potentials with fractional powers are more favored than the simplest versions of

chaotic inflation. However, these models suffer from a firm field theoretical foundation which seems difficult to be achieved from usual field theories [258, 259]. The chaotic inflation with a fractional power-law potential in the context of supergravity is presented in Refs. [260, 261, 262]. Also, the fractional power-law potentials derived in string theories are presented in [252]. In [201, 203], people studied the chaotic inflationary models with fractional powers in the framework of strongly coupled supersymmetric gauge theories. In the following, we consider both types of powers integer and fractional which have been studied in different inflationary literature in particular in Planck 2015 and the BICEP2/Keck array data releases [263, 264] in which $p = 1, 2, 3, 4$ and $p = 2/3, 4/3$ are considered for integer and fractional powers, respectively.
Let's begin the analysis in the Einstein frame with writing the effective potential for the general form of power-law potential as

$$\hat{V}(\hat{\varphi}) = \frac{c\varphi^n}{(1+\kappa^2\xi\varphi^2)^2}. \tag{5.27}$$

Under the slow-roll approximation, the slow-roll parameters (5.26) can be written as

$$\hat{\epsilon} = \frac{\xi(n^2+2n(n-4)\kappa^2\xi\varphi^2+(n-4)^2\kappa^4\xi^2\varphi^4)}{2\kappa^2\xi\varphi^2(1+\kappa^2\xi\varphi^2(1+6\xi))}, \tag{5.28}$$

$$\hat{\eta} = \frac{1}{\kappa^2\xi\varphi^2(1+\kappa^2\xi\varphi^2(1+6\xi))^2}\Big[n(n-1)\xi+\xi\Big(3n^2(1+2\xi)-2n(5+6\xi)-4\Big)\kappa^2\xi\varphi^2$$
$$+\xi\Big(3n^2(1+4\xi)-n(17+60\xi)+12\Big)\kappa^4\xi^2\varphi^4+\xi\Big((1+6\xi)(n^2-8n+16)\Big)\kappa^6\xi^3\varphi^6\Big]$$

and

$$\hat{\zeta}^2 = \frac{1}{\kappa^4\varphi^4(1+\kappa^2\xi\varphi^2(1+6\xi))^4}$$
$$\Big[\Big(n^2(n-1)(n-2)\Big)+\Big(6n^4(1+2\xi)-n^3(31+54\xi)+2n^2(11+18\xi)-8n\Big)\kappa^2\xi\varphi^2+$$
$$+\Big(3n^4(12\xi^2+16\xi+5)-2n^3(108\xi^2+153\xi+55)+4n^2(72\xi^2+63\xi+41)+$$
$$+24n(1+4\xi)\Big)\kappa^4\xi^2\varphi^4+\Big(4n^4(36\xi^2+30\xi+5)-2n^3(612\xi^2+546\xi+95)+$$
$$+4n^2(612\xi^2+612\xi+119)-4n(288\xi^2+120\xi+34)-32(7+12\xi)\Big)\kappa^6\xi^3\varphi^6+$$
$$+\Big(3n^4(72\xi^2+34\xi+5)-n^3(2376\xi^2+1152\xi+175)+2n^2(3744\xi^2+1944\xi+317)+$$
$$-4n(1296\xi^2+756\xi+158)-192(1+9\xi)\Big)\kappa^8\xi^4\varphi^8+\Big(6n^4(24\xi^2+10\xi+1)+$$
$$-n^3(1944\xi^2+822\xi+83)+n^2(8784\xi^2+3852\xi+398)-n(13248\xi^2+6528\xi+720)+$$
$$+288(1+6\xi)\Big)\kappa^{10}\xi^5\varphi^{10}+\Big((1+6\xi)^2(n^4-16n^3+96n^2-256n+256)\Big)\kappa^{12}\xi^6\varphi^{12}\Big].$$

Let us now consider the value of the inflaton field at the end of inflation φ_e and at

the start of inflation, i.e., at the time of Hubble Crossing, φ_{HC}. Setting $\hat{\epsilon} = 1$ at the end of inflation, and considering the quantity $\beta^2 = \kappa^2\xi\varphi_e^2$, using Eq. (5.28) we get

$$\beta^2 = \frac{\left(-(1 - n(n-4)\xi) \pm \sqrt{1 + 8\xi n + 12\xi^2 n^2} \right)}{(2(1+6\xi) - \xi(n-4)^2)}. \tag{5.31}$$

On the other hand, defining $m^2 = \kappa^2\xi\varphi_{HC}^2$, we can write the slow-roll parameters at the beginning of inflation as

$$\hat{\epsilon} = \frac{\xi n + m^2(4-n)^2}{2m^2(1 + m^2(1+6\xi))}, \tag{5.32}$$

$$\hat{\eta} = \frac{\xi}{m^2(1+m^2(1+6\xi))^2}\Big[n(n-1) + \Big(3n^2(1+2\xi) - 2n(5+6\xi) - 4\Big)m^2 + \\ + \Big(3n^2(1+4\xi) - n(17+60\xi) + 12\Big)m^4 + \Big((1+6\xi)(n^2 - 8n + 16)\Big)m^6\Big]$$

and

$$\hat{\zeta}^2 = \frac{\xi^2}{m^4(1+m^2(1+6\xi))^4} \\ \Big[\Big(n^2(n-1)(n-2)\Big) + \Big(6n^4(1+2\xi) - n^3(31+54\xi) + 2n^2(11+18\xi) - 8n\Big)m^2 + \\ + \Big(3n^4(12\xi^2+16\xi+5) - 2n^3(108\xi^2+153\xi+55) + 4n^2(72\xi^2+63\xi+41) + 24n(1+4\xi)\Big)m^4 + \\ + \Big(4n^4(36\xi^2+30\xi+5) - 2n^3(612\xi^2+546\xi+95) + 4n^2(612\xi^2+612\xi+119) + \\ -4n(288\xi^2+120\xi+34) - 32(7+12\xi)\Big)m^6 + \Big(3n^4(72\xi^2+34\xi+5) - n^3(2376\xi^2+1152\xi + \\ +175) + 2n^2(3744\xi^2+1944\xi+317) - 4n(1296\xi^2+756\xi+158) - 192(1+9\xi)\Big)m^8 + \\ + \Big(6n^4(24\xi^2+10\xi+1) - n^3(1944\xi^2+822\xi+83) + n^2(8784\xi^2+3852\xi+398) + \\ -n(13248\xi^2+6528\xi+720) + 288(1+6\xi)\Big)m^{10} + \Big((1+6\xi)^2(n^4 - 16n^3 + 96n^2 \\ -256n + 256)\Big)m^{12}\Big].$$

The amount of inflation is usually specified considering the number of e-folds N defined as the logarithm of the ratio of the value of the scale factor at the end and beginning of inflation,

$$e^N \equiv \frac{\hat{a}(\hat{t}_e)}{\hat{a}(\hat{t}_{HC})} = \frac{a(t_e)}{a(t_{HC})}\frac{\Omega(x_{end})}{\Omega(x_{HC})}. \tag{5.35}$$

where the hat denotes, as usual, the Einstein frame. It is well-know that the number of e-folds is strongly connected with the amount of perturbations generated during inflation and. Therefore, to the cosmological parameters describing them. In NMC

theories, however also the coupling constant ξ enters those definitions. In the following, we will consider several value of the exponential n for the potential $V(\phi)$, for each of them we will derive the relations connecting the coupling constant ξ and the number of e-folds N to the cosmological parameters r, n_s and n_{run}. We will then use these relations to obtain constraints on the parameter space of ξ and N using Planck data.

5.4.1 Case of $n = 4$

Probably the most famous form of large field inflationary potential is $V(\varphi) = \frac{1}{4}\lambda\varphi^4$. It corresponds to the quartic potential where the inflaton has a self-interacting feature. It is assumed that $\lambda < 1$ because otherwise, the interaction would become so strong that φ would not correspond to a physical particle (the non-perturbative regime). On the other hand, values of λ much smaller than 1 are not usually envisaged since they would represent fine-tuning. The slow-roll parameters for this potential in the Einstein frame are given by Eqs. (5.32) to (5.34)

$$\hat{\epsilon} = \frac{8\xi}{m^2(1+m^2(1+6\xi))} \tag{5.36}$$

$$\hat{\eta} = \frac{4\xi\left(3+m^2(1+12\xi)-2m^4(1+6\xi)\right)}{m^2(1+m^2(1+6\xi))^2} \tag{5.37}$$

and

$$\hat{\zeta}^2 = \frac{32\xi^2\left(3+2m^2(-2+3\xi)-15m^4(1+6\xi)-6m^6(1+6\xi)^2+2m^8(1+6\xi)^2\right)}{m^4(1+m^2(1+6\xi))^4}. \tag{5.38}$$

In order to connect the number of e-folds with the inflaton field and the slow-roll parameters, we need an expression for the scale factor $a(t)$ during inflation. This can be found in solving the Fiedmann equation (2.16) without the cosmological constant under the slow-roll conditions (3.16) and (3.17), which left us with

$$\frac{a(t)}{a_0} = \left(\frac{1+\kappa^2\xi\varphi^2(t)}{1+\kappa^2\xi\varphi_0^2}\right)^{5/4} \exp\left((\frac{1+6\xi}{8})\kappa^2(\varphi_0^2-\varphi^2(t))\right), \tag{5.39}$$

where the subscribe "0" denotes the value of the inflaton field and scale factor at some time t_0. Taking t_0 to be the time of the Hubble crossing and using Eq. (5.35), one obtains

$$e^N = (\frac{1+\beta^2}{1+m^2})^{5/4} \exp\left(\frac{1+6\xi}{8\xi}(m^2-\beta^2)\right) \tag{5.40}$$

for the e-folds number. If we now impose the consistency condition for large-potentials field $m \geq \beta$, we find the relation

$$m^2 = \beta^2 + \frac{8\xi N}{1+6\xi}. \tag{5.41}$$

In what follows we restrict our analysis on the effect of non-minimal coupling under the approximation $|\xi| \ll 1$ and $\psi \ll 1$ $m^2 \ll 1$. In this case the slow-roll parameters rewrite

$$\hat{\epsilon} \simeq \frac{8\xi}{m^2}, \qquad \hat{\eta} \simeq \frac{4\xi\Big(3+m^2(1+12\xi)-2m^4(1+6\xi)\Big)}{m^2} \tag{5.42}$$

and

$$\hat{\zeta}^2 \simeq \frac{32\xi^2\Big(3+2m^2(-2+3\xi)-15m^4(1+6\xi)-6m^6(1+6\xi)^2+2m^8(1+6\xi)^2\Big)}{m^4} \tag{5.43}$$

We can now derive from the above equations the expressions for the scalar spectral index n_s, its running $\alpha_s = dn_s/d\log k$ and the tensor-to-scalar ratio r such as

$$\hat{n}_s = 1-6\hat{\epsilon}+2\hat{\eta} \simeq 1-\frac{1}{N}(3-8\xi N), \tag{5.44}$$

$$\hat{\alpha}_s = 16\hat{\epsilon}\hat{\eta}-24\hat{\epsilon}^2-2\hat{\zeta}^2 \simeq \frac{1}{N^2}(-3+96\xi N-64\xi^2N^2) \tag{5.45}$$

and

$$\hat{r} = 16\hat{\epsilon} \simeq \frac{16}{N}(1-8\xi N) \tag{5.46}$$

The above equations can be reduced to $\hat{n}_s \simeq 1-\frac{3}{N}$, $\hat{\alpha}_s \simeq -\frac{3}{N^2}$ and $\hat{r} \simeq \frac{16}{N}$ in the limit of $\xi \to 0$.

5.4.2 Case of $n \neq 4$ with $n \geq 1$

Following the same strategy, we continue here the analysis of the power-law potentials by considering other values of n. For potential with $n \neq 4$ we cannot use Eq. (5.40), therefore we need to restart by the definition of the e-folds number in the Einstein frame

$$N = -\sqrt{\frac{\kappa^2}{2}}\int \frac{1}{\sqrt{\hat{\epsilon}}}d\hat{\varphi} \tag{5.47}$$

which once integrated, gives

$$e^N = \frac{1+\beta^2}{1+m^2}^{\frac{5}{4}}\left(\frac{n+(n-4)\beta^2}{n+(n-4)m^2}\right)^{\frac{(n-4)-n(1+6\xi)}{8\xi(n-4)}}, \tag{5.48}$$

where β^2 is defined by Eq. (5.31). Assuming again the consistency condition $m \geq \beta$, we obtain

$$\left(\frac{n+(n-4)\beta^2}{n+(n-4)m^2}\right) \simeq e^{-2\xi N(n-4)} \quad for \quad n \neq 4. \tag{5.49}$$

With this equation we can specify the expressions for the scalar spectral index n_s, its running $\alpha_s = dn_s/d\log k$, and the tensor-to-scalar ratio r for each of the potential we are considering in the present work with $n \neq 4$.

5.4.2.1 Case of $V \propto \varphi$

In the case of $n = 1$ and with the assumption $|\xi| \ll 1$, we have from Eq. (5.49)

$$m^2 \simeq \frac{1}{3}1-(1-3\beta^2)e^{-6\xi N} \simeq 2N\xi. \tag{5.50}$$

For the spectral index, its running and the tensor-to-scalar ratio, using Eqs. (5.42) and (5.43), we have

$$\hat{n}_s \simeq 1-\frac{1}{2N}(3+8\xi N), \quad \hat{\alpha}_s \simeq \frac{1}{2N^2}(-3+6\xi N+4\xi^2N^2), \quad \hat{r} \simeq \frac{4}{N}(1-12\xi N). \tag{5.51}$$

Also, for $\xi \to 0$ the above equations are reduced to $\hat{n}_s \simeq 1-\frac{3}{2N}$, $\hat{\alpha}_s \simeq -\frac{3}{2N^2}$ and $\hat{r} \simeq \frac{4}{N}$.

5.4.2.2 Case of $V \propto \varphi^2$

The simplest form of chaotic inflation is a non-interacting (free) field with a potential $V = \frac{1}{2}\mu^2\varphi^2$ where μ is the mass of the inflaton. The field equations have a time-independent, spatially homogeneous, solution $\varphi = 0$, which represents the vacuum. Plane waves, related to oscillations around the vacuum state, correspond after quantization to non-interacting particles φ, which have mass μ. Another feature of this potential is that in the presence of NMC between gravity and inflaton, the mass can be deformed to an effective mass by the shape of NMC term it is consequently more difficult to achieve slow-roll inflation. In the case of $n = 2$ and with the assumption $|\xi| \ll 1$, we have from Eq. (5.49)

$$m^2 \simeq 1-(1-\beta^2)e^{-4\xi N} \simeq 4\xi N. \tag{5.52}$$

The scalar spectral index, its running and tensor-to-scalar ratio are

$$\hat{n}_s \simeq 1-\frac{2}{N}(1+\frac{4}{3}\xi^2N^2), \quad \hat{\alpha}_s \simeq \frac{2}{N^2}(-1+4\xi N-96\xi^2N^2), \quad \hat{r} \simeq \frac{8}{N}(1-8\xi N). \tag{5.53}$$

and $\hat{n}_s \simeq 1-\frac{2}{N}$, $\hat{\alpha}_s \simeq -\frac{2}{N^2}$ and $\hat{r} \simeq \frac{8}{N}$ when $\xi \to 0$.

5.4.2.3 Case of $V \propto \varphi^3$

In the case of $n = 3$ and with the assumption $|\xi| \ll 1$, we have from Eq. (5.49)

$$m^2 = 3-(3-\beta^2)e^{-2\xi N} \simeq 6\xi N \tag{5.54}$$

In this case, the inflationary parameters take the following form

$$\hat{n}_s \simeq 1-\frac{1}{2N}(5-8\xi N), \quad \hat{\alpha}_s \simeq \frac{5}{6N^2}(-3+42\xi N-468\xi^2N^2), \quad \hat{r} \simeq \frac{12}{N}(1-4\xi N). \tag{5.55}$$

For $\xi \to 0$, the above equations are expressed as $\hat{n}_s \simeq 1-\frac{5}{2N}$, $\hat{\alpha}_s \simeq -\frac{5}{2N^2}$, and $\hat{r} \simeq \frac{12}{N}$.

5.4.2.4 Case of $V \propto \varphi^{\frac{2}{3}}$

In the case of $n = 2/3$ and with the assumption $|\xi| \ll 1$, we have from Eq. (5.49)

$$m^2 = \frac{1}{5}1-(1-5\beta^2)e^{-20\xi N/3} \simeq \frac{4}{3}\xi N. \tag{5.56}$$

The first order of spectral index, its running and tensor-to-scalar ratio are therefore

$$\hat{n}_s \simeq 1-\frac{4}{3N}(1+4\xi N), \quad \hat{\alpha}_s \simeq \frac{4}{81N^2}(-27+84\xi N+464\xi^2 N^2), \quad \hat{r} \simeq \frac{8}{9N}(3-40\xi N). \tag{5.57}$$

In the limit $\xi \to 0$, we have $\hat{n}_s \simeq 1-\frac{4}{3N}$, $\hat{\alpha}_s \simeq -\frac{4}{3N^2}$ and $\hat{r} \simeq \frac{8}{3N}$.

5.4.2.5 Case of $V \propto \varphi^{\frac{4}{3}}$

In the case of $n = 4/3$ and with the assumption $|\xi| \ll 1$, we have from Eq. (5.49)

$$m^2 = \frac{1}{2}1-(1-2\beta^2)e^{-\frac{16}{3}\xi N} \simeq \frac{8}{3}\xi N \tag{5.58}$$

the inflationary parameters, we have

$$\hat{n}_s \simeq 1-\frac{1}{3N}(5+8\xi N), \quad \hat{\alpha}_s \simeq \frac{5}{81N^2}(-27+48\xi N-704\xi^2 N^2), \quad \hat{r} \simeq \frac{16}{9N}(3-32\xi N). \tag{5.59}$$

The above equations for $\xi \to 0$ are turned to $\hat{n}_s \simeq 1-\frac{5}{3N}$, $\hat{\alpha}_s \simeq -\frac{5}{3N^2}$ and $\hat{r} \simeq \frac{16}{3N}$.

5.5 Analysis Method

CMB constraints on inflationary parameters can be performed by letting the parameters n_S, r and α_S to vary freely and by then comparing the predictions of a specific inflationary model with the allowed region of the parameters. Our approach here is different: an inflationary model is imposed *ab initio*, and we investigate the constraints on the parameters of that specific model. In particular, as we discussed in the previous section, our inflationary parameters are reduced to two: the number of e-foldings N and the coupling term ξ. While this kind of analysis is indeed more model dependent, it may provide constraints that are not achievable in a more general study where any value of n_S, r and α_S is permitted. Given a likelihood that compare data with theory [1] constraints on cosmological parameters are extracted using the publicly available version of the Monte Carlo Markov Chain (MCMC) code Cosmological Monte Carlo (CosmoMC) [266] (Nov2016 version [2]), based on the Metropolis-Hastings algorithm with chains convergence tested by the Gelman and Rubin method. We compare our theoretical models with data using the 2015 Planck likelihood, containing temperature and polarization spectra and their cross-correlation. We consider two cases for the Planck data: In the Planck high-ℓ case we consider only the CMB data at high multipoles $\ell > 30$ and we impose an external prior on the optical depth $\tau = 0.055 \pm 0.02$, i.e., we remove the large scale temperature and polarization data. In the Planck TTTEEE case, we consider the full Planck 2015 temperature and polarization dataset, including also the low multipoles and we disregard the prior on τ. Eventually, those two datasets are combined with the Bicep-Keck-Planck (BKP) B-mode likelihood [267]. We modified the code CosmoMC to accommodate N and ξ as independent parameters they are randomly sampled in a given range, and to calculate the, now, derived parameters as function of the

[1] The theoretical models are computed using the latest version of the Boltzmann integrator CAMB [265]

[2] https://cosmologist.info/

Parameter	Prior
ω_b	$[0.02 \div 0.25]$
ω_c	$[0.1 \div 0.3]$
θ_s	$[0.5 \div 2]$
τ	$[0.01 \div 0.8]$
$\ln(10^{10} A_s)$	$[3.01 \div 3.2]$
N	$[20 \div 100]$
ξ	$[-0.2 \div 0.2]$

TABLE 5.1: Range of the flat prior on the parameters varied in the MCMC analysis.

inflationary ones throughout Eqs. (5.44) to (5.46) or $n = 4$ and Eqs. (5.51), (5.53), (5.55), (5.57) and (5.59) for $n \neq 4$. Note that in the publicly available version of CosmoMC the parameters r, n_s and α_s are independent. An hard prior is imposed on the tensor-to-scalar ratio to assure is positiveness since for $N\xi > \alpha^{-1}$, where α is a constant value depending on the model we are considering, r is a negative quantity. The spectral index of tensor perturbations instead is evaluated using the inflationary consistency condition $n_t = -r/8$ as in the standard version of CosmoMC. Along with the number of e-folds N and the coupling constant ξ, we allow to vary the baryon $\omega_b = \Omega_b h^2$ and the CDM density $\omega_c = \Omega_c h^2$, the angular size of the sound horizon at decoupling θ_s, the reionization optical depth τ and the amplitude A_s and the spectral index n_s of scalar perturbations. The assumed flat priors on these parameters are reported in Table 5.1.

5.6 The Results

The constraints on the inflationary parameters from the Planck 2015 data and from their combination with the BICEP2/Keck Array release are reported in Tables 5.2 and 5.3. In Figures 5.1 and 5.2 we show the contour plots at 68% and 95% C.L. from the Planck highℓ and Planck TTTEEE data, respectively. In Figures 5.3 and 5.4 we show the analogous constraints obtained now with the inclusion of the BKP dataset. Let us first consider the results obtained from the Planck 2015 datasets (with and without the low multipoles data) alone. As we can see from the first column of Tables 5.2 and 5.3 and also Figure 5.1, we found no evidence for a coupling ($\xi \neq 0$) from the Planck high-ℓ+τ_{prior} data in any of the power-law models considered. Moreover, by looking at the reported values of the χ^2_{eff}, we see that models with $n > 2$ have a $\Delta\chi^2 \sim 4$ with respect to models with $n = 1$, i.e., they provide a worse fit to the data at about two standard deviations. In practice, the Planck high-ℓ data alone is unable to rule out significantly models with $n = 2, 3, 4$. This fact is mainly due to the poor constraints on the tensor to scalar ratio r achievable from this dataset. It is however compelling, that all models, except for the $n = 2/3$ case, shows an indication for a negative running $n_{run} \sim -0.001$. This result is not due to an actual presence of running in the data but to the specific correlations between n_{run} and the other inflationary parameters present in the models considered. So one should be careful in claiming any general indication for n_{run} from this analysis. However, this shows either the potential of future measurements of n_{run} of discriminating between these models, either the fact that a running at this level could be easily produced and that it should not be discarded in the analysis of future data.

As we can see from the second column of Tables 5.2 and 5.3 and also Figure 5.2, the inclusion of the low multipole CMB data, without a prior on the optical depth, has the main effect of substantially increasing (by a factor ~ 2) the constraint on r. The main consequence of this is that in this case, an indication for a coupling ξ starts to emerge. If we consider the values reported in Tables 5.2 and 5.3 and also the corresponding posteriors plotted in Figure 5.2 (left panel) we see that for models with $n < 2$, the indication is slightly above one standard deviation (consider that the posterior on ξ is non-gaussian in this case), while, considering the posteriors ξ in Figure 5.4, right panel, it is above the two standard deviations for $n > 2$ (and close to two standard deviation for $n = 2$). Again, as we pointed out in the previous paragraph, this indication for $\xi \neq 0$ is not generic and must be considered valid only for models with an NMC term and power-law potential with $n > 2$. Considering the values of the χ^2_{eff} we see that they are almost identical for any value of n considered. In few words, the inclusion of an NMC term at the level of $\xi \sim 0.004$ makes models with $n = 2, 3, 4$ back into agreement with the full Planck 2015 dataset. Considering the running, we can also notice that models with $n < 2$ all show an indication for a negative running but at the level of $n_{run} \sim 0.0006$. Models with $n \geq 2$ show on the contrary a significantly lower negative running with $n_{run} \sim 0.001$. Again, a future accurate measurement of n_{run} could significantly discriminate between inflationary models.
In the third and fourth columns of Tables 5.2 and 5.3 we report the constraints obtained by combing the Planck 2015 data with the BKP dataset. As expected, the inclusion of the BKP dataset significantly increase the limits on r. It is interesting to notice that the constraint on r from the full Planck dataset are similar to those obtained by the Planck high-ℓ+BKP dataset, showing a good agreement between the low multipole data from Planck and BKP. As we can see from the results reported in Tables 5.2 and 5.3 and the posteriors in Figures 5.3 and 5.4 the inclusion of the BKP dataset improves the indication for $\xi > 0$ obtained from the Planck dataset alone. We have now from the Planck high-ℓ+BKP dataset an indication for coupling above one standard deviation for $n = 1$ and $n = 4/3$, at about two standard deviation for $n = 2$, and, finally, above 95% C.L. for $n = 3$ and $n = 4$. When the Planck TTTEEE+BKP dataset is considered, the indication for ξ is above one standard deviation for $n = 1$ and $n = 2/3$, at about two standard deviations for $n = 4/3$ and above two standard deviations for $n \geq 2$.
Considering now the constraints on the running of the spectral index n_{run}, we see that while models with $n \leq 2$ prefer a running around $n_{run} \sim -0.001$ at the 95% C.L., models with $n > 2$ are suggesting an higher value around $n_{run} \sim -0.006$. These values are both consistent with the latest constraints from Planck ($n_{run} = -0.007 \pm 0.0068$, see [268] and clearly indicates that future constraints on n_{run} could significantly constrain models with NMC.

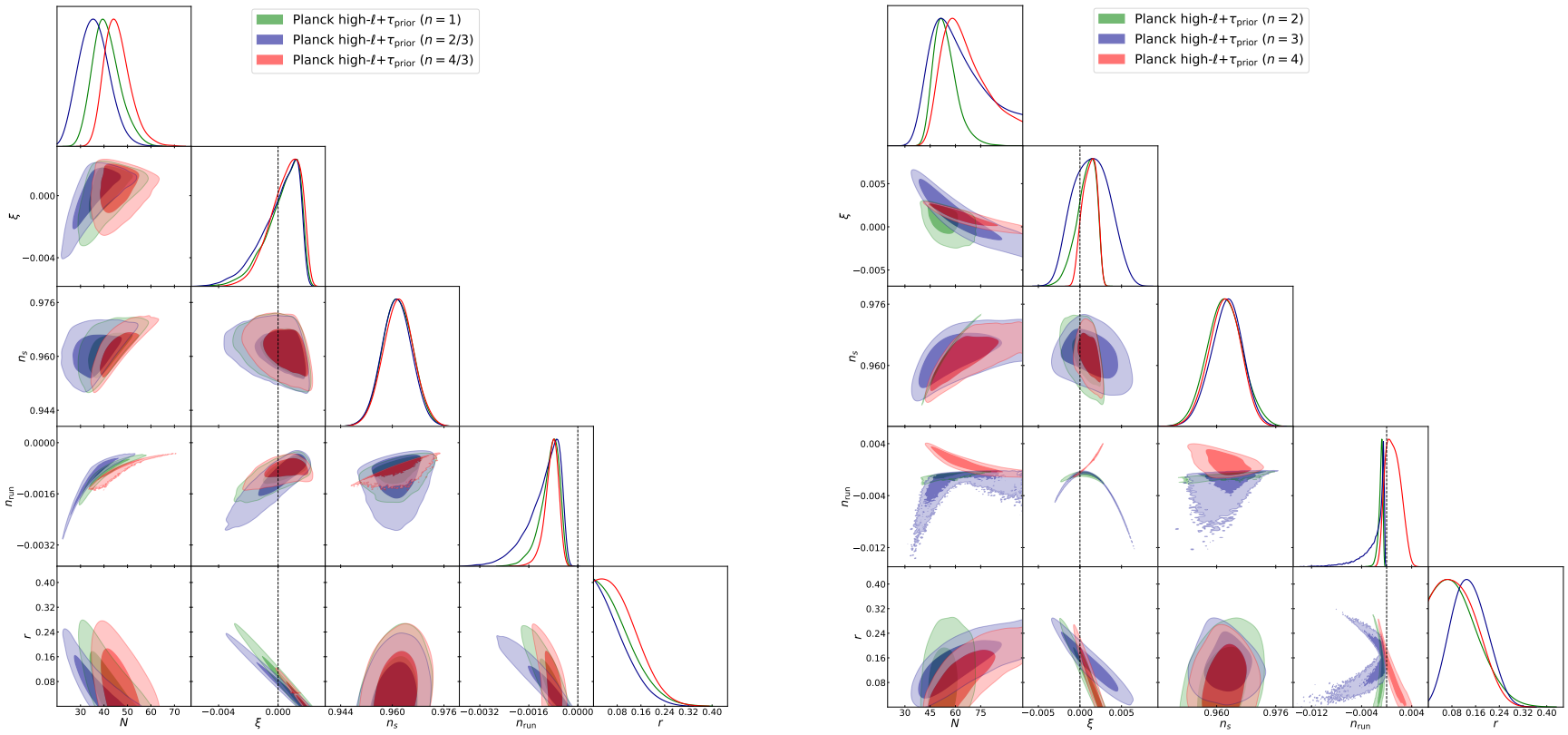

FIGURE 5.1: Constraints at 68% and 95% C.L. on cosmological and inflationary parameters from Planck anisotropy and polarization data at high multipoles ($\ell > 30$) with the inclusion of a prior on the reionization optical depth. Power-law potentials with $n < 2$ are on the left and power-law potentials with $n \geq 2$ are on the right.

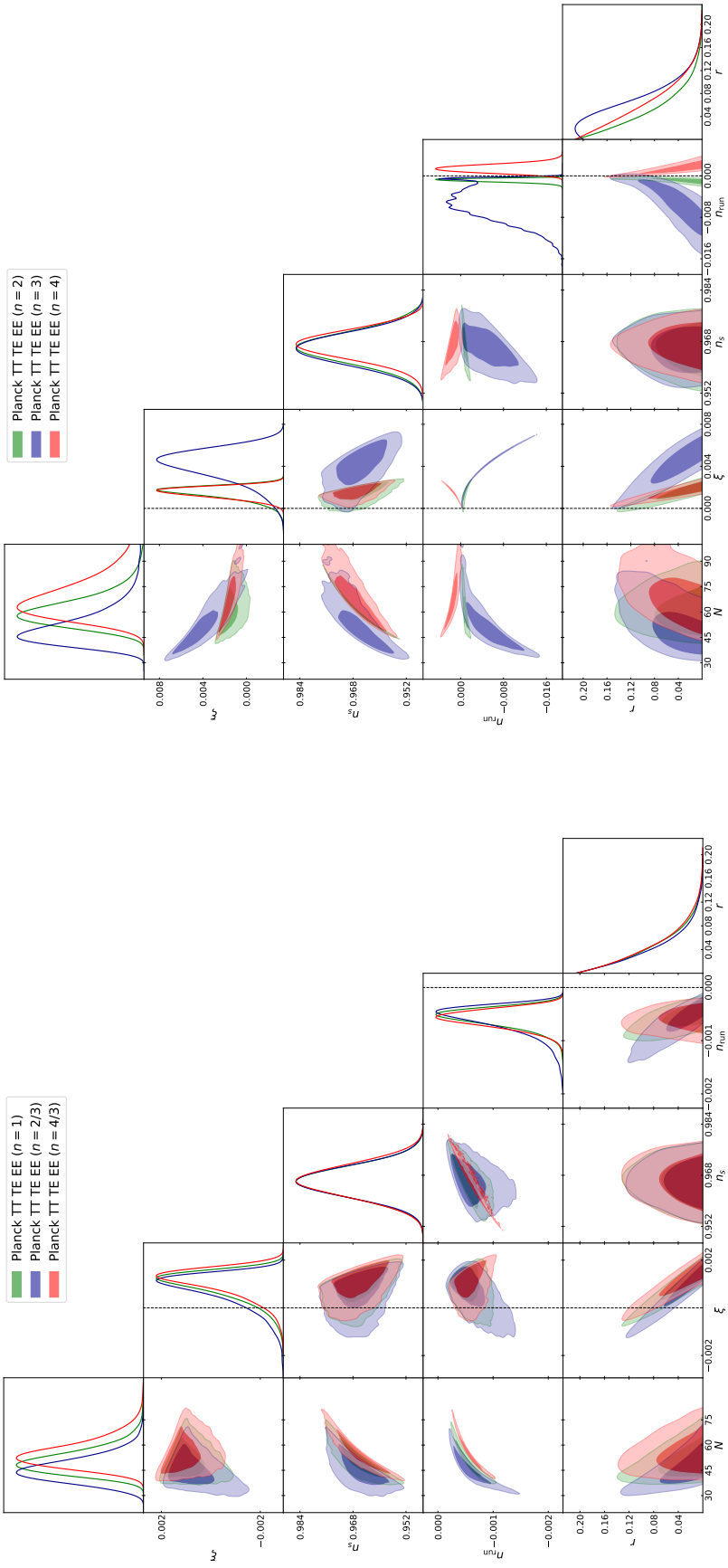

FIGURE 5.2: Constraints at 68% and 95% C.L. on cosmological and inflationary parameters from Planck anisotropy and polarization data. Power-law potentials with $n < 2$ are on the left and power-law potentials with $n \geq 2$ are on the right.

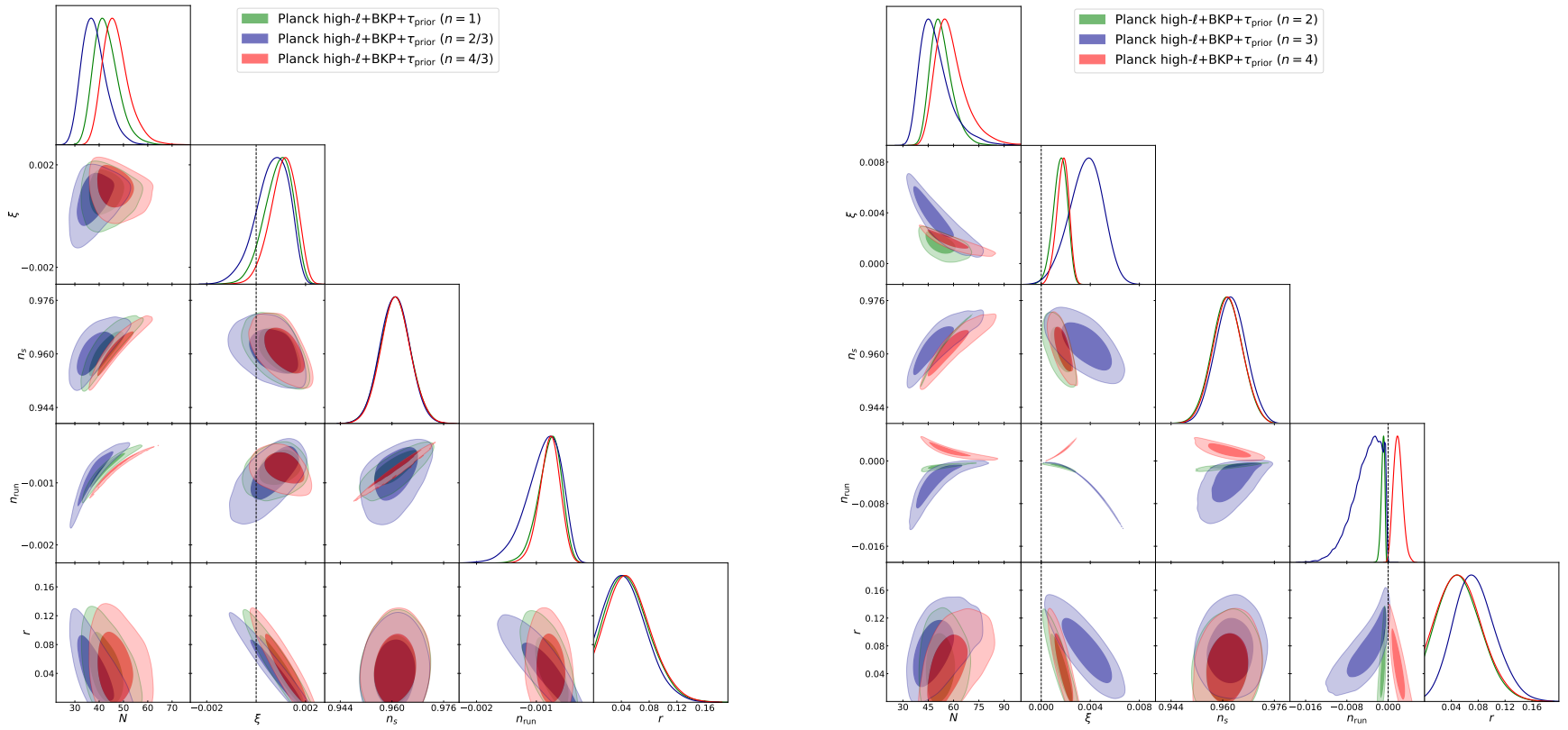

FIGURE 5.3: Constraints at 68% and 95% C.L. on cosmological and inflationary parameters from Planck anisotropy and polarization data combined with the BKP likelihood and with the inclusion of a prior on the reionization optical depth. Power-law potentials with $n < 2$ are on the left and power-law potentials with $n \geq 2$ are on the right.

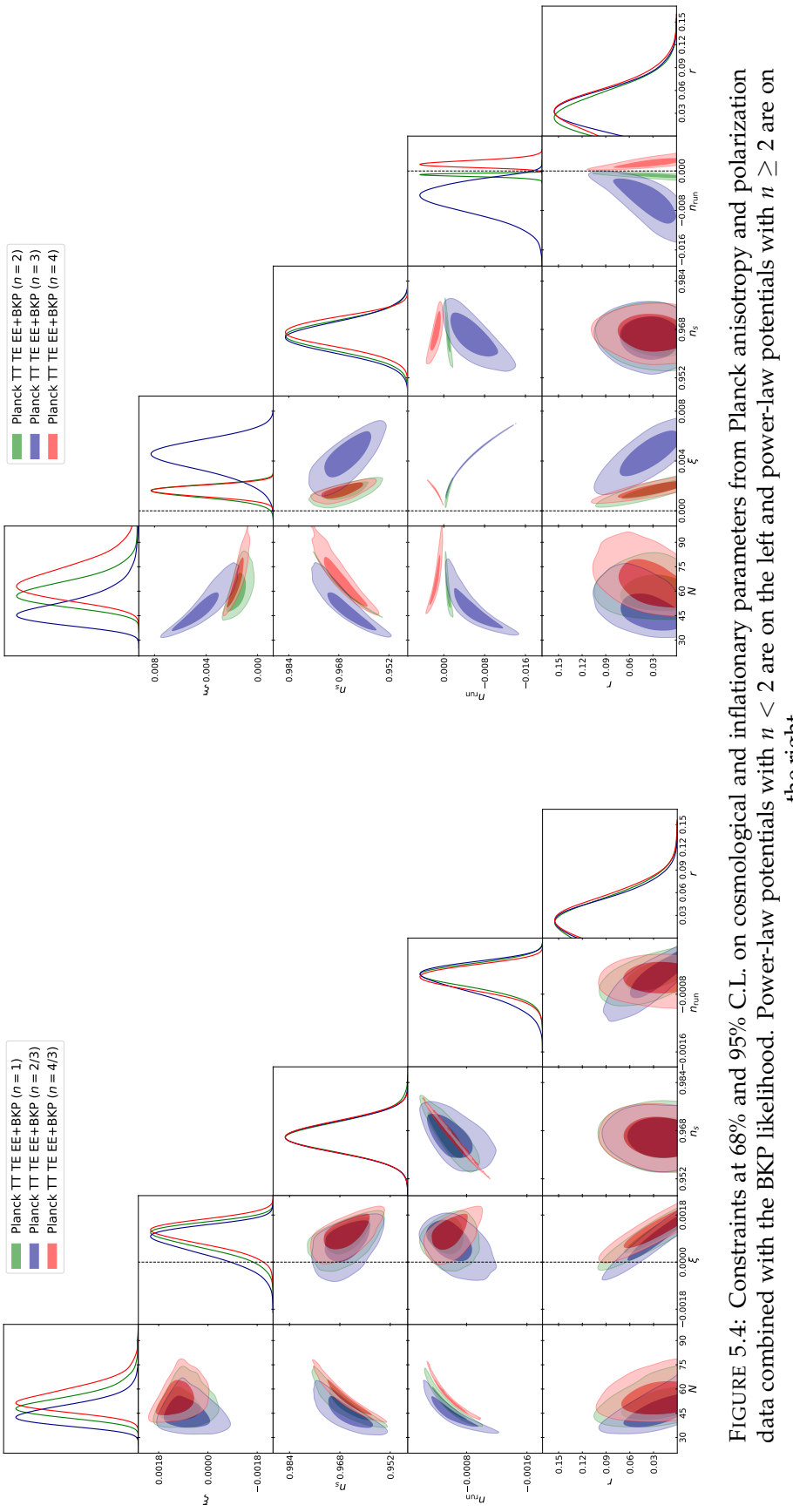

FIGURE 5.4: Constraints at 68% and 95% C.L. on cosmological and inflationary parameters from Planck anisotropy and polarization data combined with the BKP likelihood. Power-law potentials with $n < 2$ are on the left and power-law potentials with $n \geq 2$ are on the right.

	Parameter	Planck high-ℓ+$\tau_{\rm prior}$	Planck TTTEEE	Planck high-ℓ+$\tau_{\rm prior}$+BKP	Planck TTTEEE+BKP
n = 1	N	41^{+5}_{-7}	50^{+5}_{-9}	43^{+4}_{-6}	51^{+5}_{-9}
	ξ	$0.0003^{+0.0014}_{-0.0006}$	$0.0009^{+0.0007}_{-0.0003}$	$0.0009^{+0.0007}_{-0.0005}$	$0.0009^{+0.0006}_{-0.0004}$
	n_s	0.962 ± 0.005	0.966 ± 0.005	0.961 ± 0.005	0.966 ± 0.005
	$n_{\rm run}$	$-0.0009^{+0.0004}_{-0.0002}$	$-0.0006^{+0.0002}_{-0.0001}$	-0.0008 ± -0.0002	$-0.0006^{+0.0002}_{-0.0001}$
	r	< 0.213	< 0.100	< 0.106	< 0.081
	χ^2	2453	12992	2495	12992
n = 2/3	N	36^{+6}_{-7}	45^{+6}_{-8}	38^{+4}_{-6}	45^{+5}_{-8}
	ξ	$0.0000^{+0.0016}_{-0.0006}$	$0.0008^{+0.0008}_{-0.0003}$	$0.0006^{+0.0008}_{-0.0005}$	$0.0007^{+0.0007}_{-0.0004}$
	n_s	0.961 ± 0.005	$0.966^{+0.005}_{-0.004}$	0.961 ± 0.005	0.966 ± 0.005
	$n_{\rm run}$	$-0.0011^{+0.0007}_{-0.0002}$	$-0.0006^{+0.0003}_{-0.0001}$	$-0.0009^{+0.0004}_{-0.0002}$	$-0.0006^{+0.0003}_{-0.0001}$
	r	< 0.188	< 0.094	< 0.101	< 0.077
	χ^2	2452	12949	2495	12992
n = 4/3	N	46^{+4}_{-6}	55^{+5}_{-10}	47^{+4}_{-6}	55^{+5}_{-9}
	ξ	$0.0004^{+0.0013}_{-0.0006}$	$0.0011^{+0.0007}_{-0.0003}$	$0.0011^{+0.0006}_{-0.0004}$	0.0011 ± 0.0005
	n_s	0.962 ± 0.005	0.966 ± 0.005	0.961 ± 0.005	0.966 ± 0.005
	$n_{\rm run}$	-0.0009 ± 0.0003	$-0.0006^{+0.0002}_{-0.0001}$	-0.0008 ± 0.0002	$-0.0006^{+0.0002}_{-0.0001}$
	r	< 0.215	< 0.106	< 0.108	< 0.082
	χ^2	2454	12950	2495	12992

TABLE 5.2: Constraints on cosmological and inflationary parameters in case of power-law potentials (case of $n < 2$) with non-minimal coupling from Planck and Planck+BKP datasets. Constraints on parameters are at the 68% C.L. (upper limits at 95% C.L.)

	Parameter	Planck high-ℓ+$\tau_{\rm prior}$	Planck TTTEEE	Planck high-ℓ+$\tau_{\rm prior}$+BKP	Planck TTTEEE+BKP
n = 2	N	54^{+5}_{-8}	61^{+6}_{-11}	53^{+5}_{-8}	60^{+6}_{-10}
	ξ	$0.0007^{+0.0015}_{-0.0008}$	$0.0014^{+0.0008}_{-0.0004}$	0.0015 ± 0.0006	0.0015 ± 0.0005
	n_s	0.962 ± 0.005	0.966 ± 0.005	0.961 ± 0.005	0.966 ± 0.005
	$n_{\rm run}$	$-0.0010^{+0.0004}_{-0.0002}$	$-0.0009^{+0.0004}_{-0.0002}$	$-0.0010^{+0.0004}_{-0.0002}$	$-0.0009^{+0.0004}_{-0.0002}$
	r	< 0.238	< 0.115	< 0.109	< 0.087
	χ^2	2452	12950	2495	12992
n = 3	N	62^{+10}_{-21}	52^{+5}_{-13}	53^{+5}_{-8}	51^{+5}_{-12}
	ξ	0.0014 ± 0.0023	$0.0040^{+0.0018}_{-0.0011}$	$0.0036^{+0.0015}_{-0.0012}$	$0.0042^{+0.0014}_{-0.0010}$
	n_s	$0.963^{+0.005}_{-0.004}$	$0.966 \pm +0.005$	$0.962 \pm +0.005$	$0.966 \pm +0.005$
	$n_{\rm run}$	$-0.0022^{+0.0019}_{-0.0002}$	$-0.0053^{+0.0050}_{-0.0021}$	$-0.0042^{+0.0038}_{-0.0012}$	$-0.0055^{+0.0035}_{-0.0024}$
	r	$0.139^{+0.056}_{-0.066}$	< 0.123	$0.075^{+0.027}_{-0.034}$	< 0.087
	χ^2	2456	12950	2497	12991
n = 4	N	66^{+9}_{-17}	66^{+8}_{-14}	59^{+6}_{-11}	67^{+8}_{-13}
	ξ	$0.0012^{+0.0010}_{-0.0014}$	$0.0015^{+0.0006}_{-0.0004}$	$0.0018 \pm +0.0005$	0.0016 ± 0.0004
n_s	$0.962^{+0.005}_{-0.004}$	0.966 ± 0.004	0.962 ± 0.005	$0.967^{+0.005}_{-0.004}$	
	$n_{\rm run}$	$0.0011^{+0.0010}_{-0.0014}$	$0.0014^{+0.0007}_{-0.0008}$	$0.0019^{+0.001}_{-0.001}$	$0.0015^{+0.0005}_{-0.0008}$
	r	< 0.219	< 0.121	< 0.111	< 0.089
	χ^2	2453	12950	2495	12993

TABLE 5.3: Constraints on cosmological and inflationary parameters in case of power-law potentials (case of $n \geq 2$) with non-minimal coupling from Planck and Planck+BKP datasets. Constraints on parameters are at the 68% C.L. (upper limits at 95% C.L.)

Chapter 6

R^{2p} Inflationary Models

In addition to the inflationary model based on a single scalar field, the models from modified theories of gravity are very conventional among the inflationary literature. One of the most interesting models can be investigated in the context of $f(R)$ gravity [53, 54] in which one can obtain the acceleration phase in the early stages of the universe by considering some modifications in geometry instead of the inflaton. The most well-known model which gained many successes was proposed by A. A. Starobinsky in 1980 [108] by introducing the form of R^2 wherein the model has a graceful exit from inflation to the next stage of the universe by reheating phase [269, 270, 271]. Interestingly the R^2 has also a crucial role in solving the shortcomings of $f(R)$ theories which have been proposed as one of the possible alternatives to the cosmological constant of the concordance Λ Cold Dark Matter (ΛCDM) model [272, 273, 274, 275, 276, 277, 278, 279, 280, 281, 282, 283]. Because of its agreement with current observations, the Starobinski model is now considered as a "target" model for several future CMB experiments as, for example, the Simons Observatory [284], CMB-S4 [285], and the LiteBIRD satellite experiment [286]. Assuming the current best-fit values of the scalar spectral index n_S from the Planck experiment, the Starobinski model predicts a tiny tensor amplitude namely $r \simeq 0.003$ for 60 e-folds. The goal of these future experiments is therefore to have enough experimental sensitivity to measure such signal with enough statistical significance with $\delta r < 0.001$. However the prediction of $r \simeq 0.003$ is a first approximation that does not consider several caveats. First of all, there is an experimental uncertainty on the value of n_S derived under ΛCDM and this affect the predicted value for r, since, for example, for higher values of n_S the expected value of r is smaller. Secondly, there is a severe anomaly in the Planck data on the amount of gravitational lensing present in the CMB angular spectra. The lensing signal, parameterized by the parameter A_{lens}, is indeed larger than what expected in the ΛCDM scenario by more than two standard deviations. Since A_{lens} correlates with n_S, the lensing anomaly could affect the predictions on r. Finally, there is clearly no fundamental reason to believe that the Starobinski model is the correct inflationary scenario and, for example, several generalization could be considered.

The main purpose of this chapter is evaluating the amount of gravitational waves predicted by Starobinski model considering the current uncertainties on n_S and the possibility of an extension to the ΛCDM model parametrized by A_{lens}. Hence, we consider a minimal generalization of Starobinsky inflation, the so-called R^{2p} models (with $p \approx 1$). These inflationary models were first proposed by [287, 288] in the context of higher derivative theories and subsequently were applied to inflation providing a simple and elegant generalization of the R^2 inflation [289, 290, 54, 202, 291]. In [292], the authors showed that the tensor-to-scalar ratio r can be raised by some small derivations of the Starobinsky model. Also, the connection between Higgs

inflation and R^p form is investigated in [293, 294]. While the introduction of a variable index of the Ricci scalar in the inflationary action complicates the simplicity of R^2 inflation it allows significant deviations from the benchmark value of the tensor amplitude of the Starobinsky model and could in principle results in a better agreement with data.In this chapter, we provide constraints on Starobinsky inflation and the more general R^{2p} model using CMB anisotropies data. In particular, we make use of the publicly available Planck 2015 and Biceps2/Keck array data releases. Notice that the chapter is based on our research paper published on the Physics of Dark Universe Journal.

6.1 The Model

We start with the form of action for R^{2p} inflation as

$$S_f = -\frac{1}{2\kappa^2}\int d^4x f(R), \qquad f(R) = R - \frac{R^{2p}}{M^{4p-2}} \qquad with \qquad p = 1,2,3,... \quad (6.1)$$

By applying the conformal transformation introduced in appendix A for the above action, we can move to the Einstein frame with defining a scalar field φ which is called *scaleron*. Then, the action Eq. (6.1) can be rewrite as

$$S_\varphi = \int d^4x\sqrt{-g}\left(-\frac{R}{2\kappa^2} + \frac{1}{2}g^{\mu\nu}\partial_\mu\varphi\partial_\nu\varphi - V(\varphi)\right) \quad (6.2)$$

and the potential can be wrote as

$$V(y) = V_0 e^{-2y}(e^y - 1)^{\frac{2p}{2p-1}} \quad with \quad y = \sqrt{\frac{2}{3}}\frac{\varphi}{m_{pl}}, \quad (6.3)$$

where $V_0 = (\frac{2p-1}{4p})m_{pl}^2 M^2(\frac{1}{2p})^{\frac{1}{2p-1}}$ and $M \simeq 10^{13}$ GeV is the energy scale determined by the amplitude of the observed power spectrum for primordial perturbations. In Figure 6.1, we report the behaviour of the potential (6.3) for different values of the index p, we note that:

- for $p > 1$ the potential has a maximum $\varphi_m = m_{pl}\sqrt{\frac{2}{3}}\ln\frac{2p-1}{p-1}$ but goes asymptotically to zero for large value of the scalar field φ. Inflation therefore can happen both for $0 \leq \phi \leq \varphi_m$ and $\varphi > \varphi_m$. The behavior of R^{2p} inflation significantly differs from the Starobinsky model in the latter region and since we are interested only in small deviations from R^2 inflation we neglect the inflationary behavior in the potential region where $\varphi > \varphi_m$.
- for $p < 1$ the potential increases indefinitely but its decreasing towards zero is steeper than in R^2 model therefore leading to larger tensor-to-scalar ratios.
- for $p = 1$ we recover the potential of Starobinsky inflation asymptotically approaching a constant value $V_0 = \frac{3}{4}M^2 m_{pl}$ for large φ

$$V(\varphi) = \frac{3}{4}M^2 m_{pl}\left(1 - e^{-\sqrt{\frac{2}{3}}\frac{\varphi}{m_{pl}}}\right)^2. \quad (6.4)$$

In the Einstein frame, the slow-roll parameters can be expressed through the potential as

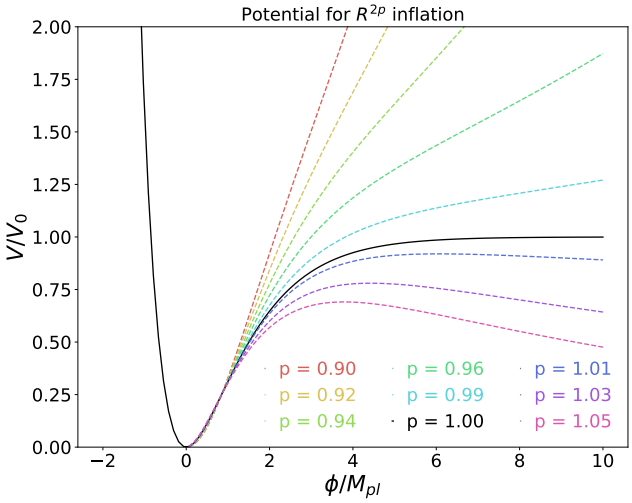

FIGURE 6.1: The potential of R^{2p} inflation for different values of p.

$$\epsilon = \frac{1}{2\kappa^2}\left(\frac{V'(\varphi)}{V(\varphi)}\right)^2, \qquad \eta = \frac{1}{\kappa^2}\left(\frac{V''(\varphi)}{V(\varphi)}\right), \qquad \zeta^2 = \frac{1}{\kappa^4}\left(\frac{V'(\varphi)V'''(\varphi)}{V^2(\varphi)}\right), \tag{6.5}$$

where prime denotes to the derivation respect to φ. Also, the number of e-folds between the start and the end of inflation can be defined by

$$N \equiv \int_{t_i}^{t_e} H dt \simeq \sqrt{\frac{\kappa^2}{2}} \int_{\varphi_e}^{\varphi_i} \frac{1}{\sqrt{\epsilon}} d\varphi. \tag{6.6}$$

Since the case of $p = 1$ leads to a singularity for the number of e-folds, we start with the general form of $p \neq 1$. Then, the case of $p = 1$ will be explained separately. The slow-roll parameters Eqs. (6.5) for $p \neq 1$ can be found by [295]

$$\epsilon = \frac{4\left((p-1)e^{\sqrt{\frac{2}{3}}\frac{\varphi}{m_{pl}}} - 2p + 1\right)^2}{3(2p-1)^2\left(e^{\sqrt{\frac{2}{3}}\frac{\varphi}{m_{pl}}}, -1\right)^2} \tag{6.7}$$

$$\eta = \frac{4}{3(2p-1)^2\left(e^{\sqrt{\frac{2}{3}}\frac{\varphi}{m_{pl}}} - 1\right)^2}\left((2p^2 - 4p + 2)e^{2\sqrt{\frac{2}{3}}\frac{\varphi}{m_{pl}}} + (-10p^2 + 13p - 4)e^{\sqrt{\frac{2}{3}}\frac{\varphi}{m_{pl}}} + 8p^2 - 8p + 2\right) \tag{6.8}$$

and

$$\zeta^2 = \frac{16}{9(2p-1)^4\left(e^{\sqrt{\frac{2}{3}}\frac{\varphi}{m_{pl}}}-1\right)^4}\Bigg[\Big((p-1)(4p^3-12p^2+12p-4)\Big)e^{4\sqrt{\frac{2}{3}}\frac{\varphi}{m_{pl}}}$$
$$-\Big(48p^4-150p^3+173p^2-87p+16\Big)e^{3\sqrt{\frac{2}{3}}\frac{\varphi}{m_{pl}}}+\Big(148p^4-388p^3+373p^2-156p+24\Big)e^{2\sqrt{\frac{2}{3}}\frac{\varphi}{m_{pl}}}$$
$$-\Big(168p^4-380p^3+318p^2-117p+16\Big)e^{\sqrt{\frac{2}{3}}\frac{\varphi}{m_{pl}}}.+4\Big(16p^4-32p^3+24p^2-8p+1\Big)\Bigg]$$

Notice that by setting the condition $\epsilon = 1$, we have the value of scaleron for the end of inflation φ_e. Also, the number of e-folds (6.6) for this case is given by

$$N = -\frac{3p}{4(p-1)}\ln\left(\frac{(p-1)e^{\sqrt{\frac{2}{3}}\frac{\varphi_i}{m_{pl}}}-2p+1}{(p-1)e^{\sqrt{\frac{2}{3}}\frac{\varphi_e}{m_{pl}}}-2p+1}\right) \tag{6.10}$$

and by removing the role of scalar field at the end of inflation, the above equation can be reduced to

$$N \simeq -\frac{3p}{4(p-1)}\ln\left(\frac{(p-1)e^{\sqrt{\frac{2}{3}}\frac{\varphi_i}{m_{pl}}}}{1-2p}+1\right). \tag{6.11}$$

For our purposes, it is very nice to rewrite the Eq. (6.11) as

$$e^{\sqrt{\frac{2}{3}}\frac{\varphi_i}{m_{pl}}} = \frac{(1-2p)}{(p-1)}\left(e^{\frac{-4N(p-1)}{3p}}-1\right) \quad with \quad \mathcal{C} \equiv e^{\frac{-4N(p-1)}{3p}}. \tag{6.12}$$

In order to obtain the inflationary parameters, we require to rewrite the slow-roll parameters (6.7) to (6.9) at the beginning of inflation as follow

$$\epsilon = \frac{4\mathcal{C}^2(p-1)^2}{3(\mathcal{C}(1-2p)+p)^2}, \tag{6.13}$$

$$\eta = \frac{4(p-1)}{3((1-2p)\mathcal{C}+p)^2}\Big(2\mathcal{C}^2(p-1)+p\mathcal{C}-p\Big) \tag{6.14}$$

and

$$\zeta^2 = \frac{16\mathcal{C}(p-1)^2}{9((1-2p)\mathcal{C}+p)^4}\Big(4(p-1)^2\mathcal{C}^3+p(8p-7)\mathcal{C}^2-p(11p-9)\mathcal{C}+p(3p-2)\Big) \tag{6.15}$$

Now we can calculate the first order of spectral index, its running and the tensor-to-scalar ratio which are invariant under the conrformal transformation [296, 297], by

$$n_s = 1-6\epsilon+2\eta, \qquad \alpha_s = 16\epsilon\eta-24\epsilon^2-2\zeta^2, \qquad r = 16\epsilon, \tag{6.16}$$

where for the R^p model, we obtain

$$n_s = 1 - \frac{8(p-1)\Big(\mathcal{C}^2(p-1) - p(\mathcal{C}-1)\Big)}{3\Big(\mathcal{C}(1-2p)+p\Big)^2}, \tag{6.17}$$

$$\alpha_s = -\frac{32p\mathcal{C}(p-1)^2(\mathcal{C}-1)(\mathcal{C}-3p+2)}{9\Big(\mathcal{C}(1-2p)+p\Big)^4}, \qquad r = \frac{64\mathcal{C}^2(p-1)^2}{3\Big(\mathcal{C}(1-2p)+p\Big)^2}. \tag{6.18}$$

The consistency relations between above equations take the following form

$$n_s - 1 = -\frac{(3p-2)\sqrt{r}}{\sqrt{3}p} + \frac{8(1-p)}{3p} - \frac{r(3p-1)}{8p} \tag{6.19}$$

and

$$\begin{aligned}\alpha_s = \frac{4(1-p)(3p-2)\sqrt{r}}{3\sqrt{3}p^2} - \frac{(15p^2-20p+6)r}{6p^2} \\ - \frac{(3p-2)(8p-3)r^{\frac{3}{2}}}{16\sqrt{3}p^2} - \frac{(2p-1)(3p-1)r^2}{64p^2}\end{aligned} \tag{6.20}$$

Now, let us consider the singular case of $p = 1$. In this case, the slow-roll parameters (6.5) are given by

$$\epsilon = \frac{4}{3(e^{\sqrt{\frac{2}{3}}\frac{\varphi}{m_{pl}}} - 1)^2}, \qquad \eta = -\frac{4(e^{\sqrt{\frac{2}{3}}\frac{\varphi}{m_{pl}}} - 2)}{3(e^{\sqrt{\frac{2}{3}}\frac{\varphi}{m_{pl}}} - 1)^2}, \qquad \zeta = \frac{16(e^{\sqrt{\frac{2}{3}}\frac{\varphi}{m_{pl}}} - 4)}{9(e^{\sqrt{\frac{2}{3}}\frac{\varphi}{m_{pl}}} - 1)^3}. \tag{6.21}$$

By using the Eq. (6.6), the number of e-folds in this case is obtained as

$$N \simeq \frac{3}{4}e^{\sqrt{\frac{2}{3}}\frac{\varphi_i}{m_{pl}}}. \tag{6.22}$$

For the spectral index, the running spectral index and the tensor-to-scalar ratio from Eqs. (6.16) we have

$$n_s = 1 - \frac{2}{N}, \qquad \alpha_s = -\frac{2}{N^2}, \qquad r = \frac{12}{N^2}. \tag{6.23}$$

We show in Figure 6.2 the scalar spectral index n_S (left panel) and its running α_S (right panel) as function of the tensor-to-scalar ratio r for different value of the index p. We superimpose on the curves drawn according to Eqs. (6.19) and (6.20) the Planck 2015 bounds on n_S to show how the models considered in the present work can fit with observations of CMB anisotropies. We see from the left panel of Figure 6.2 that for arbitrary small values of r the scalar index saturates to a maximum value which depends only on p, namely

$$n_S - 1 = \frac{8(1-p)}{3p} \tag{6.24}$$

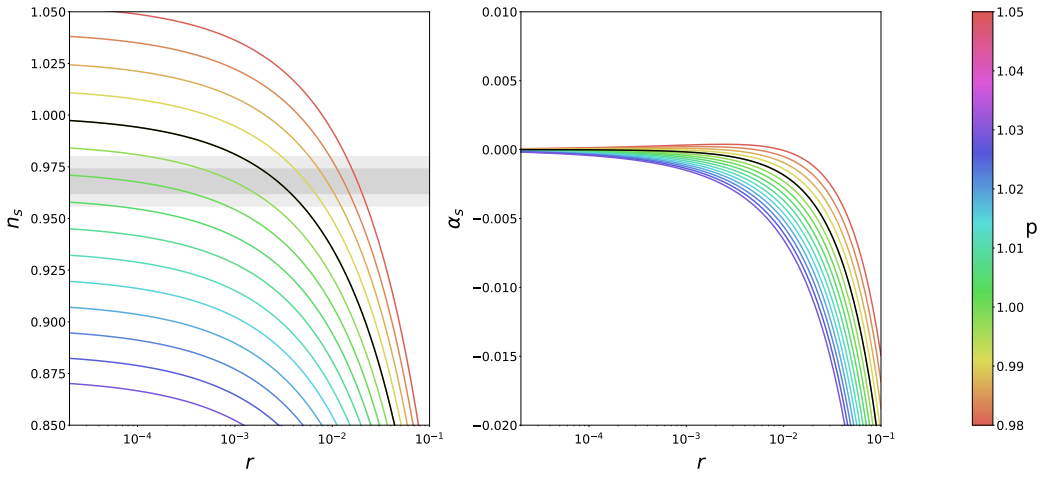

FIGURE 6.2: The spectral index (left) and the running spectral index (right) versus tensor-to-scalar ratio with respect to the different values of p. The dashed line on the left panel shows the case for $p = 1$. The gray band show the 68% and 95% C.L. constraints on the spectral index from Planck 2015. The black lines show the case $p = 1$

for $1.01 \lesssim p \lesssim 1.02$, the saturation value falls well within the Planck bound on n_S, this model are therefore well in agreement with Planck data for a tensor-to-scalar ratio consistent with zero. For $p \gtrsim 1.02$ the value of n_S is always outside the Planck bounds, thus we expect these models to be ruled out by current data. Model with $p \lesssim 1.01$ are within the Planck bounds only for a finite range of values of the tensor amplitude r these models are not ruled out only if their range is contained in the Planck upper limit for $r < 0.1$. For α_S we see a similar behavior as $r \to 0$ (right panel of Figure 6.2), but the saturation value now is zero for every value of the index p since $\alpha_S \propto \sqrt{r}$ for $r \to 0$. Therefore we expect that Planck data will be able to give a bound on p if it is let free to vary while the bounds on r and α_S will be consistent with zero. Conversely for the Starobinsky model we expect to have a bound on r in the range $10^{-4} - 10^{-3}$ and thus an indication for a non zero running at more than two standard deviation.

6.2 Comparison with Recent Experimental Data and Expected Signal

As stated in the previous sections the aim of this chapter is to show how stable are the prediction of the Starobinsky model on inflationary parameters when a model-dependent approach is used to sample the cosmological parameter space. The general approach when looking at constraints from observations on inflationary models (see e.g. [298, 299, 300, 264]) is to let the parameters n_S, r and α_S free to vary assuming them to be independent from one another and then comparing the prediction of a specific model with the allowed parameter space. On the one hand, this allows to explore the inflationary sector in a model independent way but has the drawback of not allowing to sample the whole parameter space of a specific theory. Furthermore the assumption that n_S, r and α_S are independent from one another is also in contrast with the prediction of any theory of inflation that assumes the validity of the slow-roll conditions (see e.g Eqs. (6.19) and (6.20)). In this work, we choose

Parameter	Prior
ω_b	$[0.005 \div 0.1]$
ω_c	$[0.001 \div 0.99]$
θ_s	$[0.5 \div 10]$
τ	$[0.01 \div 0.8]$
$\ln(10^{10} A_s)$	$[2 \div 4]$
N	$[20 \div 100]$
p	$[0.9 \div 1.05]$
A_{lens}	$[0 \div 2]$

TABLE 6.1: Range of the flat prior on the parameters varied in the MCMC analysis.

a different approach: we impose an inflationary model *a priori* (here, R^{2p} inflation) and we extract the posterior distribution of the parameters of that specific model. In particular, we exploit Eqs. (6.16) to reduce the number of inflationary parameters to only two: the number of e-folds, N, and the index, p. While this approach is more model-dependant, it may results in constraints that are not achievable with the standard approach in which the inflationary parameter are independently sampled and any value of n_S, r and α_S is permitted. The theoretical models are calculated using the latest version of the Boltzmann integrator Code for Anisotropies in the Microwave Background (CAMB) [266], and we use publicily available version of the MCMC code CosmoMC [265] (Nov 2016 version) to extract constraints on cosmological parameters. To compare our theoretical models with data, we use the full 2015 Planck temperature and polarization datasets which also includes multipoles $\ell < 30$. Eventually we combine the Planck likelihood with the Biceps/Keck 2015 B-mode likelihood. We modified the code CosmoMC to include the number of e-folds, N, and the index, p, as new independent parameters and to calculate the inflationary parameters n_S, r and α_S throughout Eqs. (6.13) - (6.15). Along with these parameters, we consider also the baryon $\omega_b = \Omega_b h^2$ and the CDM density $\omega_c h^2$, the angular size of the sound horizon at decoupling θ_S, the optical depth τ, the amplitude of scalar perturbations A_S and the phenomenological lensing parameter $A_{\rm lens}$. The flat prior imposed for these parameters are reported in Table 6.1.

6.3 Results for Starobinsky Inflation

We report the bounds on the inflationary parameters for the Starobinsky model obtained using the full Planck 2015 likelihood (Planck) and its combination with Bicep/Keck 2015 data (Planck+BK14) in Table 6.2. The 68% and 95% C.L. contour plots are showed in Figure 6.3 instead. Let us start by discussing the results from the Planck datasets alone (without the inclusion of $A_{\rm lens}$). As we can see from the first column of Table 6.2, we found evidence for a non-zero tensor-to-scalar ratio at the 2-σ level when using the full Planck 2015 data ($r_{0.002} \sim 0.0036$). This result is not coming from an actual presence of tensor perturbations in Planck data but rather it is arising from the correlation between $r_{0.002}$ and n_S present in the model considered. In fact, Planck data are only able to place an upper bound on the value of the tensor-to-scalar ratio due to the poor polarization data at large scales ($r_{0.002} < 0.11$ in a one-parameter extension of the ΛCDM model) while they are able to place a strong constraint on the scalar spectral index at the accuracy of $\sim 0.6\%$ ($n_S = 0.968 \pm 0.006$)

when the standard approach is used to sample these parameters. Enforcing a dependence of n_S from $r_{0.002}$ therefore limits the parameter space for the tensor-to-scalar ratio and force its value to fit in the available range for n_S. This situation can be better understood looking at Figure 6.2, where we show the behavior of the scalar index as a function of tensor-to-scalar ratio. The same argument can be applied to the running of the scalar index α_S for which we find an evidence to be negative ($\alpha_S \sim 0.0006$) at the 3-σ level. Again, we stress that this is not due to an indication of a running in the data but to the specific correlation which arises in Starobinsky inflation between the running and the other inflationary parameters. However these bounds show either that future measurements of $r_{0.002}$ and α_S have the potential to rule out the Starobinsky inflation, either that they should be considered in the analysis of future data being key parameters in studying the feasibility of inflationary models (see also [301]). We can see from Figure 6.3 and the third column of Table 6.2 that the combination of BK14 and Planck data do not significantly modify the bounds coming from the Planck datasets alone. The main reason for this is that the combination of Planck and Biceps2 data is compatible with every value of the tensor-to-scalar ratio satisfying $r_{0.002} < 0.07$ [263] and therefore is not able to improve the constraints of Planck data alone since the bounds on $r_{0.002}$ now fall well within this limit. It is worth noting that, the slight decrease in the best-fit value of $r_{0.002}$ when including BK14 is caused by an increase in the best-fit value of the reionization optical depth that requires a smaller scalar spectral index which in turns demand a smaller tensor ratio and a more negative running. We see from Figure 6.3 and the second column of Table 6.2 the addition of the parameter $A_{\rm lens}$ leads to changes in the best-fit of all other parameters while not affecting their bounds. Here, the main difference with our base model is an increasing in n_S of the 0.4% and a reduction of 1.8% of the scalar amplitude A_S. This in turn leads to a reduction of the optical depth τ from 0.08 to 0.06. To account for this shift, Planck data requires $A_{\rm lens} > 1$ to give more smoothing on the acoustic peaks of the scalar spectrum than in the base ΛCDM model (see e.g. [302, 263] for a more detailed discussion). The parameters N, α_S and $r_{0.002}$ best-fit values are consequently shifted due to the correlation with n_S introduced by Starobinsky inflation. The combination of Planck and BK14 data do not significantly modify the situation described here, since again the bound on $r_{0.002}$ are around an order of magnitude smaller than the sensibility of the two datasets $\delta r \sim 10^{-1}$. It is worth noting that both for Planck alone and for Planck+BK14 the inclusion of A_{lens} provides a better fit to the data with $\Delta\chi^2 = 4$ again underlying the preference for more lensing power in Planck data.

6.4 Results for Near-Starobinsky Inflation

We report the constraints on the inflationary parameters for general R^{2p} model with $p \simeq 1$ in Table 6.3. The 68% and 95% C.L. contour plots are showed in Figure 6.4 instead. We start again discussing the results from the Planck datasets alone (without the inclusion of $A_{\rm lens}$) reported in the first column of Table 6.3. As expected the inclusion of the index p in the analysis does not significantly modify the bounds on the standard cosmological parameters ($\Omega_b h^2$, $\Omega_c h^2$, A_S, n_S and τ) coming from the Planck datasets alone. Conversely the constraints on inflationary parameters are largely changed by the inclusion of the index p. When p is varied, the number of e-folds of inflation are basically unconstrained within the flat range we imposed in our runs while the 2-σ bound on the tensor-to-scalar ratio is relaxed to only an upper bound. We note however that the upper limit on r is halved with respect to the

bound reported in the Planck 2015 release ($r < 0.11$), again this is due to the correlation between the inflationary parameters arising in R^{2p} inflationary models. The bound on α_S is also worsen by a factor ~ 4 leading to a running consistent with zero nearly at 2-σ level. Interestingly instead we are able to constraints the index p with an accuracy of the $0.2\% - 0.3\%$. In order to understand why this is happening we should look again at Figure 6.2. As we can see from the left panel of Figure 6.2, for arbitrary small value of r, the scalar index saturates to a constant value which is only a function of the index p (see also Eq. (6.19)). For $1.0 \lesssim p \lesssim 1.02$, the saturation value of n_S falls well within the Planck constraints for $r \to 0$ therefore for these models we do not find any lower limit on the amplitude of tensor modes. For $p > 1.02$ the value of n_S is always outside the Planck bound making these models incompatible with Planck data, instead models with $p < 1.0$ are compatible with Planck data only for value of the tensor-to-scalar ratio in the range $10^{-2} < r < 10^{-1}$. This behavior of the scalar index for different value of p leads to the highly non-Gaussian posteriors for p and α_s of Figure 6.4 and to the disappearance of the lower bound on r. Including , we again see the shift in the best fit values of A_S and n_S as for the case where p is kept fixed leading to a worsening of the limit on r of the 45% and of the constraints on p of the 20%. We see from the third column of Table 6.3 and Figure 6.4 that the combination of Planck and BK14 datasets improves sligtly the upper limit on tensor amplitudes while the other parameter bounds are virtually unchanged. The inclusion of now only changes the bound on α_S shifting the best-fit toward zero by the 14% and improving the 2-σ constraints by the same amount. Again we notice that the inclusion of provides a better fit to the data with $\Delta\chi^2 \simeq 4 - 5$.

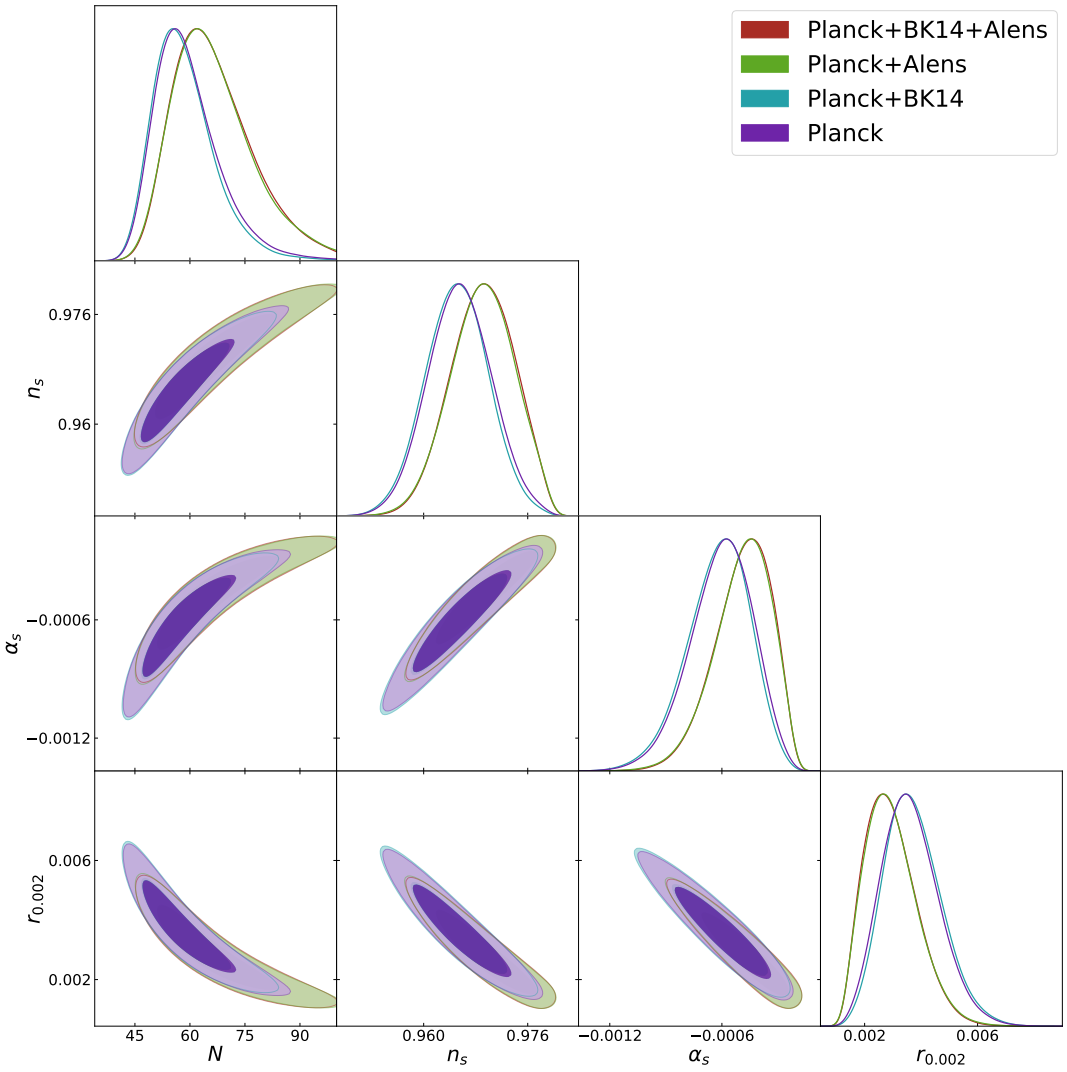

FIGURE 6.3: Constraints at 68% and 95% C.L. for the full Planck 2015 likelihood (Planck) and its combination with the Biceps/Keck 2015 B-mode likelihood (Planck+BK14) for the inflationary parameters for Starobinsky inflation $p = 1$.

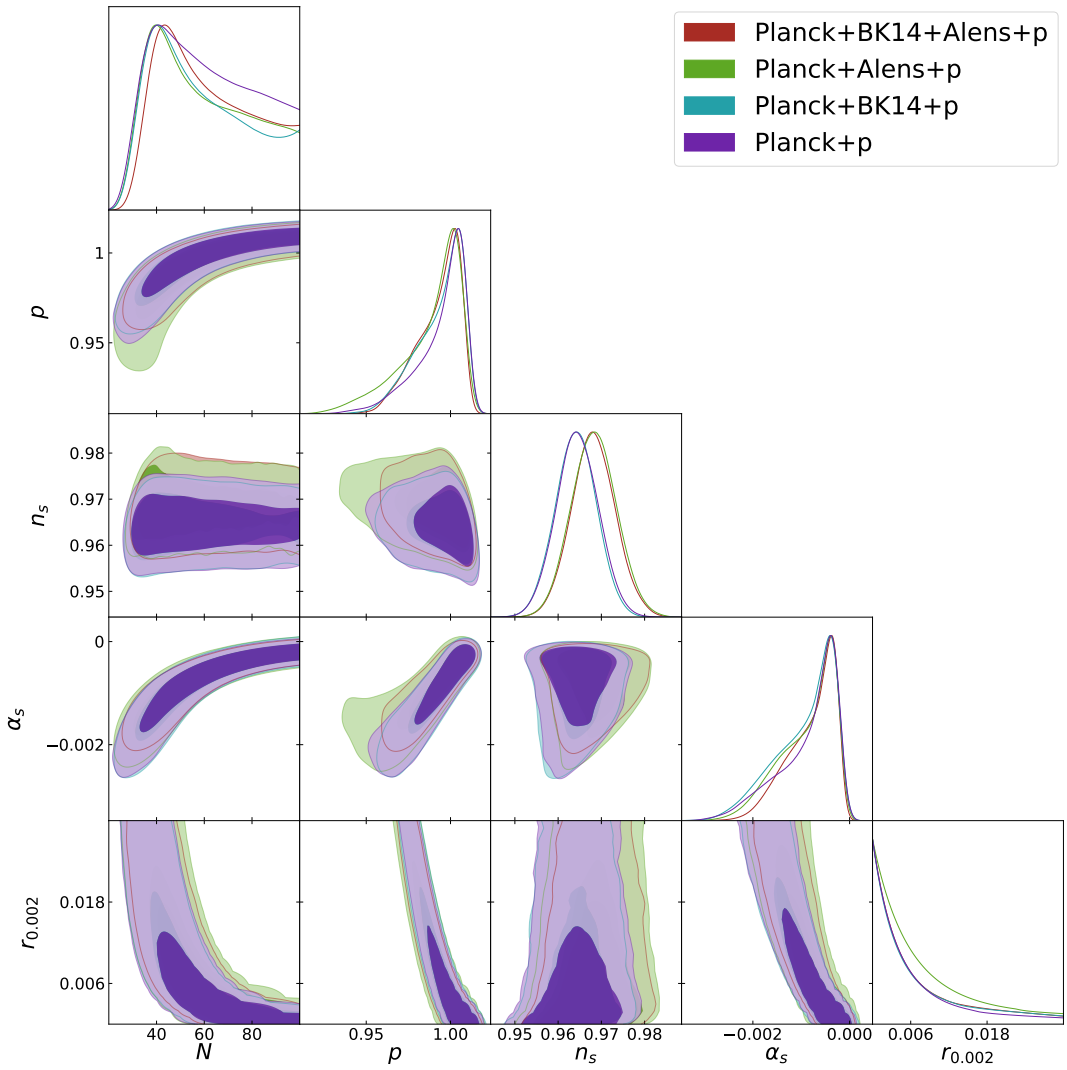

FIGURE 6.4: Constraints at 68% and 95% C.L. for the full Planck 2015 likelihood (Planck) and its combination with the Biceps/Keck 2015 B-mode likelihood (Planck+BK14) for the inflationary parameters for R^{2p} models

	Planck	Planck+$A_{\rm lens}$	Planck+BK14	Planck+BK14+$A_{\rm lens}$
$\Omega_{\rm b}h^2$	0.02226 ± 0.00016	0.02241 ± 0.00017	0.02224 ± 0.00016	0.02242 ± 0.00017
$\Omega_{\rm c}h^2$	0.1196 ± 0.0015	0.1182 ± 0.0016	0.1198 ± 0.0015	0.1182 ± 0.0015
$\ln(10^{10}A_{\rm s})$	3.096 ± 0.033	3.045 ± 0.041	3.104 ± 0.032	3.045 ± 0.040
N	59^{+6}_{-10}	66^{+8}_{-10}	59^{+6}_{-10}	67^{+8}_{-10}
n_S	0.9656 ± 0.0048	$0.9691^{+0.0053}_{-0.0047}$	0.9652 ± 0.0048	0.9692 ± 0.0049
α_S	$-0.00060^{+0.00019}_{-0.00014}$	$-0.00049^{+0.00018}_{-0.00012}$	$-0.00062^{+0.00019}_{-0.00015}$	$-0.00049^{+0.00018}_{-0.00012}$
$r_{0.002}$	$0.00363^{+0.00085}_{-0.0011}$	$0.00294^{+0.00070}_{-0.0011}$	$0.00371^{+0.00089}_{-0.0011}$	$0.00292^{+0.00070}_{-0.0011}$
τ	0.081 ± 0.017	0.057 ± 0.020	0.084 ± 0.017	0.057 ± 0.020
χ^2	12948	12944	13594	13590

TABLE 6.2: Constraints on inflationary parameters for a Starobinsky inflation ($p = 1$) from the Planck and Planck+BK14 datasets with and without the inclusion of the parameter $A_{\rm lens}$. Constraints on parameters are at the 68% C.L.

	Planck+p	Planck+p+$A_{\rm lens}$	Planck+BK14+p	Planck+BK14+p+$A_{\rm lens}$
$\Omega_{\rm b}h^2$	0.02223 ± 0.00016	0.02240 ± 0.00018	0.02223 ± 0.00016	0.02240 ± 0.00018
$\Omega_{\rm c}h^2$	0.1198 ± 0.0015	0.1184 ± 0.0016	0.1201 ± 0.0015	0.1184 ± 0.0016
$\ln(10^{10}A_{\rm S})$	3.092 ± 0.033	3.043 ± 0.041	3.101 ± 0.032	3.046 ± 0.041
N	60^{+40}_{-30}	59^{+40}_{-30}	59^{+40}_{-30}	61^{+40}_{-30}
p	$0.995^{+0.021}_{-0.033}$	$0.990^{+0.025}_{-0.039}$	$0.994^{+0.021}_{-0.030}$	$0.993^{+0.020}_{-0.027}$
n_S	0.9644 ± 0.0049	0.9683 ± 0.0051	0.9640 ± 0.0049	0.9683 ± 0.0051
α_S	$-0.00084^{+0.00084}_{-0.0013}$	$-0.00083^{+0.00080}_{-0.0011}$	$-0.00090^{+0.00088}_{-0.0013}$	$-0.00077^{+0.00072}_{-0.0010}$
$r_{0.002}$	< 0.0515	< 0.0750	< 0.0483	< 0.0422
τ	0.079 ± 0.017	0.056 ± 0.020	0.082 ± 0.017	0.057 ± 0.020
χ^2	12949	12945	13595	13590

TABLE 6.3: Constraints on inflationary parameters for near-Starobinsky inflation ($p \simeq 1$) from the Planck and Planck+BK14 datasets with and without the inclusion of the parameter $A_{\rm lens}$. Constraints on parameters are at the 68% C.L. for $\Omega_{\rm b}h^2, \Omega_{\rm c}h^2$ and A_S while constraints on α_S, N and p are at 95% C.L. since their posteriors are highly non-Gaussian. Upper bound are also at 95% C.L.

Chapter 7

Conclusion

As we learned, in modern cosmology, the idea of inflation is known as the most desirable candidate to remove HBB theory weaknesses, including flatness, horizon and monopole puzzles. Also, it provides the seed of structure formation of the universe due to the quantum fluctuations of the scalar field as scalar perturbations produced during the inflation period. Moreover, the scalar perturbations are recognized as one of the most significant factors of the temperature anisotropies of CMB photons. In addition to the scalar perturbations, tensor perturbations generated during inflation are responsible for composing the primordial gravitational waves which are detectable by B-mode polarization anisotropies of CMB photons. The simplest description of cosmic inflation is based on inflaton as a single field coming from particle physics which decays at the end of inflation into other particles due to a reheating process. Regarding the potential of the inflaton, we define two main divisions, including large field models in which the value of inflaton at the start of inflation is bigger than its value at the end of inflation and small field models in which the value of inflaton at the beginning of inflation is smaller than its value when inflation ends. Another class of basic inflationary models deals with more than one scalar field to drive inflation, in particular, the hybrid model in which an assistant scalar field is engaged to aid inflaton in order to terminate inflation. Moreover, the inflationary models founded on the modified theories of gravity have been noticed in recent years, significantly. The eternal inflation also presents an unconventional approach to inflation by considering some little bubbles of space that could have randomly held inflating instead of ending inflation all at once. As a consequence of the above study, one can find a wide range of inflationary models among the cosmological papers and the most reliable way to discriminate the models is using the inflationary observations which come from the analysis of the temperature and polarisation anisotropies of CMB photons. Hence, the main aim of the present thesis is finding the observational constraints on some inflationary models by using the CMB anisotropies observations.

The main purpose of our first research work was finding the CMB anisotropies constraints on parameters space of power-law inflationary potentials, as the main generator of large field models, in the context of non-minimal coupling of gravity and inflaton. Also, we studied the effects of the presence of the NMC term on the predicted amount of gravitational waves in such models. We carried out the inflationary analysis for the power-law potentials with the NMC term in the Einstein frame as the easier frame which is conformally connected to the Jordan frame as the non-minimal frame. We considered two main classes of large field potentials, e.g., $n = 4$ and $n \neq 4$ with contains integer and fractional values. The inflationary parameters in both cases presented up to the first order of the slow-roll parameters, where we are assured that the results of the two frames are the same. In order to engage the observational datasets for investigation of the model, we used a model-depended

analysis method wherein N and ξ as the independent parameters driven by modified CosmoMC code can be randomly sampled in a given range and to calculate the inflationary parameters of the model. Then, we provided the final results by corresponded plots and tables.

Our results can be summarized as follows:

- If we conservatively consider only the Planck data at high-ℓ plus an external prior on the optical depth, the bounds on r are rather weak, and we found no indication for coupling from this dataset.
- If consider the full Planck dataset we obtain an indication for a coupling $\xi \sim 0.001$ at the level above one standard deviation for power-law potentials with $n = 1, 2/3, 4/3$, and a sign for a more substantial coupling in the range $\xi \sim 0.002 - 0.004$ for $n = 2, 3, 4$ at two standard deviations. These results are confirmed and reinforced by the inclusion of the BKP data.
- The models considered also show a significant running n_{run}. When we consider the full Planck dataset in combination with the BKP dataset we get an indication above two standard deviations for running $n_{run} \sim -0.0006$ for $n < 2$ and for larger negative running in the range $[-0.007\,;\,-0.001]$ from $n \geq 2$.

Therefore, we not only confirmed that NMC inflationary models with a power law potential with $n \geq 2$ could provide a good fit to current Planck+BKP data but also obtained constraints on the value of the coupling ξ needed to achieve this result. Moreover, we found that models with $n < 2$ predict a negative value of the running of the spectral index of $n_{run} \sim -0.0006$ while models with $n \geq 2$ predict a even more negative value in the range $n_{run} \sim -0.0015 : -0.006$. Given the current constraints from Planck on n_{run} that show a sensitivity of $\Delta n_{run} \sim 0.007$ is therefore possible that near future measurements could significantly constrain power law NMC models with $n \geq 2$.
Our second research work dedicated to finding constraints on inflationary parameters using a set of recent CMB data and under the assumption of the Starobinski model. Also, we considered a particular class of inflationary models that generalize Starobinsky inflation and the possibility of an extension to ΛCDM described by the A_{lens} parameter. We presented the inflationary analysis for the generalized form of the Starobinsky model and used the conformal transformation to transit to the Einstein frame as the conformal frame. Then, we followed the inflationary investigation in the presence of a new scalar field, which is called scaleron, created due to using the conformal transformation. We calculated the inflationary parameters up to the first order of the slow-roll parameters as two main classes, $p = 1$ or Starobinsky model and $p \neq 1$ for a generalized case. Similar to the previous model, we used a model-depended analysis method wherein N and p as the independent parameters driven by modified CosmoMC code, can be randomly sampled in a given range and to calculate the inflationary parameters of the model. Lastly, we examined the final results by corresponded plots and tables.

We can summarize our results as follows:

- When conservatively considering Starobinsky inflation, corresponding to $p = 1$, and using the full Planck 2015 likelihood we obtain an upper limit on the tensor to scalar ratio $r > 0.0017$ at 95% C.L. and an indication for a negative

running at more than two standard deviations. While smaller values for r are allowed, also values of $r \sim 0.006$ are now inside the 95% C.L. Interestingly, models with a larger value of r would also predict a more negative value of the running α_s. The maximum value of $\alpha_s \sim -0.001$ (see Figure 6.3), however, is not within the reach of the future CMB-S4 experiment that is expected to have a sensitivity on the running of $\Delta\alpha_s \sim 0.0026$ [285]. The combination of the Planck and BK14 datasets leaves our results almost unchanged. As discussed above, this is related to the fact that our results are coming from the Planck bound on n_S and from assuming inflationary consistency relations between n_S, r and α_S and therefore they are not significantly affected from the inclusion of the BICEP2 B-mode likelihood.

- Considering the phenomenological lensing parameter shifts the best-fit values of r and α_S due to the degeneracy between and the scalar parameters n_S and A_S. When is considered, the upper limit is now $r > 0.0013$ at 95% C.L., i.e., the amount of gravitational waves predicted is significantly smaller. Future CMB experiments should, therefore, target to a $\Delta r \sim 0.0003$ sensitivity if they plan to falsify the Starobinski model at the level of five standard deviations. This sensitivity is about a factor two better than the one predicted for the CMB-S4 experiment.

- For a more general R^{2p} inflation and using the full Planck likelihood, we found no lower limit for the tensor mode amplitude. Conversely, we obtain a tight constraint on the index p at the 95% C.L. confirming that small departures from the Starobinsky model are allowed by the Planck data with values in the range $0.962 \leq p \leq 1.016$. The inclusion of worsen this constraint by the 20%. When considering the combination of the full Planck dataset with the BK14 dataset again we do not find any improvement w.r.t. to the Planck datasets alone. However, including now do not worsen the constraints on p but only shift the best fit of α_S to a less negative value.

We confirmed that Starobinsky inflation provides an excellent fit to the most recent data, but that uncertainties on n_s and on the value of A_{lens} could easily bring the expected value of r in the region of $r \sim 0.001$. If the primordial inflationary background is at this level, it will not be detectable either by the Simons Observatory [284], that has an expected sensitivity around $\Delta r \sim 0.002$, either by the LiteBIRD satellite that is planned to have a sensitivity of $\Delta r \sim 0.001$. It will also be barely detectable by CMB-S4 [285] that is expected to reach a target sensitivity of $\Delta r \sim 0.0006$. Moreover, the goal of the CMB-S4 mission to "achieve a 95% confidence upper limit of $r < 0.001$" [285] can be severely affected if the primordial gravitational waves background is in the region of $r \sim 0.001$. However, values of r could also reach the $r \sim 0.006$ region, allowing, in this case, a statistically significant detection at about three standard deviations for the Simons Observatory and at about ten standard deviations for CMB-S4. In the optimistic case of $r \sim 0.006$ we also expect a running of the spectral index $\alpha_s \sim -0.001$. Unfortunately this value can't be detectable even by future CMB experiments as CMB-S4 (with expected sensitivity of $\Delta\alpha_s \sim 0.002$ [285]), but it could be reachable when information from future lensing or galaxy clustering measurements are included. Finally, small departures from the Starobinski model are also possible and in agreement with observations. In this case, we found no predicted lower limit to r.

Appendix A

Conformal Transformation

In this appendix, first, we introduce the conformal transformation as a useful mathematical tool for diverse gravitational scenarios. Then, we apply the conformal transformation for some gravitational theories under consideration.

A.1 Introduction

The conformal transformation plays an essential role in many physics fields e.g. electromagnetism [303] and quantum theories [304]. Also, it is widely engaged in relativity and cosmology so that it can be exploited to introduce the conformally flat spacetimes [305] and even to construct Penrose diagrams [306], which are one of the most important techniques for the study of black hole physics. Moreover, it is used for a wide range of gravitational theories which are based on scalar fields through the dependence of the conformal factor $\Omega = \Omega(x(\varphi))$ to scalar field φ. This can be addressed to some modified theories of gravity including the scalar-tensor, nonlinear gravity theories and also the theories dealing with the extra dimensions like Kaluza-Klein theories [50, 51, 52, 53, 54, 135, 136, 137, 307, 308, 309, 310, 311, 312]. Moreover, the conformal transformation can be engaged to the inflationary models based on scalar fields in the presence of a non-minimal coupling between gravity and scalar field [313, 314, 210]. Since working with such theories is followed by some difficulties compared to GR, we apply the conformal transformation to ease calculations due to mapping from the *Jordan frame* as the main frame to the *Einstein frame* as the conformal frame. In other words, the conformal transformation is employed as a mathematical tool to map the equations of a system into mathematically equivalent sets of equations for easier study. Hence, the physical equivalency of two frames would be expected as a consequence of mathematical equivalency at the classical level.
On the quantum level, the equivalence between two frames is disturbed by anomaly which is essential and manifests itself at the level of the one-loop divergences already. In a framework of Einstein gravity, the one-loop counterterms vanish on the classical mass shell and the theory is finite [315]. Indeed this property does not hold if the matter fields are incorporated [316] or if the two-loop effects are taken into account [317]. In our new conformal frame, the one-loop S-matrix is not finite because of the anomaly. This fact can be interpreted as the non-invariance of the measure of the path integral with respect to (generalized) conformal transformations. Earlier, a similar objection has been made in a quantum conformal (Weyl) gravity [318, 319] which is power counting renormalizable. In the case of Weyl gravity, the lack of renormalizability is caused by anomaly which affects even the one-loop divergences. The difference is that here, we lack the one-loop on shell renormalizability which is lost in a new frame. Now, let's review some applications of the conformal transformation for gravitational theories at the classical level.

A.2 Einstein's Gravity

In order to present the conformal transformation, let us consider an arbitrary manifold M described by two different metrics $\hat{g}_{\mu\nu}$ and $g_{\mu\nu}$ which are connected conformally if

$$\hat{g}_{\mu\nu} = \Omega^2 g_{\mu\nu} \tag{A.1}$$

where $\Omega = \Omega(x)$ is the conformal factor and is a non-zero, differentiable function. In other words, one can find two different coordinates sets on the manifold M with the metrics $\hat{g}_{\mu\nu}$ and $g_{\mu\nu}$ which are equivalent mathematically and it leads to the physical equivalency between two structures. Mathematically, under the conformal transformation, the angles between the vectors and their values are conserved but not necessarily the lengths. We can translate this property of the conformal transformation into the relativity language. In fact, by conformal mapping, the lengths of spacelike and timelike intervals and also their vectors are affected, but it leaves the light cones unchanged. Thus, two sets have the same casual structure. Through the conformal connection of two metrics, $\hat{g}_{\mu\nu}$ and $g_{\mu\nu}$ (A.1), other geometrical parameters in two frames can also be linked to each other conformally. The conformal relations between two sets for the Christoffel symbol, Riemann tensor, Ricci tensor and Ricci scalar are given respectively as [309]

$$\hat{\Gamma}^{\alpha}_{\beta\gamma} = \Gamma^{\alpha}_{\beta\gamma} + \Omega^{-1}(\delta^{\alpha}_{\beta}\nabla_{\gamma}\Omega + \delta^{\alpha}_{\gamma}\nabla_{\beta}\Omega - g_{\beta\gamma}\nabla^{\alpha}\Omega), \tag{A.2}$$

$$\begin{aligned}\hat{R}_{\alpha\beta\gamma}{}^{\delta} = R_{\alpha\beta\gamma}{}^{\delta} + 2\delta^{\delta}_{[\alpha}\nabla_{\beta]}\nabla_{\gamma}(\ln\Omega) - 2g^{\delta\sigma}g_{\gamma[\alpha}\nabla_{\beta]}\nabla_{\sigma}(\ln\Omega) + 2\nabla_{[\alpha}(\ln\Omega)\delta^{\delta}_{\beta]} \\ \nabla_{\gamma}(\ln\Omega) - 2\nabla_{[\alpha}(\ln\Omega)g_{\beta]\gamma}g^{\delta\sigma}\nabla_{\sigma}(\ln\Omega) - 2g_{\gamma[\alpha}\delta^{\delta}_{\beta]}g^{\sigma\rho}\nabla_{\sigma}(\ln\Omega)\nabla_{\rho}(\ln\Omega),\end{aligned} \tag{A.3}$$

$$\begin{aligned}\hat{R}_{\alpha\beta} = R_{\alpha\beta} - (n-2)\nabla_{\alpha}\nabla_{\beta}(\ln\Omega) - g_{\alpha\beta}g^{\rho\sigma}\nabla_{\rho}\nabla_{\sigma}(\ln\Omega) + (n-2)\nabla_{\alpha}(\ln\Omega) \\ \nabla_{\beta}(\ln\Omega) - (n-2)g_{\alpha\beta}g^{\rho\sigma}\nabla_{\rho}(\ln\Omega)\nabla_{\sigma}(\ln\Omega)\end{aligned} \tag{A.4}$$

and

$$\hat{R} \equiv \hat{g}^{\alpha\beta}\hat{R}_{\alpha\beta} = \Omega^{-2}\left(R - 2(n-1)\Box(\ln\Omega) - (n-1)(n-2)\frac{g^{\alpha\beta}\nabla_{\alpha}\Omega\nabla_{\beta}\Omega}{\Omega^2}\right), \tag{A.5}$$

where n is the dimension of the manifold M. For our 4D universe ($n = 4$), the Ricci scalar takes the following form

$$\hat{R} = \Omega^{-2}\left(R - \frac{6\Box\Omega}{\Omega}\right) = \Omega^{-2}\left(R - \frac{12\Box(\sqrt{\Omega})}{\sqrt{\Omega}} - \frac{3g^{\alpha\beta}\nabla_{\alpha}\Omega\nabla_{\beta}\Omega}{\Omega^2}\right), \tag{A.6}$$

where $\Box = g^{\rho\sigma}\nabla_{\rho}\nabla_{\sigma}$. Finally, the Einstein tensor under the conformal transformation (A.1), takes the following form as

$$\hat{G}_{\mu\nu} = G_{\mu\nu} + \frac{n-2}{2\Omega^2}\left(4\Omega_{,a}\Omega_{,b} + (n-5)\Omega_{,c}\Omega^{,c}g_{\mu\nu}\right) - \frac{n-2}{\Omega}\left(\Omega_{;ab} - g_{\mu\nu}\Box\Omega\right). \tag{A.7}$$

An important feature of the conformal transformations is that it preserves the Weyl conformal curvature tensor

$$C_{abcd} = R_{abcd} + \frac{2}{n-2}(g_{a[d}R_{c]b} + g_{b[c}R_{d]a}) + \frac{2}{(n-1)(n-2)}Rg_{a[c}g_{d]b} \tag{A.8}$$

which means we have $\hat{C}_{\alpha\beta\gamma}{}^{\delta} = C_{\alpha\beta\gamma}{}^{\delta}$ and the null geodesics are also conformally invariant. Notice that the conservation law of the energy-momentum tensor $\nabla^{\nu}T_{\mu\nu} = 0$ is not conformally invariant unless the tensor is traceless. Also, the Klein-Gordon equation of a scalar field is not conformally invariant, but its generalization as

$$\Box\varphi - \frac{(n-2)}{4(n-1)}R\varphi = 0 \tag{A.9}$$

is invariant for $n \geq 2$.

A.3 Scalar-Tensor Theories of Gravity

One of the most known modifications of GR is the scalar-tensor theories of gravity in which we consider a scalar field coupled with gravity in the Einstein-Hilbert action. Thus the form of standard action modifies as presented by the Eq. (3.48). Also, we pointed out that due to the coupling between gravity and scalar field, we can apply the conformal transformation to transit from the Jordan frame (main frame) to the Einstein frame (3.49) as the easier frame for calculations in which we deal with a new form of scalar field and appropriated potential (3.50). As we know, in the case of $w = constant$ and $\Lambda = constant$, the scalar-tensor theory reduces to the Brans-Dicke theory and now that would be worth to see how the conformal transformation work for such theory. Let's start with the form of action in the Brans-Dicke theory as [135, 136, 137]

$$S_{BD} = \int d^4x \frac{1}{2\kappa^2}\sqrt{-g}\left(\varphi R - \frac{w}{\varphi}\partial^{\mu}\varphi\partial_{\mu}\varphi\right) + S_M \tag{A.10}$$

and by varying the above action respect to the metric, we obtain the field equation as

$$R_{\mu\nu} - \frac{R}{2}g_{\mu\nu} = \frac{\kappa^2}{\varphi}T_{\mu\nu} + \frac{w}{\varphi^2}\left(\partial_{\mu}\varphi\partial_{\nu}\varphi - \frac{1}{2}g_{\mu\nu}\partial^{\gamma}\varphi\partial_{\gamma}\varphi\right) + \frac{1}{\varphi}(\partial_{\mu}\partial_{\nu}\varphi - g_{\mu\nu}\Box\varphi). \tag{A.11}$$

By using the conformal factor $\Omega = \frac{\varphi}{m_{PL}^2}$, we can change from the Jordan frame to the conformal frame with the familiar form of the Einstein action as

$$S_E = \int d^4x\left[\frac{1}{2}\sqrt{-\hat{g}}\left((\frac{\hat{R}}{\kappa^2}) - \hat{\partial}^{\mu}\hat{\varphi}\hat{\partial}_{\mu}\hat{\varphi}\right) + \exp\left(-8\sqrt{\frac{\kappa^2}{8(2w+3)}}\hat{\varphi}\right)\mathcal{L}_M(\hat{g})\right], \tag{A.12}$$

where $\hat{\varphi}$ as the redefined form of scalar field is connected to the Brans-Dicke scalar field φ by

$$d\hat{\varphi} = \sqrt{\frac{2w+3}{2\kappa^2}}\frac{d\varphi}{\varphi}. \tag{A.13}$$

As we can see, the gravitational sector of the action in the Jordan frame (A.10) is described by the coupling between gravity R and Brans-Dicke field φ. However, by using the conformal transformation, gravity is expressed only by the redefined Ricci scalar $\hat{R}$ and the new free scalar field $\hat{\varphi}$ takes the role of ordinary matter. We remind that the conformal transformation applied for a general form of action in scalar-tensor gravity in the previous chapter.

A.4 Non-Minimally Coupled Theories of Gravity

By using the conformal transformation, we can ease the calculations of cosmological scenarios equipped with non-minimal coupling term between gravity R and scalar field φ. Based on theoretical considerations, we can not neglect the role of direct interaction between two fields. Hence the standard gravitational action is modified by joining a non-minimal term as [313, 314, 210]

$$S = \int \sqrt{-g}\left((1-\kappa^2\xi\varphi^2)\frac{R}{2\kappa^2} - \frac{1}{2}g^{\mu\nu}\partial_\mu\varphi\partial_\nu\varphi - V(\varphi)\right)d^4x + S_M(g_{\mu\nu},\Psi_M), \tag{A.14}$$

where $V(\varphi)$ is the potential describing the scalar field and S_{matter} is associated with matter fields other than φ. In the non-minimal term $\xi\varphi^2R$, ξ is known as coupling constant and its value is crucial for our cosmological aims. By varying the action respect with the metric, the field equation is given as

$$(1-\kappa^2\xi\varphi^2)(R_{\mu\nu} - \frac{R}{2}g_{\mu\nu}) = \kappa^2(\tilde{T}_{\mu\nu}(\varphi) + \tilde{T}_{\mu\nu}(\Psi_M)), \tag{A.15}$$

where

$$\tilde{T}_{\mu\nu}(\varphi) = \partial_\mu\varphi\partial_\nu\varphi - \frac{1}{2}g_{\mu\nu}\partial^\gamma\varphi\partial_\gamma\varphi - V(\varphi)g_{\mu\nu} + \xi\left(g_{\mu\nu}\Box\varphi^2 - \partial_\mu\partial_\nu\varphi^2\right), \tag{A.16}$$

$$\tilde{T}_{\mu\nu}(\Psi_M) = -\frac{2}{\sqrt{-g}}\frac{\delta S_M(\Psi_M, g_{\mu\nu})}{\delta g^{\mu\nu}}, \tag{A.17}$$

$$\Omega^2 = 1-\kappa^2\xi\varphi^2 \tag{A.18}$$

then, the action in the Einstein frame can be expressed by

$$S = \int d^4x\sqrt{-\hat{g}}\left(\frac{\hat{R}}{2\kappa^2} - \frac{1}{2}\hat{\partial}^\mu\hat{\varphi}\hat{\partial}_\nu\hat{\varphi} - \hat{V}(\hat{\varphi})\right) + \int d^4x\mathcal{L}_M(\Omega^{-2}(\varphi)\hat{g}_{\mu\nu},\Psi_M), \tag{A.19}$$

where $\hat{V}(\hat{\varphi})$ is the potential of the new scalar field $\hat{\varphi}$ and is defined as

$$\hat{V}(\hat{\varphi}) = \frac{V(\varphi)}{(1-\kappa^2\xi\varphi^2)^2}. \tag{A.20}$$

Also, two scalar fields are connected by

$$\frac{d\varphi}{d\hat{\varphi}} = \frac{1-\kappa^2\xi\varphi^2}{\sqrt{1-\kappa^2\xi\varphi^2(1-6\xi)}}. \tag{A.21}$$

Using the conformal transformation for large field inflationary models with a non-minimal coupling term will be studied in chapter 5.

A.5 f(R) Theories of Gravity

Another conventional modification of gravity presented to explain DE is f(R) theory. Based on such gravity, we do not require to consider the cosmological constant to drive the late time acceleration (even for inflation as early time acceleration) and only by changing the geometry, we can provide the acceleration phase for the universe. The f(R) gravity theory is a type of nonlinear gravity since it deals with a general and nonlinear function of Ricci scalar R. The form of action in this theory is given by [53, 54]

$$S = \frac{1}{2\kappa^2}\int d^4x\sqrt{-g}f(R) + \int d^4x\mathcal{L}_M(g_{\mu\nu},\Psi_M), \tag{A.22}$$

where $\mathcal{L}_{matter}$ denotes to matter Lagrangian and Ψ_{matter} implies to matter fields. The field equations are driven by variation of the action (A.22) respect with metric $g_{\mu\nu}$ as

$$\frac{\partial f}{\partial R}R_{\mu\nu} - \frac{1}{2}f(R)g_{\mu\nu} - \nabla_\mu\nabla_\nu\frac{\partial f}{\partial R} + g_{\mu\nu}\Box\frac{\partial f}{\partial R} = \kappa^2 T^M_{\mu\nu}, \tag{A.23}$$

where the energy-momentum tensor $T^M_{\mu\nu}$ is defined by

$$T^M_{\mu\nu} = -\frac{2}{\sqrt{-g}}\frac{\delta\mathcal{L}_M}{\delta g^{\mu\nu}}. \tag{A.24}$$

In order to move to the Einstein frame, we apply the conformal transformation (A.1) by definition of the conformal factor as

$$\Omega^2 = \mathcal{F} \equiv e^{\sqrt{\frac{2\kappa^2}{3}}\varphi} \tag{A.25}$$

and then the form of action in the Einstein frame takes the following form

$$S = \int d^4x\sqrt{-\hat{g}}\left(\frac{\hat{R}}{2\kappa} - \frac{1}{2}\hat{g}^{\mu\nu}\partial_\mu\varphi\partial_\nu\varphi - V(\varphi)\right) + \int d^4x\mathcal{L}_M(\mathcal{F}^{-1}(\varphi)\hat{g}_{\mu\nu},\Psi_M) \tag{A.26}$$

where the potential of new scalar field φ can be defined by

$$V(\varphi) = \frac{\mathcal{F}R - f}{2\kappa\mathcal{F}^2} \tag{A.27}$$

In chapter 6, the discussed transformation will be applied to investigate the R^{2p} inflationary model as a customary form of the Starobinsky R^2 model.

Bibliography

[1] R. M. Wald, *General Relativity*. University of Chicago Press, 1984.

[2] E. W. Kolb and M. S. Turner, *The Early Universe*. Review of Scientific Instruments, 1990.

[3] P. Peebles, *Principles of physical cosmology*. Princeton University Press, 1994.

[4] A. R. Liddle, *An introduction to modern cosmology*. Wiley, 1998.

[5] A. R. Liddle and D. Lyth, *Cosmological inflation and large scale structure*. Cambridge University Press, 2000.

[6] B. Ryden, *Introduction to Cosmology*. Addison-Wesley, 2002.

[7] S. M. Carroll, *Spacetime and Geometry: An Introduction to General Relativity*. Addison-Wesley, 2001.

[8] S. Dodelson, *Modern cosmology*. Amsterdam, Netherlands: Academic Press, 2003.

[9] Ø. Grøn and S. Hervik, *Einstein's General Theory of Relativity*. Springer-Verlag New York, 2007.

[10] S. Weinberg, *Cosmology*. Oxford University Press, 2008.

[11] D. H. Lyth and A. R. Liddle, *The primordial density perturbation*. Cambridge University Press, 2009.

[12] A. Einstein, "The foundation of the general theory of relativity," *Annalen der Physik*, vol. 49, p. 769–822, (1916).

[13] E. Mach, "The science of mechanics," *Open Court, La Salle*, (1960).

[14] M. Born and G. Leibfried, *Einstein's Theory of Relativity*. Courier Dover Publications, 1965.

[15] H. Bondi and J. Samuel, "The lense–thirring effect and mach's principle," *Phys. Lett. A.*, vol. 228, p. 121–126, (1996).

[16] M. P. Haugen and C. Lämmerzahl, "Principles of equivalence: Their role in gravitation physics and experiments that test them," *Gyros.*, vol. 562, p. 195–212, (2001).

[17] F. Giannoni, A. Masiello, and P. Piccione, "The fermat principle in general relativity and applications," *[arXiv:math-ph/9906023]*.

[18] L. Bel and J. Martín, "Fermat's principle in general relativity," *Gyros.*, vol. 26, p. 567–585, (1994).

[19] A. Einstein, "On the electrodynamics of moving bodies," *Annalen der Physik*, vol. 17, pp. 891–921, (1905).

[20] C. W. Misner, K. S. Thorne, and J. A. Wheeler, *Gravitation*. Princeton University Press.

[21] N. Bohr, "About the serial spectra of the element," *Zeitschrift für Physik*, vol. 2, p. 423–478, (1920).

[22] U. L. Verrier, "Letter from mr. le verrier to mr. faye on the theory of mercury and on the movement of the perihelion of this planet," *Comptes rendus hebdomadaires des séances de l'Académie des sciences*, vol. 49, p. 379–383, (1859).

[23] F. W. Dyson, A. S. Eddington, and C. Davidson, "A determination of the deflection of light by the sun's gravitational field, from observations made at the total eclipse of 29 may 1919," *Philosophical Transactions of the Royal Society*, vol. 220A, p. 291–333, (1920).

[24] R. V. Pound and J. G. A. Rebka, "Gravitational red-shift in nuclear resonance," *Phys. Rev. Lett..*, vol. 3, p. 439–441, (1959).

[25] A. Einstein, "Approximately integration of the field equations of gravitation," *Sitzungsberichte der Königlich Preussischen Akademie der Wissenschaften Berlin*, vol. 1, p. 688–696, (1916).

[26] J. H. Taylor, L. A. Fowler, and P. M. McCulloch, "Overall measurements of relativistic effects in the binary pulsar psr 1913 + 16," *Nature*, vol. 277, p. 437–440, (1979).

[27] B. P. Abbott *et al.*, "Observation of gravitational waves from a binary black hole merger," *Phys. Rev. Lett.*, vol. 116, pp. 061102–061116, (2016).

[28] A. Einstein, "On the general theory of relativity," *Sitzungsber. Preuss. Akad. Wiss. Berlin*, vol. 1915, p. 778–786, (1915).

[29] D. Hilbert, "The basics of physics. 1.," *Gott. Nachr.*, vol. 27, p. 395–407, (1915).

[30] H. Stephani, D. Kramer, M. MacCallum, C. Hoenselaers, and E. Herlt, *Exact Solutions of Einstein's Field Equations*. Cambridge University Press, 2003.

[31] A. Friedmann, "On the possibility of a world with constant negative curvature of space," *Z. Phys.*, vol. 21, p. 326–332, (1924).

[32] G. Lemaitre, "A homogeneous universe of constant mass and growing radius accounting for the radial velocity of extragalactic nebulae," *Annales Soc. Sci. Brux. Ser. I Sci. Math. Astron. Phys.*, vol. A47, p. 49–59, (1927).

[33] H. Robertson, "Kinematics and world-structure," *Astrophysical Journal*, vol. 82, p. 284–301, (1935).

[34] A. G. Walker, "On the formal comparison of milne's kinematical system with the systems of general relativity," *Mon. Not. Roy. Astron. Soc.*, vol. 95, p. 263–269, (1935).

[35] K. Schwarzschild, "About the gravitational field of a mass point according to einstein's theory," *Sitzungsberichte der Königlich Preussischen Akademie der Wissenschaften*, vol. 7, p. 189–196, (1916).

[36] R. P. Kerr, "Gravitational field of a spinning mass as an example of algebraically special metrics," *Phys. Rev. Lett.*, vol. 11, p. 237–238, (1963).

[37] H. Reissner, "About the gravitational field of a mass point according to einstein's theory," *Annalen der Physik*, vol. 50, p. 106–120, (1916).

[38] H. Weyl, "To the theory of gravitation," *Annalen der Physik*, vol. 54, p. 117–145, (1917).

[39] G. Nordström, "On the energy of the gravitational field in Einstein's theory," *Verhandl. Koninkl. Ned. Akad. Wetenschap. Afdel. Natuurk.*, vol. 26, p. 1201–1208, (1918).

[40] G. B. Jeffery, "The field of an electron on Einstein's theory of gravitation," *Proc. Roy. Soc. Lond. A.*, vol. 99, p. 123–134, (1921).

[41] E. Newman, E. Couch, K. Chinnapared, A. Exton, A. Prakash, and R. Torrence, "Metric of a rotating, charged mass," *Journal of Mathematical Physics.*, vol. 6, p. 918–919, (1965).

[42] A. Friedmann, "On the curvature of space,," *Z. Phys.*, vol. 10, p. 377–386, (1922).

[43] A. Raychaudhuri, "Relativistic cosmology. 1.," *Phys. Rev.*, vol. 98, p. 1123–1126, (1955).

[44] E. A. Milne, "A newtonian expanding universe," *The Quarterly Journal of Mathematics*, vol. 5, p. 64–72, (1934).

[45] A. Einstein and W. de Sitter, "On the relation between the expansion and the mean density of the universe," *Proceedings of the National Academy of Sciences*, vol. 18, p. 213–214, (1932).

[46] P. A. R. Ade *et al.*, "Planck 2013 results. xvi. cosmological parameters," vol. 18, p. 213–214, (2018).

[47] A. G. Riess *et al.*, "Observational evidence from supernovae for an accelerating universe and a cosmological constant," *Astronomical Journal.*, vol. 116, p. 1009–1038, (1998).

[48] S. Perlmutter *et al.*, "Measurements of omega and lambda from 42 high redshift supernovae," *Astronomical Journal*, vol. 517, p. 565–586, (1999).

[49] J. Martin, "Everything you always wanted to know about the cosmological constant problem (but were afraid to ask)," *Comptes Rendus Physique*, vol. 13, p. 566–665, (2012).

[50] S. Capozziello and V. Faraoni, *Beyond Einstein Gravity*. Springer Netherlands, 2011.

[51] S. Capozziello and M. D. Laurentis, "Extended theories of gravity," *Phys. Rep.*, vol. 509, pp. 167–321, (2011).

[52] S. Nojiri, S. D. Odintsov, and V. K. Oikonomou, "Modified gravity theories on a nutshell: Inflation, bounce and late-time evolution," *Phys. Rep.*, vol. 692, pp. 1–104, (2017).

[53] T. Sotiriou and V. Faraoni, "f(R) theories of gravity," *Rev. Mod. Phys.*, vol. 82, p. 451–497, (2008).

[54] A. D. Felice and S. Tsujikawa, "f(R) theories," *Liv. Rev. Relativ.*, vol. 13, pp. 3–158, (2010).

[55] R. Maartens and K. Koyama, "Brane-world gravity," *Liv. Rev. Relativ.*, vol. 13, pp. 5–223, (2010).

[56] S. W. Allen, A. E. Evrard, E. August, and A. B. Mantz, "Cosmological parameters from clusters of galaxies," *Annual Review of Astronomy and Astrophysics*, vol. 49, p. 409–470, (2011).

[57] J. G. de Swart, G. Bertone, and D. J. van Dongen, "How dark matter came to matter," *Nature Astronomy.*, vol. 1, pp. 0059–0066, (2017).

[58] E. Amaldi, "From the discovery of the neutron to the discovery of the nuclear fission," *Nature Astronomy.*, vol. 111, pp. 1–331, (1984).

[59] B. Follin, L. Knox, M. Millea, and Z. Pan, "First detection of the acoustic oscillation phase shift expected from the cosmic neutrino background," *Phys. Rev. Lett.*, vol. 115, pp. 091301–091304, (2015).

[60] D. D. Clayton, *Principles of Stellar Evolution and Nucleosynthesis*. University of Chicago Press, (1983).

[61] D. Kirzhnits and A. D. Linde, "Macroscopic consequences of the weinberg model," *Phys. Lett. B*, vol. 42, p. 471–474, (1972).

[62] S. Weinberg, "Gauge and global symmetries at high temperature," *Phys. Rev. D*, vol. 9, p. 3357–3378, (1974).

[63] D. Kirzhnits, "Weinberg model in the hot universe," *JETP Lett.*, p. 529–531, (1972).

[64] L. Dolan and R. Jackiw, "Symmetry behavior at finite temperature," *Phys. Rev. D*, vol. 9, p. 3320–3341, (1974).

[65] D. Kirzhnits and A. D. Linde, "A relativistic phase transition," *Sov. Phys. JETP*, vol. 40, pp. 628–640, (1975).

[66] D. Kirzhnits and A. D. Linde, "Symmetry behavior in gauge theories," *Annals Phys.*, vol. 101, p. 195–238, (1976).

[67] P. Y. H. A. D. L. M. Dine, R. G. Leigh and D. A. Linde, "Towards the theory of the electroweak phase transition," *Phys. Rev. D*, vol. 46, p. 550–571, (1992).

[68] K. A. Olive, "The thermodynamics of the quark - hadron phase transition in the early universe," *Nucl. Phys. B*, vol. 483-503, p. 190, (1981).

[69] E. Suhonen, "The quark - hadron phase transition in the early universe," *Nucl. Phys. B*, vol. 81-84, p. 119, (1982).

[70] M. Crawford and D. N. Schramm, "Spontaneous generation of density perturbations in the early universe," *Nature*, vol. 298, p. 538–540, (1982).

[71] J. Applegate and C. Hogan, "Relics of cosmic quark condensation," *Phys. Rev. D*, vol. 31, p. 3037–3045, (1985).

[72] H. Satz, "The transition from hadron matter to quark-gluon plasma," *Ann. Rev. Nucl. Part. Sci*, vol. 35, p. 245–270, (1985).

[73] G. M. G. Fuller and C. Alcock, "The quark - hadron phase transition in the early universe: Isothermal baryon number fluctuations and primordial nucleosynthesis," *Phys. Rev. D*, vol. 37, pp. 1380–1400, (1988).

[74] H. B. R. Alpher and G. Gamow, "The origin of chemical elements," *Phys. Rev.*, vol. 73, p. 803–804, (1948).

[75] W. A. F. R. V. Wagoner and F. Hoyle, "On the synthesis of elements at very high temperatures," *Astrophysical Journal*, vol. 148, p. 3–49, (1967).

[76] S. Sarkar, "Big bang nucleosynthesis and physics beyond the standard model," *Rept. Prog. Phys.*, vol. 59, p. 1493–1610, (1996).

[77] D. N. Schramm and M. S. Turner, "Big bang nucleosynthesis and physics beyond the standard model," *Rept. Prog. Phys.*, vol. 70, p. 303–318, (1998).

[78] A. A. Penzias and R. W. Wilson, "A measurement of excess antenna temperature at 4080-mc/s," *Astrophysical Journal*, vol. 142, p. 419–421, (1965).

[79] J. E. Gunn and B. A. Peterson, "On the density of neutral hydrogen in intergalactic space," *Astrophysical Journal*, vol. 142, pp. 1633–1636, (1965).

[80] R. H. Becker *et al.*, "Evidence for reionization at $z \sim 6$: Detection of a gunn-peterson trough in a $z = 6.28$ quasar," *Astrophysical Journal*, vol. 122, pp. 2850–2857, (2001).

[81] R. Barkana and A. Loeb, "In the beginning: The first sources of light and the reionization of the universe," *Phys. Rept.*, vol. 349, p. 125–238, (2001).

[82] E. Hubble, "A relation between distance and radial velocity among extra-galactic nebulae," *Proc. Nat. Acad. Sci.*, vol. 15, p. 168–173, (1929).

[83] G. Gamow, "The origin of elements and the separation of galaxies," *Phys. Rev.*, vol. 74, p. 505–506, (1948).

[84] G. Gamow, "The evolution of the universe," *Nature*, vol. 162, p. 680–682, (1948).

[85] R. A. Alpher and C. R. Herman, "On the relative abundance of the elements," *Phys. Rev.*, vol. 74, p. 1737–1742, (1948).

[86] R. A. Alpher and C. R. Herman, "Evolution of the universe," *Nature*, vol. 162, p. 774–775, (1948).

[87] G. F. Smoot *et al.*, "Structure in the cobe differential microwave radiometer first-year maps," *Astrophysical Journal*, vol. 396, p. L1–L5, (1992).

[88] C. L. Bennett *et al.*, "Four-year cobe dmr cosmic microwave background observations: Maps and basic results," *Astrophysical Journal*, vol. 464, p. L1–L4, (1996).

[89] G. Hinshaw *et al.*, "Three-year wilkinson microwave anisotropy probe (wmap) observations: temperature analysis," *Astrophysical Journal*, vol. 170, p. 288–334, (2007).

[90] P. A. R. Ade *et al.*, "Detection of b-mode polarization at degree angular scales by bicep2," *Phys. Rev. Lett.*, vol. 112, pp. 241101–241113, (2014).

[91] R. Dicke, *Gravitation and the Universe: The Jayne Lectures for 1969*. American Philosophical Society.

[92] R. Dicke and P. Peebles, *General Relativity: An Einstein Centenary Survey*. Cambridge University Press, (1979).

[93] W. Rindler, "Visual horizons in world-models," *Mon. Not. Roy. Astron. Soc.*, vol. 116, p. 662–677, (1956).

[94] C. W. Misner, "The isotropy of the universe," *Astrophysical Journal*, vol. 151, pp. 431–457, (1967).

[95] A. H. Guth and S. Tye, "Phase transitions and magnetic monopole production in the very early universe," *Phys. Rev. Lett.*, vol. 44, pp. 631–13, (1980).

[96] D. S. M. B. Einhorn and D. Toussaint, "Are grand unified theories compatible with standard cosmology?," *Phys. Rev. D*, vol. 21, pp. 3295–3298, (1980).

[97] W. O. P. Price, E. Shirk and L. S. Pinsky, "Evidence for detection of a moving magnetic monopole," *Phys. Rev. Lett*, vol. 35, p. 487–490, (1975).

[98] B. Cabrera, "First results from a superconductive detector for moving magnetic monopoles," *Phys. Rev. Lett*, vol. 48, p. 1378–1380, (1982).

[99] S. A. P. Price, S.-l. Guo and R. Fleischer, "Search for gut magnetic monopoles at a flux level below the parker limit," *Phys. Rev. Lett*, vol. 52, pp. 1265–1268, (1984).

[100] M. Ambrosio *et al.*, "Search for nucleon decays induced by gut magnetic monopoles with the macro experiment," *Eur. Phys. J. C*, vol. 26, p. 163–172, (2002).

[101] J. Pinfold, "Moedal becomes the lhc's magnificent seventh," *CERN Cour.*, vol. 50N4, p. 19–20, (2010).

[102] A. H. Guth, "The inflationary universe: A possible solution to the horizon and flatness problems," *Phys. Rev. D*, vol. 23, p. 347–356, (1981).

[103] A. D. Linde and R. Brandenberger, *Inflation and quantum cosmology*. Boston USA Academic, (1990).

[104] A. D. Linde, "Particle physics and inflationary cosmology," *Contemp. Concepts Phys.*, vol. 5, pp. 1–362, (1990).

[105] A. H. Guth, *The inflationary universe: The quest for a new theory of cosmic origins.* Addison-Wesley, (1997).

[106] S. Winitzki, *Eternal inflation*. World Scientific Press, (2008).

[107] M. Lemoine, J. Martin, and P. Peter, *Inflationary cosmology*. Springer-Verlag Press, (2008).

[108] A. A. Starobinsky, "A new type of isotropic cosmological models without singularity," *Phys. Lett. B*, vol. 91, p. 99–102, (1980).

[109] D. H. Lyth and A. Riotto, "Particle physics models of inflation and the cosmological density perturbation," *Phys. Rep.*, vol. 314, p. 1–146, (1999).

[110] A. R. Liddle, P. Parsons, and J. D. Barrow, "Formalising the slow-roll approximation in inflation," *Phys. Rev. D*, vol. 50, pp. 7222–7232, (1994).

[111] D. J. Schwarz, C. A. Terrero-Escalante, and A. A. Garcia, "Higher order corrections to primordial spectra from cosmological inflation," *Phys. Lett. B*, vol. 517, p. 243–249, (2001).

[112] D. J. Schwarz and C. A. Terrero-Escalante, "Primordial fluctuations and cosmological inflation after wmap 1.0," *JCAP*, vol. 0408, pp. 003–0021, (2004).

[113] M. S. Turner, "Coherent scalar field oscillations in an expanding universe," *Phys. Rev. D*, vol. 28, pp. 1243–1254, (1983).

[114] L. Kofman, A. D. Linde, and A. A. Starobinsky, "Towards the theory of reheating after inflation," *Phys. Rev. D*, vol. 56, p. 3258–3295, (1997).

[115] B. A. Bassett, D. I. Kaiser, and R. Maartens, "General relativistic preheating after inflation," *Phys. Lett. B*, vol. 455, p. 84–89, (1999).

[116] F. Finelli and R. H. Brandenberger, "Parametric amplification of metric fluctuations during reheating in two field models," *Phys. Rev. D*, vol. 62, pp. 083502–083514, (2000).

[117] S. T. B. A. Bassett and D. Wands, "Inflation dynamics and reheating," *Rev. Mod. Phys.*, vol. 78, p. 537–589, (2006).

[118] A. Mazumdar and J. Rocher, "Particle physics models of inflation and curvaton scenarios," *Phys. Rep.*, vol. 497, p. 85–215, (2011).

[119] K. Jedamzik, M. Lemoine, and J. Martin, "Collapse of small-scale density perturbations during preheating in single field inflation," *JCAP*, vol. 1009, pp. 034–040, (2010).

[120] K. Jedamzik, M. Lemoine, and J. Martin, "Generation of gravitational waves during early structure formation between cosmic inflation and reheating," *JCAP*, vol. 2010, pp. 021–031, (2010).

[121] R. Easther, R. Flauger, and J. B. Gilmore, "Delayed reheating and the breakdown of coherent oscillations," *JCAP*, vol. 1104, pp. 027–044, (2011).

[122] A. Albrecht, P. J. Steinhardt, M. S. Turner, and F. Wilczek, "Reheating an inflationary universe," *Phys. Rev. Lett.*, vol. 48, pp. 1437–1440, (1982).

[123] L. Kofman, A. D. Linde, and A. A. Starobinsky, "Reheating after inflation," *Phys. Rev. Lett.*, vol. 73, p. 3195–3198, (1994).

[124] Y. S. J. H. Traschen and R. H. Brandenberger, "Universe reheating after inflation," *Phys. Rev. D*, vol. 51, p. 5438–5455, (1995).

[125] V. Kuzmin and V. Rubakov, "Ultrahigh-energy cosmic rays: A window to postinflationary reheating epoch of the universe?," *Phys. Atom. Nucl.*, vol. 61, p. 1028–1030, (1998).

[126] F. Finelli and R. H. Brandenberger, "Parametric amplification of gravitational fluctuations during reheating," *Phys. Rev. Lett.*, vol. 82, p. 1362–1365, (1999).

[127] E. W. Kolb, "Dynamics of the inflationary era," *[arXiv:hep-ph/9910311]*.

[128] S. Dodelson, W. H. Kinney, and E. W. Kolb, "Cosmic microwave background measurements can discriminate among inflation models," *Phys. Rev. D*, vol. 56, pp. 3207–3215, (1997).

[129] A. D. Linde, "Chaotic inflation," *Phys. Lett. B*, vol. 129, pp. 177–181, (1983).

[130] K. Freese, J. A. Frieman, and A. V. Olinto, "Natural inflation with pseudo nambu-goldstone bosons," *Phys. Rev. Lett.*, vol. 65, pp. 3233–3236, (1990).

[131] S. R. Coleman and E. J. Weinberg, "Radiative corrections as the origin of spontaneous symmetry breaking," *Phys. Rev. D*, vol. 7, pp. 1888–1910, (1888).

[132] A. D. Linde and A. Riotto *Phys. Rev. D*, vol. 56, pp. 1841–1844, (1997).

[133] E. J. Copeland, A. R. Liddle, D. H. Lyth, E. D. Stewar, and D. Wands, "False vacuum inflation with einstein gravity," *Phys. Rev. D*, vol. 49, pp. 6410–6433, (1994).

[134] A. D. Linde, "Hybrid inflation," *Phys. Rev. D*, vol. 49, pp. 748–754, (1994).

[135] V. Faraoni, *Cosmology in Scalar-Tensor Gravity*. Springer Press, (2004).

[136] Y. Fujii and K. Maeda, *Scalar-Tensor Theory of Gravitation*. Cambridge University Press, (2007).

[137] I. Quiros, "Selected topics in scalar–tensor theories and beyond," *Int. J. Mod. Phys. D*, vol. 28, pp. 1930012–1930192, (2019).

[138] L. Randall and R. Sundrum, "Large mass hierarchy from a small extra dimension," *Phys. Rev. Lett.*, vol. 83, p. 3370–3373, (1999).

[139] L. Randall and R. Sundrum, "An alternative to compactification," *Phys. Rev. Lett.*, vol. 83, p. 4690–4693, (1999).

[140] G. Dvali, G. Gabadadze, and M. Porrati, "4D gravity on a brane in 5D minkowski space," *Phys. Lett. B*, vol. 485, p. 208–214, (2000).

[141] G. Dvali and S. H. H. Tye, "Brane inflation," *Phys. Lett. B*, vol. 450, pp. 72–82, (1999).

[142] R. Maartens, D. Wands, B. A. Bassett, and I. Heard, "Chaotic inflation on the brane," *Phys. Rev. D*, vol. 62, pp. 041301–041305, (2000).

[143] A. H. Guth, "Eternal inflation and its implications," *Journal of Physics A*, vol. 40, pp. 6811–6826, (2007).

[144] P. Zhang and M. C. Johnson, "Testing eternal inflation with the kinetic sunyaev zel'dovich effect," *JCAP*, vol. 1506, pp. 046–078, (2015).

[145] C. L. Wainwright, M. C. Johnson, H. V. Peiris, A. Aguirre, L. Lehner, and S. L. Liebling, "Simulating the universe(s): from cosmic bubble collisions to cosmological observables with numerical relativity," *JCAP*, vol. 1403, pp. 030–085, (2014).

[146] S. M. Feeney, M. C. Johnson, and H. V. P. J. D. McEwen, D. J. Mortlock, "Hierarchical bayesian detection algorithm for early-universe relics in the cosmic microwave background," *Phys. Rev. D*, vol. 88, pp. 043012–043039, (2013).

[147] M. C. Johnson, H. V. Peiris, and L. Lehner, "Determining the outcome of cosmic bubble collisions in full general relativity," *Phys. Rev. D*, vol. 85, pp. 083516–083552.

[148] S. M. Feeney, M. C. Johnson, D. J. Mortlock, and H. V. Peiris, "First observational tests of eternal inflation: Analysis methods and wmap 7-year results," *Phys. Rev. D*, vol. 84, pp. 043507–043542, (2011).

[149] H. Kodama and M. Sasaki, "Cosmological perturbation theory," *Prog. Theor. Phys. Suppl.*, vol. 78, p. 1–166, (1984).

[150] A. Linde, "Particle physics and inflationary cosmology," *[arXiv:hep-th/0503203]*.

[151] D. H. Lyth and A. Riotto, "Inflation dynamics and reheating," *Phys. Rep.*, vol. 314, pp. 1–146, (1999).

[152] A. Riotto, "Inflation and the theory of cosmological perturbations," *[arXiv:hep-ph/0210162]*.

[153] J. E. Lidsey, A. R. Liddle, E. W. Kolb, and E. J. Copeland, "Reconstructing the inflaton potential—an overview," *Rev. Mod. Phys.*, vol. 69, pp. 373–410, (1997).

[154] B. A. Bassett, S. Tsujikawa, and D. Wands, "Inflation dynamics and reheating," *Rev. Mod. Phys.*, vol. 78, pp. 537–589, (2006).

[155] D. W. K. Malik, "Cosmological perturbations," *Phys. Rep.*, vol. 475, pp. 1–51, (2009).

[156] V. Acquaviva, N. Bartolo, S. Matarrese, and A. Riotto, "Second-order cosmological perturbations from inflation," *Nucl. Phys. B*, vol. 119-148, p. 667, (2003).

[157] J. M. Bardeen, "Gauge-invariant cosmological perturbations," *Phys. Rev. D*, vol. 22, pp. 1882–1905, (1980).

[158] V. N. Lukash, "Production of phonons in an isotropic universe," *Sov. Phys. JETP*, vol. 52, pp. 807–814, (1980).

[159] D. H. Lyth, "Large-scale energy-density perturbations and inflation," *Phys. Rev. D*, vol. 31, pp. 1792–1798, (1985).

[160] V. F. Mukhanov, H. A. Feldman, and R. H. Brandenberger, "Theory of cosmological perturbations," *Phys. Rev. D*, vol. 215, pp. 203–333, (1992).

[161] V. F. Mukhanov, "Gravitational instability of the universe filled with a scalar field," *Pisma Zh. Eksp. Teor. Fiz*, vol. 41, pp. 493–496, (1985).

[162] M. Sasaki, "Large scale quantum fluctuations in the inflationary universe," *Prog. Theor. Phys.*, vol. 76, p. 1036–1046, (1986).

[163] V. F. Mukhanov, "Quantum theory of gauge-invariant cosmological perturbations," *Sov. Phys. JETP*, vol. 67, pp. 1297–1302, (1988).

[164] D. H. Lyth and D. Wands, "Conserved cosmological perturbations," *Phys. Rev. D*, vol. 68, pp. 103515–103535, (2003).

[165] J. c. Hwang and H. Noh, "Cosmological perturbations in generalized gravity theories," *Phys. Rev. D*, vol. 54, pp. 1460–1473, (1996).

[166] E. D. Stewart and D. H. Lyth, "A more accurate analytic calculation of the spectrum of cosmological perturbations produced during inflation," *Phys. Lett. B*, vol. 302, pp. 171–175, (1993).

[167] E. F. Bunn, A. R. Liddle, and M. J. White *Phys. Rev. D*, vol. 54, pp. 5917–5921, (1996).

[168] A. Miller *et al.*, "A measurement of the angular power spectrum of the microwave background made from the high chilean andes," *Astrophysical Journal*, vol. 521, p. L79 – L82, (1999).

[169] A. M. *et al.*, "A measurement of from the north american test flight of boomerang," *Astrophysical Journal*, vol. 536, p. L63 – L66, (2000).

[170] S. Hanany *et al.*, "Maxima-1: A measurement of the cosmic microwave background anisotropy on angular scales of 10'-5 ," *Astrophysical Journal*, vol. 545, p. L5–L9, (2000).

[171] P. de Bernardis *et al.*, "A flat universe from high-resolution maps of the cosmic microwave background radiation," *Nature*, vol. 404, p. 955–959, (2000).

[172] D. J. Fixsen *et al.*, "The cosmic microwave background spectrum from the full cobe firas data set," *Astron. J*, vol. 473, pp. 576–587, (1996).

[173] J. Bond and G. Efstathiou, "The statistics of cosmic background radiation fluctuations," *Mon. Not. R. Ast. Soc.*, vol. 226, pp. 655–687, (1987).

[174] A. Kosowsky, "Cosmic microwave background polarization," *Ann. Phys.*, vol. 246, pp. 49–85, (1996).

[175] M. Kamionkowski, A. Kosowsky, and A. Stebbins, "Statistics of cosmic microwave background polarization," *Phys. Rev. D*, vol. 55, pp. 73688–7388, (1997).

[176] M. Zaldarriaga and U. Seljak, "An all-sky analysis of polarization in the microwave background," *Phys. Rev. D*, vol. 55, pp. 1830–1840, (1997).

[177] E. Newman and R. Penrose, "Note on the bondi-metzner-sachs group," *J. Math Phys.*, vol. 7, pp. 863 –870, (1966).

[178] U. Seljak, "Measuring polarization in the cosmic microwave background," *J. Math Phys.*, vol. 482, pp. 6–16, (1997).

[179] A. G. Riess *et al.*, "Observational evidence from supernovae for an accelerating universe and a cosmological constant," *Astron. J*, vol. 116, pp. 1009–1038, (1998).

[180] S. Perlmutter *et al.*, "Measurements of omega and lambda from 42 high-redshift supernovae," *Astron. J*, vol. 517, pp. 565–586, (1999).

[181] P. J. E. Peebles and J. Yu, "Primeval adiabatic perturbation in an expanding universe," *Astrophys. J*, vol. 162, pp. 815–836, (1970).

[182] C. P. Ma and E. Bertschinger, "Cosmological perturbation theory in the synchronous and conformal newtonian gauges," *Astrophys. J*, vol. 455, pp. 7–25, (1995).

[183] W. Hu and N. Sugiyama, "Anisotropies in the cosmic microwave background: An analytic approach," *Astrophys. J*, vol. 444, pp. 489–506, (1995).

[184] N. Kaiser *Mon. Not. R. Ast. Soc.*, vol. 202, pp. Small–angle anisotropy of the microwave background radiation in the adiabatic theory, (1983).

[185] A. H. Guth and S. Y. Pi, "Fluctuations in the new inflationary universe," *Phys. Rev. Lett.*, vol. 49, pp. 1110–1113, (1982).

[186] S. W. Hawking, "The development of irregularities in a single bubble inflationary universe," *Phys. Lett. B*, vol. 115, pp. 295–297, (1982).

[187] J. M. Bardeen, P. J. Steinhardt, and M. S. Turner, "Spontaneous creation of almost scale-free density perturbations in an inflationary universe," *Phys. Rev. D*, vol. 28, pp. 679–693, (1983).

[188] V. A. Rubakov, M. V. Sazhin, and A. V. Veryaskin, "Graviton creation in the inflationary universe and the grand unification scale," *Phys. Lett. B*, vol. 115, pp. 189–192, (1982).

[189] V. R. Fabbri and M. D. Pollock, "The effect of primordially produced gravitons upon the anisotropy of the cosmological microwave background radiation," *Phys. Lett. B*, vol. 125, (1983).

[190] J. Peacock, "The power spectrum of galaxy clustering," *Mon. Not. R. Ast. Soc.*, vol. 253, pp. 1P–5P, (1991).

[191] M. White and W. Hu, "The sachs-wolfe effect," *Astron. Astrophys.*, vol. 321, pp. 8–9, (1997).

[192] R. K. Sachs and A. M. Wolfe, "Perturbations of a cosmological model and angular variations of the microwave background," *Astrophys. J*, vol. 147, pp. 73–90, (1967).

[193] A. Albrecht, D. Coulson, P. Ferreira, and J. Magueijo, "Causality, randomness, and the microwave background," *Phys. Rev. Lett.*, vol. 76, pp. 1413–1416, (1996).

[194] B. Allen, R. R. Caldwell, S. Dodelson, L. Knox, and E. P. S. Shellard, "Cosmic microwave background anisotropy induced by cosmic strings on angular scales $z \leq 15'$," *Phys. Rev. Lett.*, vol. 79, pp. 2624–2627, (1997).

[195] U. Seljak, U. Pen, and N. Turok, "Polarization of the microwave background in defect models," *Phys. Rev. Lett.*, vol. 79, pp. 1615–1618, (1997).

[196] L. Knox, N. Christensen, and C. Skordis, "The age of the universe and the cosmological constant determined from cosmic microwave background anisotropy measurements," *Astrophys. J Lett.*, vol. 563, pp. L95–L98, (2001).

[197] X. Wang, M. Tegmark, and M. Zaldarriaga, "Is cosmology consistent?," *Phys. Rev. D*, vol. 65, p. 123001, (2002).

[198] W. J. Percival *et al.*, "Parameter constraints for flat cosmologies from cmb and 2dfgrs power spectra," *Mon. Not. R. Ast. Soc.*, vol. 337, p. 1068, (2002).

[199] L. Knox and Y. S. Song, "Limit on the detectability of the energy scale of inflation," *Phys. Rev. Lett.*, vol. 89, p. 011303, (2002).

[200] A. D. Linde, "Chaotic inflation," *Phys. Lett. B*, vol. 129, pp. 177–181, (1983).

[201] K. Harigaya, M. Ibe, K. Schmitz, and T. T. Yanagida, "Chaotic inflation with a fractional power-law potential in strongly coupled gauge theories," *Phys. Lett. B*, vol. 720, pp. 125–129, (2013).

[202] J. Martin, C. Ringeval, and V. Vennin, "Encyclopaedia inflationaris," *Phys. Dark Univ.*, vol. 5-6, pp. 75–235, (2014).

[203] K. Harigaya, M. Ibe, K. Schmitz, and T. T. Yanagida, "Dynamical fractional chaotic inflation – dynamical generation of a fractional power-law potential for chaotic inflation," *Phys. Rev. D*, vol. 90, pp. 123524–123591, (2014).

[204] R. Kallosh, A. Linde, and D. Roest, "Large field inflation and double α-attractors," *JHEP*, vol. 1408, pp. 052–073, (2014).

[205] J. McDonald, "A minimal sub-planckian axion inflation model with large tensor-to-scalar ratio," *JCAP*, vol. 1501, pp. 018–023, (2015).

[206] A. D. Linde, "Gravitational waves and large field inflation," *JCAP*, vol. 1702, (2017).

[207] A. Ito, A. Iyonaga, S. Kim, and J. Soda, "Dressed power-law inflation with cuscuton," *Phys. Rev. D*, vol. 99, pp. 083502–083511, (2019).

[208] V. Faraoni, "Nonminimal coupling of the scalar field and inflation," *Phys. Rev. D*, vol. 53, pp. 6813–6821, (1996).

[209] V. Faraoni, "Does the nonminimal coupling of the scalar field improve or destroy inflation?," *[arxiv:gr-qc/9807066]*.

[210] V. Faraoni, "Inflation and quintessence with non-minimal coupling," *Phys. Rev. D*, vol. 62, pp. 023504–023539, (2000).

[211] B. L. Spokoiny, "Inflation and generation of perturbations in broken symmetric theory of gravity," *Phys. Lett. B*, vol. 147, pp. 39–43, (1984).

[212] F. Lucchin, S. Matarrese, and M. D., "Inflation with a nonminimally coupled scalar field," *Phys. Lett. B*, vol. 167, pp. 163–168, (1986).

[213] T. Futamase and K. i. Maeda, "Chaotic inflationary scenario in models having nonminimal coupling with curvature," *Phys. Rev. D*, vol. 39, pp. 399–404, (1989).

[214] R. Fakir and W. G. Unruh, "Improvement on cosmological chaotic inflation through nonminimal coupling," *Phys. Rev. D*, vol. 41, pp. 1783–1791, (1990).

[215] L. Amendola, M. Litterio, and F. Occhionero, "The phase space view of inflation. 1: The non-minimally coupled scalar field," *Int. J. Mod. Phys. A*, vol. 5, pp. 3861–3886, (1990).

[216] A. S. Salopek, J. R. Bond, and J. M. Bardeen, "Designing density fluctuation spectra in inflation," *Phys. Rev. D*, vol. 40, pp. 1753–1838, (1994).

[217] D. I. Kaiser, "Primordial spectral indices from generalized einstein theories," *Phys. Rev. D*, vol. 52, pp. 4295–4306, (1995).

[218] S. Tsujikawa and B. Gumjudpai, "Density perturbations in generalized einstein scenarios and constraints on non-minimal couplings from the cosmic microwave background," *Phys. Rev. D*, vol. 69, pp. 123523–123537, (2004).

[219] K. Nozari and S. D. Sadatian, "Non-minimal inflation after wmap3," *Mod. Phys. Lett. A*, vol. 23, pp. 2933–2945, (2007).

[220] F. Bezrukov and M. Shaposhnikov, "The standard model higgs boson as the inflaton," *Phys. Lett. B*, vol. 659, pp. 703–706, (2008).

[221] F. Bauer and D. A. Demir, "Inflation with non-minimal coupling: Metric versus palatini formulations," *Phys. Lett. B*, vol. 665, pp. 222–226, (2008).

[222] S. C. Park and S. Yamaguchi, "Inflation by non-minimal coupling," *JCAP*, vol. 0808, pp. 009–0019, (2008).

[223] K. Nozari and S. Shafizadeh, "Non-minimal inflation revisited," *Phys. Scripta*, vol. 82, pp. 015901–015917, (2010).

[224] A. Linde, M. Noorbala, and A. Westphal, "Observational consequences of chaotic inflation with non-minimal coupling to gravity," *JCAP*, vol. 1103, pp. 013–021, (2011).

[225] M. Artymowski, A. Dapor, and T. Pawlowski, "Inflation from non-minimally coupled scalar field in loop quantum cosmology," *JCAP*, vol. 1306, pp. 010–023, (2011).

[226] S. Tsujikawa, "Observational tests of inflation with a field derivative coupling to gravity," *Phys. Rev. D*, vol. 85, pp. 083518–083528, (2012).

[227] M. A. Skugoreva, S. V. Sushkov, and A. V. Toporensky, "Cosmology with non-minimal kinetic coupling and a power-law potential," *Phys. Rev. D*, vol. 88, pp. 083539–083548, (2013).

[228] R. Kallosh and A. Linde, "Non-minimal inflationary attractors," *JCAP*, vol. 1310, pp. 033–045, (2013).

[229] D. C. Edwards and A. R. Liddle, "The observational position of simple non-minimally coupled inflationary scenarios," *JCAP*, vol. 1409, p. 059, (2014).

[230] S. del Campo, C. Gonzalez, and R. Herrera, "Power law inflation with a non-minimally coupled scalar field in light of planck 2015 data: the exact versus slow roll results," *Astrophys. Space Sci.*, vol. 358, pp. 31–36, (2015).

[231] K. Nozari and N. Rashidi, "Testing an inflation model with non-minimal derivative coupling in the light of planck 2015 data," *Adv. High Energy Phys.*, vol. 2016, pp. 1252689–1252704, (2016).

[232] T. Chiba and K. Kohri, "Consistency relations for large field inflation: Non-minimal coupling," *PTEP*, vol. 2015, p. 023E01, (2015).

[233] N. Yang, Q. Fei, Q. Gao, and Y. Gong, "Inflationary models with non-minimally derivative coupling," *Class. Quantum Grav.*, vol. 33, pp. 205001–205021, (2016).

[234] L. Boubekeur, E. Giusarma, O. Mena, and H. Ramirez, "Does current data prefer a non-minimally coupled inflaton?," *Phys. Rev. D*, vol. 91, pp. 103004–103008, (2015).

[235] M. Pieroni, "β-function formalism for inflationary models with a non-minimal coupling with gravity," *JCAP*, vol. 1602, pp. 012–027, (2016).

[236] C. Geng, C. Lee, S. Sami, E. N. Saridakis, and A. A. Starobinsky, "Observational constraints on successful model of quintessential inflation," *JCAP*, vol. 1706, pp. 011–024, (2017).

[237] T. Tenkanen, "Resurrecting quadratic inflation with a non-minimal coupling to gravity," *JCAP*, vol. 1712, pp. 001–011, (2017).

[238] M. Shokri, "A revision to the issue of frames by non-minimal large field inflation," *[gr-qc:1710.04990]*.

[239] T. Markkanen, T. Tenkanen, V. Vaskonen, and H. Veermäe, "Quantum corrections to quartic inflation with a non-minimal coupling: metric vs. palatini," *JCAP*, vol. 1803, pp. 029–044, (2018).

[240] N. Kaewkhao and B. Gumjudpai, "Cosmology of non-minimal derivative coupling to gravity in palatini formalism and its chaotic inflation," *Phys. Dark Univ.*, vol. 20, pp. 20–27, (2018).

[241] N. D. Birrell and P. C. Davies, *Quantum Fields in Curved Space*. Cambridge University Press, (1980).

[242] C. G. Gallan, S. Coleman, and R. Jackiw, "A new improved energy-momentum tensor," *Ann. Phys.*, vol. 59, pp. 42–73, (1970).

[243] D. Z. Freedman and E. J. Weinberg, "The energy-momentum tensor in scalar and gauge field theories," *Ann. Phys.*, vol. 87, pp. 354–396, (1974).

[244] D. Z. Freedman, I. J. Muzinich, and E. J. Weinberg, "On the energy-momentum tensor in gauge field theories," *Ann. Phys.*, vol. 87, pp. 95–146, (1974).

[245] R. Fakir and W. G. Unruh, "Induced-gravity inflation," *phys. Rev. D*, vol. 41, pp. 1792–1795, (1990).

[246] R. Fakir and W. G. Unruh, "Quantum creation of universes with non-minimal coupling," *phys. Rev. D*, vol. 41, pp. 3012–3023, (1990).

[247] L. F. Abbott, "Gravitational effects on the $SU(5)$ breaking phase transition for a coleman-weinberg potential," *Nucl. phys. B*, vol. 185, pp. 233–238, (1981).

[248] R. Fakir and W. G. Unruh, "Cosmological density perturbations with modified gravity," *Astrophysical Journal*, vol. 394, pp. 396–410, (1992).

[249] E. W. Kolb, D. S. Salopek, and M. S. Turner, "Origin of density fluctuations in extended inflation.," *Phys. Rev. D*, vol. 42, pp. 3925–3935, (1990).

[250] N. Makino and M. Sasaki, "The density perturbation in the chaotic inflation with non-minimal coupling," *Prog. Theor. Phys. Suppl.*, vol. 86, pp. 103–118, (1990).

[251] M. Kawasaki, M. Yamaguchi, and T. Yanagida, "Natural chaotic inflation in supergravity," *Phys. Rev. Lett.*, vol. 85, pp. 3572–3575, (2000).

[252] E. Silverstein and A. Westphal, "Monodromy in the cmb: Gravity waves and string inflation," *Phys. Rev. D*, vol. 78, pp. 106003–06045, (2008).

[253] L. McAllister, E. Silverstein, and A. Westphal, "Gravity waves and linear inflation from axion monodromy," *Phys. Rev. D*, vol. 82, pp. 046003–046043, (2010).

[254] R. Flauger, L. McAllister, E. Pajer, A. Westphal, and G. Xu, "Oscillations in the cmb from axion monodromy inflation," *JCAP*, vol. 009, p. 1006, (2010).

[255] N. Kaloper and L. Sorbo, "A natural framework for chaotic inflation," *JCAP*, vol. 102, pp. 121301–121304, (2009).

[256] N. Kaloper, A. Lawrence, and L. Sorbo, "An ignoble approach to large field inflation," *JCAP*, vol. 1103, p. 023, (2011).

[257] N. Kaloper and A. Lawrence, "Natural chaotic inflation and uv sensitivity," *Phys. Rev. D*, vol. 90, pp. 023506–023513, (2014).

[258] L. Alabidi and I. Huston, "An update on single field models of inflation in light of WMAP7," *JCAP*, vol. 1008, pp. 037–042, (2010).

[259] J. Martin, C. Ringeval, and R. Trotta, "Hunting down the best model of inflation with bayesian evidence," *Phys. Rev. D*, vol. 83, pp. 063524–063535, (2011).

[260] R. Kallosh and A. Linde, "New models of chaotic inflation in supergravity," *JCAP*, vol. 1011, pp. 011–021, (2010).

[261] F. Takahashi, "Linear inflation from running kinetic term in supergravity," *Phys. Lett. B*, vol. 693, pp. 140–143, (2010).

[262] R. Kallosh, A. Linde, and T. Rube, "General inflaton potentials in supergravity," *Phys. Rev. D*, vol. 83, pp. 043507–043512, (2011).

[263] P. Ade *et al.*, "Planck 2015 results. xiii. cosmological parameters," *Astron. Astrophys.*, vol. 594, pp. A13–A75, (2016).

[264] P. Ade *et al.*, "Improved constraints on cosmology and foregrounds from bicep2 and keck array cosmic microwave background data with inclusion of 95 ghz band.," *Phys. Rev. Lett.*, vol. 116, p. 031302, (2016).

[265] A. Lewis and S. Bridle, "Cosmological parameters from cmb and other data: A monte carlo approach," *Phys. Rev. D*, vol. 66, p. 103511, (2002).

[266] A. Lewis, A. Challinor, and A. Lasenby, "Efficient computation of cosmic microwave background anisotropies in closed friedmann-robertson-walker models," *Astrophysical Journal*, vol. 538, pp. 473–476, (2000).

[267] N. Aghanim *et al.*, "Planck 2015 results. xi. cmb power spectra likelihoods and robustness of parameters," *Astrophysical Journal*, vol. 594, p. A11, (2016).

[268] Y. Akrami *et al.*, "Planck 2018 results. x. constraints on inflation," *[arXiv:astro-ph/1807.06211].*

[269] A. Vilenkin, "Classical and quantum cosmology of the starobinsky inflationary model," *Phys. Rev. D*, vol. 32, pp. 2511–2547, (1985).

[270] M. B. Mojic, M. S. Morris, and S. Wei-Mo, "The R^2 cosmology: Inflation without a phase transition.," *Phys. Rev. D*, vol. 34, pp. 2934–2962, (1986).

[271] L. H. Ford, "Gravitational particle creation and inflation," *Phys. Rev. D*, vol. 35, pp. 2955–2977, (1987).

[272] H. Motahashi, A. A. Starobinsky, and J. Yokoyama, "Phantom boundary crossing and anomalous growth index of fluctuations in viable f(R) models of cosmic acceleration," *Prog. Theor. Phys.*, vol. 123, pp. 887–902, (2010).

[273] H. Motahashi, A. A. Starobinsky, and J. Yokoyama, "Future oscillations around phantom divide in f(r) gravity," *JCAP.*, vol. 1106, pp. 006–0017, (2011).

[274] R. Gannouji, B. Moraes, and D. Polarski, "The growth of matter perturbations in f(R) models," *JCAP.*, vol. 0902, pp. 034–047, (2009).

[275] H. Motahashi, A. A. Starobinsky, and J. Yokoyama, "f(R) gravity and its cosmological implications," *Int. J. Mod. Phys. D.*, vol. 20, pp. 1347–1355, (2009).

[276] S. Tsujikawa, R. Gannouji, B. Moraes, and D. Polarski, "The dispersion of growth of matter perturbations in f(R) gravity," *Phys. Rev. D*, vol. 80, pp. 084044–084054, (2009).

[277] H. Motahashi, A. A. Starobinsky, and J. Yokoyama, "Matter power spectrum in f(R) gravity with massive neutrinos," *Prog. Theor. Phys.*, vol. 124, pp. 541–546, (2010).

[278] H. Motahashi, A. A. Starobinsky, and J. Yokoyama, "Cosmology based on f(R) gravity admits 1 ev sterile neutrinos," *Phys. Rev. Lett.*, vol. 110, pp. 121302–121306, (2013).

[279] S. Tsujikawa, "Observational signatures of f(R) dark energy models that satisfy cosmological and local gravity constraints," *Phys. Rev. D*, vol. 77, pp. 023507–023519, (2008).

[280] S. Appleby and R. Battye, "Aspects of cosmological expansion in f(R) gravity models," *JCAP*, vol. 0805, p. 019, (2008).

[281] A. V. Frolov, "A singularity problem with f(R) dark energy," *Phys. Rev. Lett.*, vol. 101, pp. 061103–061107, (2008).

[282] T. Kobayashi and K. i Maeda, "Relativistic stars in f(R) gravity, and absence thereof," *Phys. Rev. D*, vol. 78, pp. 064019–064027, (2008).

[283] S. A. Appleby, R. A. Battye, and A. A. Starobinsky, "Curing singularities in cosmological evolution of f(R) gravity," *JCAP*, vol. 1006, p. 005, (2010).

[284] J. Aguirre *et al.*, "The simons observatory: Science goals and forecasts," *JCAP*, vol. 1902, p. 056, (2019).

[285] K. N. Abazajian *et al.*, "Cmb-s4 science book, first edition," *[astro-ph:1610.02743]*.

[286] A. Suzuki *et al.*, "The litebird satellite mission: Sub-kelvin instrument," *Journal of Low Temperature Physics*, vol. 193, pp. 1048–1056, (2018).

[287] H. Schmidt, "Variational derivatives of arbitrarily high order and multi-inflation cosmological models," *JCAP*, vol. 7, pp. 1023–1031, (1989).

[288] K. i. Maeda, "Towards the einstein-hilbert action via conformal transformation," *JCAP*, vol. 39, pp. 3159–3162, (1989).

[289] V. Muller, H. Schmidt, and A. A. Starobinsky, "Power-law inflation as an attractor solution for inhomogeneous cosmological models," *Class. Quant. Grav.*, vol. 7, pp. 1163–1168, (1990).

[290] S. Gottlober, V. Muller, H. Schmidt, and A. A. Starobinsky, "Models of chaotic inflation," *Int. J. Mod. Phys. D*, vol. 1, pp. 257–279, (1992).

[291] J. Martin, C. Ringeval, R. Trotta, and V. Vennin, "Compatibility of planck and bicep2 in the light of inflation," *Phys. Rev. D*, vol. 90, p. 063501, (2014).

[292] A. Codello, J. Joergensen, F. Sannino, and O. Svendsent, "Marginally deformed starobinsky gravity," *JHEP*, vol. 1502, pp. 050–057, (2015).

[293] R. Costa and H. Nastase, "General f(R) and conformal inflation from minimal supergravity plus matter," *JHEP*, vol. 1406, p. 145, (2014).

[294] G. K. Chakravarty and S. Mohanty, "Power law starobinsky model of inflation from no-scale sugra," *[hep-ph:1405.1321]*.

[295] H. Motahashi, "Consistency relation for R^p inflation," *Phys. Rev. D*, vol. 91, p. 064016, (2014).

[296] T. Chiba and M. Yamaguchi, "Extended slow-roll conditions and rapid-roll conditions," *JCAP*, vol. 0810, pp. 021–035, (2008).

[297] J.-O. Gong, J. chan Huang, W. I. park, M. Sasaki, and Y.-S. Song, "Conformal invariance of curvature perturbation," *JCAP*, vol. 2011, pp. 023–023, (2011).

[298] H. C. Chiang *et al.*, "Measurement of cosmic microwave background polarization power spectra from two years of bicep data," *A. J.*, vol. 711, p. 1123, (2010).

[299] P. A. R. Ade *et al.*, "Planck 2013 results. xxii. constraints on inflation," *Astron. Astrophys.*, vol. 571, p. A22, (2014).

[300] P. A. R. Ade *et al.*, "Planck 2015 results. xx. constraints on inflation," *Astron. Astrophys.*, vol. 579, p. A20, (2016).

[301] M. Shokri, F. Renzi, and A. Melchiorri, "Cosmic microwave background constraints on non-minimal couplings in inflationary models with power law potentials," *Phys. Dark Univ.*, vol. 2008, pp. 2212–6864, (2019).

[302] P. A. R. Ade *et al.*, "Planck 2013 results. xvi. cosmological parameters," *A. A.*, vol. 571, p. A16, (2014).

[303] H. Bateman, "The conformal transformations of space of four dimensions and their applications to geometrical optics," *Proc. London Math. Soc.*, vol. 8, p. 223–264, (1910).

[304] H. A. Kastrup, "The transformations of the electrodynamical equations," *Annalen Phys.*, vol. 17, pp. 631–690, (2008).

[305] J. L. Synge, *Relativity: The General Theory*. Elsevier Science Publishing, (1960).

[306] S. W. Hawking and G. F. R. Ellis, *The Large Scale Structure of Space-Time*. Cambridge University Press, (1973).

[307] I. L. Shapiro and H. Takata, "Conformal transformation in gravity," *Phys. Lett. B*, vol. 361, pp. 31–37, (1995).

[308] I. L. Shapiro, "On the conformal transformation and duality in gravity," *Class. Quant. Grav.*, vol. 14, pp. 391–406, (1997).

[309] V. Faraoni, E. Gunzig, and P. Nardone, "Conformal transformations in classical gravitational theories and in cosmology," *Fund. Cosmic Phys.*, vol. 20, pp. 121–173, (1999).

[310] D. F. Carneiro, E. A. Freiras, B. Gonçalves, A. G. de Lima, and I. L. Shapiro, "On useful conformal tranformations in general relativity," *Grav. Cosmol.*, vol. 10, pp. 305–312, (2004).

[311] S. Carloni, E. Elizalde, and S. Odintsov, "Conformal transformations in cosmology of modified gravity: the covariant approach perspective," *Gen. Rel. Grav.*, vol. 42, pp. 1667–1705, (2010).

[312] M. P. Dabrowski, J. Garecki, and D. B. Blaschke, "Conformal transformations and conformal invariance in gravitation," *Annalen Phys.*, vol. 18, pp. 13–32, (2009).

[313] K. I. Maeda, "Towards the einstein-hilbert action via conformal transformation," *Fund. Cosmic Phys.*, vol. 39, pp. 3159–3166, (1989).

[314] D. Wands, "Extended gravity theories and the einstein-hilbert action," *Class. Quant. Grav.*, vol. 11, pp. 269–280, (1994).

[315] G. t'Hooft and M. Veltman, "One-loop divergencies in the theory of gravitation," *Ann. Inst. H. Poincare. A*, vol. 20, pp. 69–94, (1974).

[316] S. Deser and P. V. Nieuwenhuisen, "Nonrenormalizability of the quantized dirac-einstein system," *Phys. Rev. D*, vol. 10, pp. 411–440, (1974).

[317] A. S. M. H. Goroff, "The ultraviolet behavior of einstein gravity," *Nucl. Phys. B*, vol. 266, pp. 709–736, (1986).

[318] E. S. Fradkin and A. A. Tseytlin, "Renormalizable asymptotically free quantum theory of gravity," *Nucl. Phys. B*, vol. 201, pp. 469–491, (1982).

[319] I. L. Shapiro and A. G. Jacksenaev, "A four-dimensional theory for quantum gravity with conformal and non-conformal explicit solutions," *Phys. Lett. B*, vol. 324, p. 284, (1994).